2009

BEHAVIOUR OF GLASS PLATES UNDER WIND LOADS

Eri Gavanski

BEHAVIOUR OF GLASS PLATES UNDER WIND LOADS

(Thesis Format: Monograph)

by

Eri Gavanski

Department of Civil and Environmental Engineering
Faculty of Engineering Science

A thesis submitted in partial fulfillment
of the requirements for the degree of
Doctor of Philosophy

The School of Graduate and Postdoctoral Studies
The University of Western Ontario
London, Ontario, Canada

ABSTRACT

Glazing damage during strong windstorms has been considered to result mainly from windborne debris. However, recent windstorm damage reports have revealed the necessity of studying fluctuating wind loads, which appear to be another factor contributing to this damage. From an experimental point of view, studies on this topic have been limited to the application of rather simple loading patterns. Moreover, there is an uncertainty surrounding both load resistance and design load used in the current North American window glass design codes. It is of concern that these regulations may not offer sufficient accuracy on account of the limited understanding of time-dependent glass strength derived from the technology available at the time of codification. Unprecedented full-scale glass breakage tests under realistic wind pressure loading were conducted to investigate these issues. The obtained results revealed significant new information about the behavior of glass plates under fluctuating loads. Along with these tests, a numerical simulation using the Monte-Carlo technique was also performed with a subtle modification of the initial glass strength. This adjustment resulted in better correspondence with test results. Using the test and numerical simulation results, the current window glass design method was examined. The calculation methods of *LR*, and the reference time conversion used in the codes, were found to require further investigation. By creating a particular wind pressure time history, the practice of using peak pressures from ASCE7-05 as the design load was investigated. The results showed that there are cases when the current practice may underestimate the design load because of the duration of windstorms.

KEYWORDS: Glass, Fluctuating load, Full-scale test, Load resistance, Design load, Static fatigue, Numerical simulation, Monte-Carlo technique, Brown's integral.

ACKNOWLEDGEMENTS

I would like to thank Dr. Gregory A. Kopp for the opportunity to work in such a great research environment, the supervision to guide me in an appropriate direction of research, the expertise to improve my work, and for his continuous support.

I would also like to acknowledge the Ministry of Education, Culture, Sports, Science and Technology of Japan for their financial support over the past three years.

I would furthermore like to thank Dr. Joseph E. Minor for his sustained feedback and support throughout the research and writing process.

There are many people whose contribution to this work was necessary for the completion of my research. I am grateful to Dr. Saburo Kawabata, Dr. F. Michael Bartlett, Mr. Per S. Werthwein, Dr. Jeff T. Wood, Dr. Robert Klassen, Dr. John.R. Dryden, and Mr. Christopher Vandelaar for their skilled knowledge, and many interesting and helpful discussions.

I would like to thank Mr. Murray J. Morrison for his excellent knowledge, effort, patience, and for being a wonderful colleague. Also, I would like to express thanks to all of my colleagues and friends for their kind and continuous support.

Equipment used in this research was generously provided by grants from the Canada Foundation for Innovation and the Ontario Innovation Trust. The Institute for Catastrophic Loss Reduction, the Natural Sciences and Engineering Research Council and the Boundary Layer Wind Tunnel Laboratory at the University of Western Ontario kindly provided funding for this research.

I would like to express my affectionate appreciation to my family, both in Japan and Canada, for their encouragement and consideration during my long academic education.

Finally, I would like to express my deep gratitude to my husband Filip, for his unlimited support, patience, indulgence, and numerous discussions on the content of my thesis.

TABLE OF CONTENTS

LIST OF TABLES

LIST OF FIGURES

LIST OF APPENDICIES

NOMENCLATURE

A	Glass plate surface area upon which applied stress is acting
A''	Crack velocity parameter
A_o	Reference glass plate surface area
a	Plate width
α_k	Crack direction on glass panel
B_x	Bias limit of quantity x
b	Plate width
β	Stress loading rate
C_k	Glass design coefficient
C_p	Pressure coefficient
$C_{\hat{p}}$	Most probable peak wind pressure coefficient during one hour storm
C_{ps}	Equivalent static pressure coefficient
c	Crack length
c_i	Initial crack length
c_1	Coefficient in CAN/CGSB
c_2	Coefficient in CAN/CGSB
c_3	Coefficient in CAN/CGSB
c_4	Coefficient in CAN/CGSB
D_{crit}	Critical damage accumulation
δ	Deflection
δ_f	Deflection at glass plate failure
E	Young's modulus
F	Cumulative distribution function of failure pressure/time expressed as $F=i/(N+1)$
$f_{Cp}(Cp)$	Probability density function of pressure coefficient
$f_p(p)$	Probability density function of pressure
$f_{X,ij}$	Dimensionless function of angle
f'	Strength factor
G	Strain energy release rate
G_c	Critical Strain energy release rate
g	Dimensionless damage function 1
g'	Dimensionless damage function 2
H	Roof height
h	Plate thickness
φ	Orientation coordinate of crack location
K_e	Damage accumulation of trapezoidal loading pulse
K_g	Damage accumulation of whole pressure trace
K_I	Stress intensity factor
K_{IC}	Fracture toughness
K_{Ii}	Initial stress intensity factor
K_{ISCC}	Static fatigue limit
k	surface crack parameter (measure of location)

λ	Period of cyclic loading
M_j	Crack location on glass panel
m	Surface crack parameter (measure of dispersion) for initial glass strength
m'	Coefficient of Kawabata's modified Brown's integral
m_f	Surface crack parameter (measure of dispersion) for failure glass strength
n	Coefficient of Brown's integral
n'	Crack velocity parameter
n''	Coefficient used in CAN/ CGSB-12.20-M89
v	Penetration velocity of crack
ν'	Poisson ratio
P	Probability
p	Applied load (pressure)
p'	Pressure loading rate
p_{eq}	Equivalent static pressure
p_f	Failure pressure
p_{peak}	Peak pressure of saw-tooth loading
$p_{3\_pressure}$	Equivalent 3 seconds load based on a modification of Brown's integral
p_{3_stress}	Equivalent 3 seconds load based on Brown's integral
p_{60_eq}	60 seconds equivalent constant load
q_{ref}	Reference velocity pressure
R	Factored resistance of glass plates
R'	Universal gas constant
R_{ref}	Reference resistance under a 1-min constant pressure
R_t	Average resistance under a t-min constant pressure
r	Distance coordinate of crack location
S	Glass strength
S_i	Initial glass strength
S_0	Scale parameter
S_x	Precision index of quantity x
s	Coefficient of modified Brown's integral
σ	Stress
σ_a	Applied stress at crack
σ_{ave}	Average stress of cyclic loading
σ_{const}	Applied constant stress
σ_f	Failure stress
σ_o	Amplitude of cyclic loading
σ_p	Proof stress
σ_{peak}	Stress corresponding to p_{peak}
σ_{60}	Equivalent 60 second constant stress
T	Temperature
T_x	Total uncertainty of quantity x
t	Time
t_f	Failure time
t_{const}	Failure time under constant loading

t_{cyclic}	Failure time under cyclic loading
t_{peak}	Peak evaluation time
t_{ref}	Reference time duration
τ	Shear stress
U	Strain energy
W	Surface energy
ξ	Ratio of amplitude of cyclic loading
Y	Geometric shape factor

SYMBOLS AND ABREVIATIONS

AN	Annealed glass
°C	Celsius
CDF	Cumulative Distribution Function
CGM	Crack Growth Model
COV	Coefficient of Variation
DA	Damage Accumulation
DAQ	Damage Acquisition System
DC	Design Cyclone
DL	Design Load
FEA	Finite Element Analysis
FT	Fully Tempered Glass
GFPM	Glass Failure Prediction Model
GTF	Glass Type Factor
HS	Heat Strengthened Glass
Hz	Hertz
IG	Insulating Glass
LA	Layered Glass
LDT	Laser Displacement Transducer
LG	Laminated
LR	Load Resistance
min	Minutes
MO	Monolithic Glass
mph	Miles Per Hour
NFL	Non-Factored Load
PDF	Probability Distribution Function
PG	Plate Glass
PLA	Pressure Loading Actuator
RH	Relative Humidity
RL	Ramp Loading
SD	Standard Deviation
sec	Seconds
SG	Sheet Glass
SS	Simply-Support Condition

1.0 Introduction

1.1 Background

During severe windstorms such as hurricanes, various cladding materials tend to suffer damage, as well as the building structure itself. Among these materials, window glass damage has been outstanding in residential structures and high-rise buildings. Factors that have been identified as affecting glass damage include fluctuating pressures, windborne debris, building deformations and poor maintenance or installation (Minor & Beason 1976; Minor 1984; Beason et al. 1984; Kareem & Stevens 1985; Williams & Kareem 2003; Kareem & Bashor 2006). While building codes and standard test methods consider these issues, significant glass damage has continued to be observed in recent windstorms with substantial damage resulting from disturbances such as Hurricane Ike (Brewick et al. 2009). Much of this damage has been reported in situations where recorded wind speeds were significantly lower than design wind speeds (Minor & Beason 1976; Beason et al. 1984). While damage is undoubtedly caused by windborne debris to a significant extent, all potential factors need to be examined in order to arrive at the best possible design standards.

Figure 1.1 shows a fluctuating wind pressure trace and the pressure levels where failure has occurred for 19 pieces of 1 x 1 x 0.006 (m) annealed glass plate. If we were to try to obtain a pressure level to use for the design for annealed glass, we would soon realize that our task is challenging. This figure clearly shows that there is no single

deterministic pressure (stress) level for glass. This unique characteristic of glass makes it difficult to use for design, especially under wind loading, which varies both spatially over building surfaces, and in time. In order to suggest a better glass design method, it is necessary to have the perspective of both resistance and load. Both are examined herein.

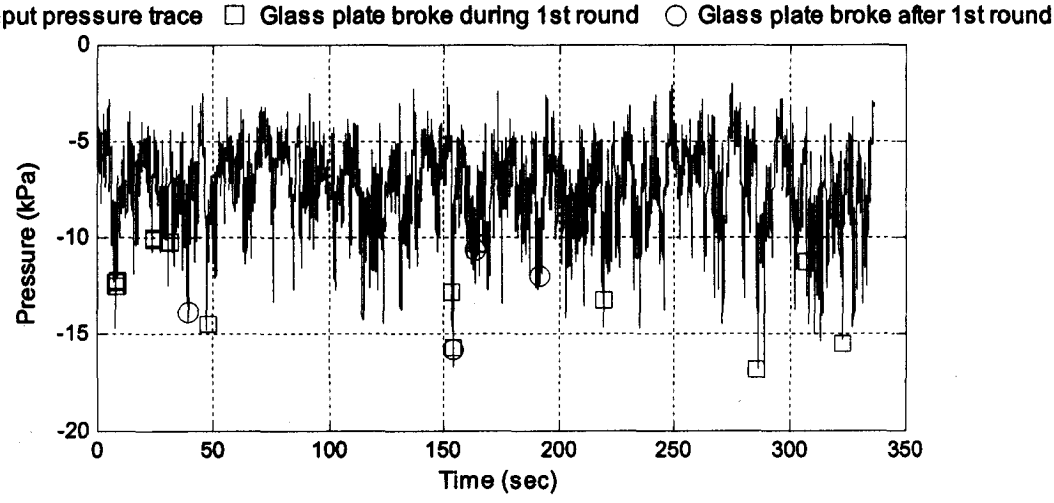

Figure 1.1 Failure pressure level in fluctuating load

1.2 Development of Load Resistance of glass

In past decades, glass design was dependent on design charts developed by glass manufacturers. Glass has some unique characteristics, such as static fatigue (delayed failure), which is a time-dependent reduction of strength after a certain duration of load application. This nature of glass had already been recognized more than 30 years ago (Minor 1981). Hence, load resistance (*LR*) needed to be expressed in a time-dependent form, and the glass manufacturers' charts referenced 60 sec as the standard load duration, without giving any specific reason for this choice (Minor 1981).

Although manufacturers' design charts were widely used, confusion eventually ensued among glass designers as a result of a controversy between two major design charts: (1) a single chart, which bases its empirical data on destructive testing of 20 glass specimens, elementary statistics and engineering judgement (Orr 1957; Hershey & Higgins 1973), and (2) the PPG glass thickness selection charts, which employs a "maximum principal stress" approach based on theoretical and experimental work (PPG Industries 1979; Tsai & Steward 1976; Krall et al. 1981). These two design charts utilized different judgements and simplifying assumptions for their respective recommendations of glass thickness, which left glass designers without any standardized design charts to which they could all refer. For further detail, see Minor 1981; Beason & Morgan 1984; and Beason et al. 1998.

The glass failure prediction model (GFPM) introduced by Beason and Morgan shed new light on glass design (Beason 1980; Beason & Morgan 1984). Widely received as a clear improvement over both glass design charts, the GFPM calculated the probability of glass failure in relation to surface flaw characteristics, induced stresses, and a number of other factors significant to glass strength such as the pane size, load duration, and the magnitude of the applied load.

The introduction of the GFPM paved the way for significant advances in current glass design. Presently, most building codes specify the use of ASTM Standard E 1300-07 "Standard practice for determining load resistance of glass in buildings", (ASTM 2007, hereafter ASTM E 1300-07) as the benchmark reference of *LR* associated with a

breakage probability less than or equal to 8 lites[1] per 1000, which corresponds to a design factor of 2.5. The basic process to calculate *LR* for annealed glass is to:

1. Determine non-factored load (NFL) for selected glass geometry from chart, which is calculated by the GFPM;
2. Determine glass type factor (GTF) for appropriate glass type (heat treatment) and load duration from table;
3. Multiply NFL and GTF to obtain *LR*.

When the standard was first finalized in the mid 1990s, only a limited number of design instances required the application of these standards, which resulted in relatively lower diligence for glass designers (Block 2002). As the relevance of various factors in glass design has come to be recognized, the application of these standards has expanded, increasing the relative complexity of usage. In addition, the 60-sec reference load duration, which had been used since the first version of the standards, was changed to a 3-sec duration, consistent with the 3-sec gust wind in Minimum Design Loads for Buildings and Other Structures (ASCE 2005, hereafter ASCE 7-05). Despite extensive use of ASTM E 1300-07 in glass design, an inherent conservatism may remain in *LR*. According to Minor and Norville (2006), there are four factors influential to the definition of NFL, which are: (1) the use of minimum glass thickness[2] in the calculation of *LR*; (2) the use of weathered window glass in the calculation of surface parameters,

---

[1] The term "lite" is defined as "one piece of glazing (preferred term) (also spelled light)" and is synonymous with "pane" (Minor & Norville 2006; ASTM 2006)

[2] "Minimum glass thickness" is the minimum value in the thickness range specified for designated glass thickness in the code. For example, nominal 6 mm glass thickness is specified to have the range of 5.56 – 6.20 mm (ASTM C 1036-01). Hence, minimum thickness in this case means 5.56 mm.

which they state produces 35 % weaker glass strength when compared to new glass; (3) the use of conservative GTF for heat treated glasses (HS, FT); and (4) the limited number of available standard glass thicknesses. It is a rational approach to make a conservative assumption in order to address an uncertainty from each factor. However, these factors are cumulative and therefore, can produce a significantly conservative *LR* (Minor & Norville 2006).

In addition, the design factor of 2.5 was selected without any guidance for specific design situations (Minor 1981), and several researchers have identified possible defects in the way that the GFPM is used to calculate the NFL, which is a uniform load associated with a failure probability of 8/1000 for monolithic annealed glass with a reference time duration (Reid 1991; Fisher-Cripps & Collins 1995; Kawabata 1996)[3]. For this reason, it seems that the reduction of glass strength in time due to static fatigue may not be properly considered through the usage of the GFPM with current input parameters. The above comments equally apply to the Canadian National standard CAN/CGSB-12.20-M89, hereafter CAN/CGSB-12.20-M89, which is based on ASTM E1300-94 (ASTM 1994). The only difference is that CAN/CGSB-12.20-M89 currently uses 60 sec as the reference load duration, which is used prior to the 2002 version of ASTM E 1300. In addition, although the basic procedure to obtain *LR* (called factored resistance of glass plates *R* in CAN/CGSB-12.20-M89) is similar, the coefficients used in order to consider several effects on glass strength are divided into a greater number of categories to:

---

[3] For greater detail, see Chapter 2.

1. Determine factored resistance of reference glass (R_{ref}) for selected glass geometry from chart, which is calculated by the GFPM;
2. Determine c_1 for appropriate glass type from table;
3. Determine c_2 for appropriate heat treatment on glass from table;
4. Determine c_3 for appropriate load duration from table;
5. Determine c_4 for appropriate load type from table;
6. Multiply R_{ref}, c_1, c_2, c_3 and c_4 to obtain R.

1.3 Development of Design Load for glass

In accordance with *LR*, the design load (*DL*) for window glass also needs to be expressed in a time-dependent form, which can be achieved by load transformation/equivalent load. Brown's integral (Brown 1972, 1974), which is the theoretical equation used to capture the idea of static fatigue, emerged as the solution:

$$DA_{crit} = \int_0^{t_f} [\sigma_a(t)]^n dt \tag{1.1}$$

where t_f is failure time, $\sigma_a(t)$ is arbitrary time-dependent applied stress at the critical crack on a glass surface, and n is constant (generally chosen to be 16 for soda-lime silicate glass). What equation (1.1) means is that when the integral of $[\sigma_a(t)]^n$ (called 'damage accumulation, DA' hereafter) reaches its critical value (critical damage accumulation), glass failure can occur.

In addition to Brown's integral, which utilizes the stress induced at a crack tip, a simplified form of Brown's integral was introduced using a power law relationship between the stress and applied pressure (Brown 1972; Dalgliesh & Taylor 1990; Kawabata 1996; Calderone 1999) so that:

$$DA_{crit} = \int_0^{t_f} [p(t)]^s dt \tag{1.2}$$

where p is applied load and s is a coefficient. A beneficial point of equation (1.2) is that the analysis of applied pressure is simpler than that of stress, and the failure location (critical crack location) on glass is not required for this calculation, as it is for equation (1.1).

The conversion to a 60-sec equivalent constant load, p_{60_eq}, which in past decades was required by the manufacturers' design charts, was achieved by various methods thanks to Brown's integral, depending on each individual researcher's interpretation of fluctuating wind loads.

Peterka and Cermak (1978) characterized a fluctuating wind load only by its peak pressure, averaged over 1 to 2 sec:

$$p_{60\_eq} = \left(t_{peak}/60\right)^{1/s} \cdot p_{peak} \tag{1.3}$$

where p_{peak} is peak pressure averaged over t_{peak} sec. From this equation, it is implicitly assumed that the peak pressure was assumed to be the only characteristic of load to bear upon glass strength (Reed & Simiu 1984).

According to Brown's integral, Davenport (1975) expressed the 1-min equivalent static load as:

$$p_{eq} = \left(\int_0^{\infty} p^s(t) \cdot f_p(p) dp \right)^{1/s} \tag{1.4}$$

where $f_p(p)$ is the probability density function of pressure $p(t)$. Using equations (1.2) and (1.4), and the statistical properties of pressure fluctuations obtained, assuming a Gaussian distribution for (positive) pressure and the exponential distribution for suction, Davenport (1983) determined that fluctuating wind loads which contain the peak pressure, p_{peak}, and sustain themselves for two hours will cause the same damage brought on by a constant load application of p_{peak} for 60 sec, which is the traditionally-used time duration for defining glass strength. This finding means that p_{peak} is well matched with the '60 sec' glass strength, and thus, p_{peak} is an appropriate comparison for a 1-min wind load in the design charts at that time.

Dalgliesh (1979), in contrast to Peterka and Cermak, considered the whole time history of a fluctuating wind load:

$$p_{60\_eq} = \left(\int_0^{t_f} p^s(t) dt \Big/ 60 \right)^{1/s} \tag{1.5}$$

Dalgliesh focused on the time duration of extreme peaks as well as the duration of the entire storm for the damage accumulation in his study, and thus, the *DL* is expressed as:

$$C_k \cdot q_{ref} = \left[(K_e + K_g) / 60 \right]^{1/s} \tag{1.6}$$

where C_k is called "glass design coefficient" and is the pressure coefficient representing the damage accumulation of turbulent wind acting on the glass, q_{ref} is reference velocity pressure, K_e is the damage accumulation contribution of trapezoidal loading pulses occurring in the specific duration, and K_g is the damage accumulation of the whole

pressure trace when it is approximated by truly Gaussian fluctuations. The comparison of C_k, which is computed from actual wind records and the 'most probable' peak wind pressure coefficient during a one-hour storm, $C_{\hat{p}}$, showed that their correspondence is generally consistent, but discrepancies could increase depending on the peak factor. Based on this study, the peak wind pressures specified by the code are currently being used in CAN/CGSB-12.20 as *DL*.

In addition to Davenport and Dalgliesh, Holmes (1985) also commented on the relationship between *DL* and peak wind pressure. Holmes calculated an equivalent static pressure coefficient C_{ps} for one-hour windstorm in order to examine the relative contributions to the critical damage accumulation from the various ranges of pressure fluctuations:

$$C_{ps} = \left[\int_0^{\infty} C_p^n \cdot f_{C_p}(C_p) dC_p \right]^{1/n} \tag{1.7}$$

where $f_{Cp}(C_p)$ is the probability density function of pressure coefficient C_p. From this examination, it was found that isolated peaks occurring at infrequent intervals during a storm most dominantly contribute to the critical damage accumulation. This finding indicates that the present use of the measured peak pressures from a wind tunnel test or full-scale test is appropriate for glass design. The latter statement was verified by comparing an equivalent glass design coefficient, following the approach of Dalgliesh (1979), with the peak pressure coefficient using an average crossing rate of one per hour.

Studies by Davenport, Dalgliesh and Holmes all indicate that the use of the peak pressure as *DL* is appropriate for glass design with small errors at certain pressure

fluctuation levels. However, the cases dealt with in their study are limited, and hence, there may be cases where their conclusion does not properly apply in glass design.

Besides the discussion centred on *DL* for glass, examinations of pressure fluctuation characteristics on glass strength were conducted experimentally and numerically using equivalent loads obtained in the way explained above to discern the important characteristics of fluctuating loads with respect to damage accumulation (Holmes 1985; Reed 1993; Kawabata 1996; Li et al. 1999; Ko et al. 2005). These studies revealed that damage accumulation on glass cladding is greatly affected by the characteristics of fluctuating wind load (turbulence intensity and scale, level of pressure fluctuation), and skewness of the probability distribution of the wind pressures (non-Gaussian nature of pressure fluctuations).

Currently the main reference for *DL* on which many codes rely is ASCE 7-05 (ASCE 2005), which specifies the wind loads for the main structural system and the cladding and components. For cladding and components, this is an area-averaged, peak pressure normalized by a 3-sec gust wind speed with a return period of 50 years. Note that the averaging times (duration) for these pressure coefficients are much shorter than 3 sec. As mentioned earlier, *DL* needs to be expressed as an equivalent load which accounts the damage accumulation due to fluctuating wind loads. Therefore, the choice of ASCE 7-05 as the main reference for *DL* seems to indicate that the error induced from the use of the peak wind pressure as *DL* has been concluded to be negligible, if the load duration is considered as 3 sec.

1.4 Previously conducted full-scale tests

A number of full-scale glass breakage tests have been conducted to understand the general characteristics and behaviour of glass under pressure, to examine factors which affect glass strength, and to develop a glass strength prediction method. Table 1.1 lists the previously conducted full-scale breakage tests, mainly on monolithic glass. In addition to these, extensive full-scale breakage tests on monolithic glass plates and on laminated glass units have been conducted at Texas Tech University. The general observations from these full-scale tests are as follows. First, glass strength is significantly affected by its surface condition (production process, weathering, etc.), edge defects, and support conditions (Abiassi 1981; Norville & Minor 1985; Kawabata 1996; Calderone 1999). Second, static fatigue is observed with different loading patterns and glass types (Abiassi 1981; Kanabolo & Norville 1985; Dalgliesh & Taylor 1990; Calderone 1999). Third, Brown's integral is valid, and n =16 is an acceptable value (Brown 1972; Abiassi 1981; Kanabolo & Norville 1985). Fourth, the modification of Brown's integral (equation (1.2)), which utilizes pressure instead of stress, is appropriate (Dalgliesh & Taylor 1990; Calderone 1999). And fifth, further full-scale tests representing in-service conditions are necessary (Overend et al. 2007a).

As seen in Table 1.1, most of the full-scale tests were conducted by applying ramp and step-up loading pressures, which are probably chosen for their relatively simple test procedures, in view of the available technology. Thus, the confirmation of the theories (3, 4) derived from these tests is valid only for these simplified loading conditions. Also, certain researchers have put forth that a glass plate can be represented

as a statically loaded structure, and dynamic amplification may be neglected since the natural frequency of glass panes is considerably higher than significant wind turbulence frequencies (Allen & Dalgliesh 1973). However, it must be noted that these loading patterns are far-removed from realistic wind loading, which varies significantly in time during windstorms. One notable exception is the work of Calderone (1999), who performed full-scale tests under cyclic loading, which is closer to real windstorm conditions when compared to ramp or step-up loading patterns. In his study, extensive parametric analysis of glass types and geometries, and the validation of a new calculation method of equivalent load were conducted. However, the nature of fluctuating wind loads on glass strength was not the primary focus of the study.

Table 1.1 Summary of previously conducted full-scale glass breakage tests

Author(s) (Year)	Loading type	Support condition	Glass type[4]	Aspect ratio	Glass nominal thickness (mm)	Number of samples
Bowles & Sugarman (1962)	Ramp loading (RL)	Simply-support (SS)	SG, PG	1-8	3.2-9.5	30-40
Miyoshi (1964)	RL, continuously increasing oscillatory loading[5]	SS	SG, PG	1-2	1.9-10	9-12
Ishizaki et al. (1972)	Step-up loading	SS	MO-AN	1.5	8-12	10-45
Abiassi (1981)	RL	SS	WE-MO-AN, MO-AN	1-2.6	2.97-5.56	10-22
Norville & Minor (1985)	RL	SS	MO-AN, WE-IG	1-3.44	5.66-6	16-60
Kanabolo & Norville (1985)	RL	SS	MO-AN	1-2	6.35	12-20
Dalgliesh & Taylor (1990)	RL	SS	MO-AN	1.6	6	21-30
Norville et al. (1991)	RL	SS	NO-FT	1	6.35	26
Norville et al. (1993)	RL	SS	MO-HS, MO-FT, LG-HS, LG-FT	2	6	20-23
Kawabata (1996)	RL	SS	MO-AN	1	6	20
Calderone (1999)	RL, Sinusoidal loading	Edges are assumed to remain in plane	MO-AN, MO-FT, LG-AN, WE-MO-AN	1-5	3-6	5

[4] Note that MO, LG, IG, LA, AN, HS, FT, PG, SG stand for monolithic, laminated, insulating, layered, annealed, heat-strengthened, fully-tempered, plate and sheet glass plate/unit, respectively. WE stands for weathered glass.
[5] This is sinusoidal loading (0.5Hz, amplitude of 30Pa), but its mean pressure increases in the manner of ramp loading.

1.5 Objectives

Through careful consideration of the development of current glass design and related fields, notice was taken of the following issues. First, it is clear that Brown's integral (or the concept of damage accumulation itself) is critical to both *LR* and *DL*. However, based on the extent of the research cited herein, this theory may only be said to have been validated for limited types of pressure loading, which are far removed from realistic wind loads. However, for the time being, most of the related research has been based on the assumption that Brown's integral is valid. Second, presuming that Brown's integral works for any loading type, an equivalent load conversion seems to be an important approach in determining both *LR* and *DL*. This conversion has been used for the calculation of *LR*. Although no explanation is provided, it is unlikely that the drafters of the code used this conversion to calculate *DL*. A conceivable explanation for this choice is that the drafters based their understanding on the work of researchers who presumed the use of peak wind pressure for *DL* as appropriate. However, it is not clear whether the representative storm duration and the appropriate evaluation time of peak pressure, both of which have a considerable effect on an equivalent load, have been sufficiently investigated in these works, even though their importance on load conversion has been commented by several researchers (Dalgliesh 1979; Holmes 1985; Kawabata 1996). Thus, the use of peak wind pressure for *DL* should be re-visited using the appropriate storm duration and evaluation time of peak pressure. Third, although *LR* in ASTM E1300-07 seems taking the appropriate method to calculate, several defects have

been detected by many researchers. Thus, the current approach used to obtain *LR* offers opportunities for improvements of the design methods.

In order to properly address the issues raised above, the necessity of further investigation of glass pane behaviour under fluctuating wind loads by full-scale glass breakage tests becomes apparent. Based on the test results which may validate or nullify the received assumptions, a better modeling method to capture the glass strength is aspired to for *LR*, and the defining characteristics of fluctuating wind loads for the purposes of glass design are identified for *DL*. Based on its findings, this study aims to obtain better glass design methods.

Before delving into the research itself, an in-depth review is conducted of the published literature on *LR*. This is done in order to understand how best to capture the unique characteristics of glass—namely, time-dependent nature of glass strength, and to select the calculation method for *LR*, best-suited to the purpose of the present study (Chapter 2). Based on the understanding of glass strength gained from a summary of the previously-conducted tests (Table 1.1), full-scale glass breakage tests under three different loading patterns are carefully conducted. Their results and the findings obtained through analysis of these data point a path to a new glass design method that is presented in Chapter 3. In Chapter 4, the calculation method for *LR* selected in Chapter 2 is carried out anew and modified in order to arrive at a better agreement with full-scale test results. Based on the findings in these discussions, the current design method used in North America is reassessed in terms of load resistance and design load in Chapter 5.

2.0 Literature review on glass strength model

2.1 Introduction

As was mentioned in Chapter 1, the Glass Failure Prediction Model (GFPM) developed by Beason and Morgan (Beason 1980; Beason & Morgan 1984) is currently used in North America in order to calculate load resistance (*LR*) in glass design. In Europe, the European draft standard prEN 13474 (CEN 1999, 2000) is based on the design method of damage equivalent load and resistance (DELR design method), with the added influence of Shen (1997) and Siebert's (1999) design methods. In addition to the methods utilized in national standards, there have been many other methods which capture the time-dependent glass strength. All of these are based on fracture mechanics, which characterizes a material's resistance to fracture, or in other words, its toughness (Fischer-Cripps 2007). One of the objectives of this study is to obtain the appropriate method to predict *LR* of glass. In order to select the most appropriate method, it is first essential to understand the existing methods as well as the theories used to develop them.

2.2 Linear elastic fracture mechanics

The failure of glass is best understood through linear elastic fracture mechanics, which characterizes the stress state around the crack tip based on the application of linear elastic fracture theory. This means that the theory is valid only when the plastic zone in the material is relatively small (Fischer-Cripps 2007). The fracture of glass is different

from that of other materials since when it is under a constant or variable load for a certain time duration, failure does not necessarily occur at the maximum nominal stress level. This phenomenon is called static fatigue or delayed failure.

The fracture of glass and other brittle materials is usually initiated due to the existing cracks on its surface, where the stress concentration occurs. Two criteria necessary for crack growth to happen were established by Griffith (1921) and Irwin (1957). Although their approaches to define the criteria are different, both are essentially equivalent (Mencik 1992).

On the one hand, Griffith (1921) based his criteria on an energy balance and postulated that crack growth occurs when the strain energy U, which is released as a crack grows, is equal to or greater than the surface energy W required for the creation of a new crack surface A. He expressed this as:

$$\frac{dU}{dA} \geq \frac{dW}{dA} \tag{2.1}$$

Later, this method was modified by Irwin (1948) and Orowan (1952) in order to apply not only to brittle materials but also to ductile ones by introducing the work of plastic deformation. The generalized energy criterion is defined as:

$$G \geq G_C \tag{2.2}$$

where G is called strain energy release rate, which is the amount of supplied elastic strain energy per unit length of crack for creating the new fracture surface and G_C is its critical value. Note that the criteria introduced above automatically results in the instantaneous fracture.

Irwin (1957), on the other hand, approached crack growth in terms of a stress analysis based on concepts of elastic theory and explained that the crack tip stress in the elastically-deformed region is decisive for crack growth in brittle materials. According to this theory, when a glass pane contains only one crack, there are three basic modes of loading corresponding to different forms of crack opening (Figure 2.1):

Mode I - Simple crack opening caused by normal stress perpendicular to the crack plane;

Mode II - Opening by shear stress acting in the crack plane and perpendicular to its leading edge;

Mode III - Opening by shear stress acting in the crack plane and parallel with its front.

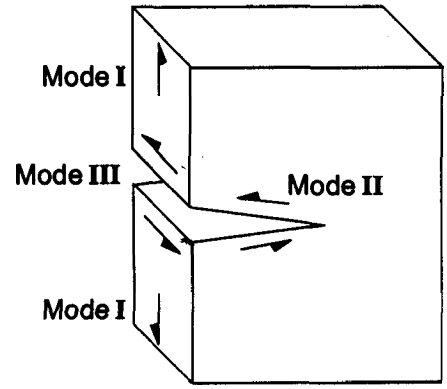

Figure 2.1 Principal modes of crack opening (after Mencik 1992)

Irwin expressed these stresses at the crack tip in the equation:

$$\sigma_{X,ij}(r,\varphi)=\frac{K_X}{\sqrt{2\pi r}}f_{X,ij}(\varphi) \tag{2.3}$$

where r, φ are the coordinates of the point considered, $f_{X,ij}(\varphi)$ is a dimensionless function of the angle between the crack plane and the respective point, X corresponds to mode of crack opening and i, j denote the direction of stress (Figure 2.2).

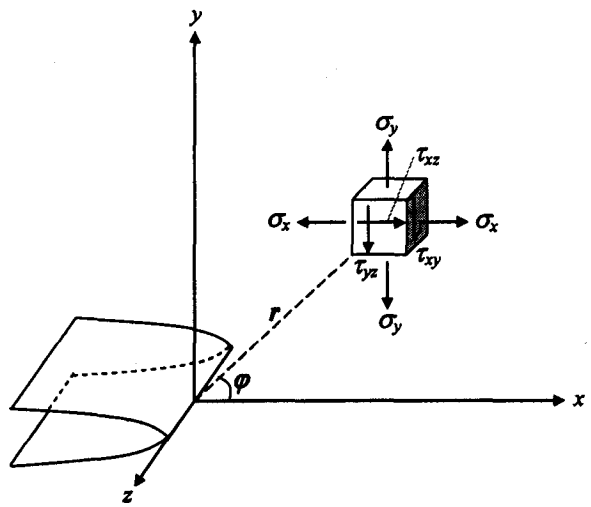

Figure 2.2 Coordinate system and stress components in vicinity of crack tip (after Mencik 1992)

In the case of Mode I, which is dominant in brittle materials, equation (2.3) becomes

$$\sigma_{I,ij}(r,\varphi)=\frac{K_I}{\sqrt{2\pi r}}f_{I,ij}(\varphi) \tag{2.4}$$

In the above equations, Irwin introduced the stress intensity factor K_I, which uniquely characterizes the magnitude of the stress field in the vicinity of the crack. This is defined as:

$$K_I = \sigma_a(t) \cdot Y \cdot \sqrt{c(t)} \tag{2.5}$$

where σ_a is the applied stress at the glass surface of the crack, Y is the geometric shape factor (which is a constant or function characterizing the influence of the body, crack size, shape and the mode of loading), c is crack length and t is time. By introducing K_I, it becomes unnecessary to know the exact information of the crack for the purpose of comparing the different cracked components. Thus, Irwin's criterion for crack growth is expressed in equation form as:

$$K_I \geq K_{IC} \tag{2.6}$$

where K_{IC} is a critical value of K_I, and is different for each material. This value is called fracture toughness and it characterizes the fracture strength.

As Fischer-Cripps (2007) pointed out, the actual fracture depends on the crack stability, and K_{IC} corresponds exclusively to the moment when the rapid crack propagation occurs. When $K_I < K_{IC}$, only slow crack growth in brittle material occurs under loading due to chemical and thermal effects of the environment. This is called subcritical crack growth. At a certain moment, however, the mechanical stress and the released strain elastic energy will overtake the chemical and thermal effects of the environment, and subcritical crack growth will change into rapid crack propagation. Once the rapid crack growth process begins (reaching K_{IC}), propagation becomes unstable and usually causes failure of the material.

Experiments on various brittle materials have shown that a limit exists in K_I, where subcritical crack growth does not occur no matter how long a load is applied. This is called the static fatigue limit (K_{ISCC}), which is the lower limit of subcritical crack

growth. K_{ISCC} varies depending on the material, and its values have been reported. For example, Wiederhorn and Bolz (1970) obtained around 0.25 ($MPa\sqrt{m}$) for soda-lime silicate glass (25° C, water), and Dauskardt (1993) obtained 2.5 and 4($MPa\sqrt{m}$) for alumina (1700° C, vacuum) and β silicon nitride (1700° C, nitrogen), respectively.

2.3 Summary of the previous studies

Based on the two criteria of crack growth, many researchers tried to explain the static fatigue of glass and to suggest a suitable method of predicting the time-dependent glass strength. There are two major approaches for this; namely, the stress corrosion theory, which tries to explain the crack growth physically, and another, which aims to describe the crack velocity and stress intensity factor relationship by using an empirical mathematical model. But before delving further into these theories, we must take account of Weibull's contribution, upon which much of the subsequent work is based.

In 1939, Weibull (1939) proposed the relationship between instantaneous failure probability and the strength of a material, expressing it as:

$$P_f = 1 - \exp\left[-kA\sigma_a{}^m\right] \tag{2.7}$$

where k and m are a measure of the location and dispersion of a surface crack, respectively, and A is the glass plate surface area upon which the applied stress σ_a is acting. The variables k and m cannot be estimated, but rather must be determined by tests. Since k and m represent the surface crack characteristics, it is important that these values be obtained in conditions as close as possible to the "in-service condition".

Furthermore, they must be obtained in the use of loading that will prevent subcritical crack growth (inert condition), which would otherwise influence surface crack coefficients. Table 2.1 lists the surface crack coefficients (k, m) obtained by different researchers. The fact that these values tend to vary significantly is possibly due to the characteristics of the surface cracks, which can be altered by the test conditions and environment.

Table 2.1 Surface crack coefficients

		m	k
Brown (1974)	As-received glass	7.3	5.10×10^{-57} ($m^{-2}Pa^{-7.3}$)
Beason (1980)	Weathered glass	6	7.19×10^{-45} ($m^{-2}Pa^{-6}$)
Beason & Morgan (1984)	As-received glass	9	1.32×10^{-69} ($m^{-2}Pa^{-9}$)
	Weathered glass	6	6.63×10^{-45} ($m^{-2}Pa^{-6}$)
	Weathered glass	6	3.01×10^{-45} ($m^{-2}Pa^{-6}$)
	Weathered glass	5	9.60×10^{-38} ($m^{-2}Pa^{-5}$)
ASTM E 1300 (2007)	Weathered glass	7	$2.86\ 10^{-53}$ ($m^{-2}Pa^{-7}$)

2.3.1 Stress corrosion theory

The stress corrosion theory proposes that the delayed failure of glass is brought about by a mechanics of differential crack growth caused by stress-activated corrosion due to water vapour. This theory was originally proposed by Charles (1958a, 1958b), who expressed the penetration velocity of a crack based on the experimental results as:

$$v = \frac{\delta c}{\delta t} = k' \cdot (\sigma_m)^n + k'' \tag{2.8}$$

where σ_m is tensile stress at the crack tip and k', k'' and n are constant.

Incorporating equation (2.8) with Inglis' stress concentration relationship (Inglis 1913) and the failure criteria for crack growth based on energy considerations, a model describing a failure process due to water vapour for both static and dynamic fatigue is introduced as:

$$\frac{\delta c}{\delta t} = k''' \cdot \sigma_m^n \cdot e^{-\frac{\gamma_0}{R' \cdot T}} \tag{2.9}$$

where R' is a universal gas constant, T is temperature, and γ_0 and k''' are constant. The value n was obtained experimentally and n =16 has been generally accepted for soda-lime silicate glass (Charles 1958b; Brown 1972). However, Charles (1958c) has remarked that the value of n depends only on the characteristics of the material and its environment, and is independent of the specific form of the stress concentration relationship which is applicable to glass failure. What equation (2.9) means is that when a crack grows to critical dimensions under the action of an atmosphere of water vapour, the rate of approach to this critical dimension is proportional to the 16^{th} power of the crack tip stress. In order to verify this equation, Charles conducted tests using exclusively constant and ramp loadings. He subsequently stated in his paper that "Any analytical model which successfully described static fatigue could also describe dynamic fatigue (Charles 1958c)". Furthermore, Charles and Hillig (1962, 1965) considered the time dependence of crack geometry due to stress corrosion by introducing the differential equation of approximate stress concentration factor. This equation enables us to clarify the relationship of the physical situation of glass strength to the corresponding crack geometry.

Brown (1972, 1974) extended the stress corrosion theory proposed by Charles, and included the relative humidity effect for soda-lime silicate glass suggested by Wiederhorn (1967). Brown's integral, which has been utilized as a basis of much subsequent research, is part of his Load Duration Theory proposed that year. The ultimately obtained equation is as follows:

$$\int RH \cdot e^{-\gamma_0/R \cdot T} \cdot \left(\frac{\sigma_a(t)}{T}\right)^n dt \cong const \tag{2.10}$$

where RH is relative humidity. Hence, at a constant temperature and relative humidity, equation (2.10) becomes

$$DA_{crit} = \int_0^{t_f} [\sigma_a(t)]^n dt \tag{1.1}$$

Essentially, Brown's integral postulates that the cumulative effect of arbitrary time-dependent stress, $\sigma_a(t)$, applied to a specimen until failure at time, t_f, is constant at the location where breakage is initiated. This value remains "constant" only for the same glass geometry (size, thickness) and glass type (annealed, heat-strengthened, etc). Note that σ_a needs to be in tension to cause the crack growth in equation (1.1). When an arbitrary loading $\sigma_a(t)$ is expressed as a linearly-increasing stress loading, $\sigma_a(t)=\beta \cdot t$, the following relationship should be attained using equation (1.1):

$$\sigma_f \approx \beta^{\frac{1}{n+1}} \tag{2.11}$$

where β is stress loading rate and σ_f is failure stress. As a verification of Brown's integral, the relationship shown in equation (2.11) was proved to be true using the ramp

loading test results with three different ramp loading rates (1, 10, 800 lb/in^2) obtained by Kropschott & Mikesell (1957). However, it should be noted that Brown proved the suitability of his equation by experiment only for constant loading and ramp loading.

Incorporating equations (2.7) and (2.10) leads to the generalized failure probability relationship for uniformly loaded rectangular plates, considering the effects of plate geometry, area, load duration, relative humidity and temperature:

$$P_f = 1 - \exp\left[C'\left(\frac{A}{A_o}\right)\{E^{n-s}\cdot\left(\frac{a}{h}\right)^{4s-2n}\int_o^{t_f}\frac{RH\cdot e^{-\gamma_0/R\cdot T}}{T^n}p^s dt\}^{\frac{m}{n+1}}\right] \tag{2.12}$$

where A_0 is reference area, C' is combined constant for square plate, E is Young's modulus, a is the plate width, and h is its thickness. Brown subsequently pointed out that the defect of this method is its inapplicability to cases of very long, time-delayed failures.

In equation (2.12), the following relationship between normalized stress at the surface σ_a and uniform pressure p is employed in the equation above:

$$\sigma_a/E(a/h)^2 \approx B\left[p/E(a/h)^4\right]^{s/n} \tag{2.13}$$

where B and s are constants dependent on edge restraint and plate shape. Based on the relationship of equations (1.1) and (2.13), a simplified form of Brown's integral is obtained as:

$$DA_{crit} = \int_0^{t_f}[p(t)]^s dt \tag{1.2}$$

Equation (1.2) represents the damage accumulation using an applied load as a function of time $p(t)$ instead of stress at the critical crack as a function of time. Brown obtained coefficient s as 12.3 from the full-scale tests of Bowles and Sugarman (1962). However,

since the relationship between p and σ_a differs at varying locations on the plate, a single value for s should not be assigned to the entire surface of a relatively large glass plate. Several researchers supported a modified form of Brown's integral and obtained the ranges of the coefficient, s depending on the parameters (glass plate geometry, glass type, etc) which affect the p-σ_a relationship (Allen & Dalgliesh 1973; Dalgliesh 1979; Dalgliesh & Taylor 1990; Calderone 1999).

Beason and Morgan (Beason 1980; Beason & Morgan 1984) extended Brown's Load Duration Theory, and combined it with a non-linear stress analysis. This so-called Glass Failure Prediction Model (GFPM) is superior to the Load Duration Theory in that it can handle a wider range of loadings and plate geometries. As a result, it has been utilized in North American design standards. In this method, an equivalent 60-sec constant stress is used to calculate the probability of failure and is expressed as:

$$\sigma_{60} = \left[\int_0^{t_f} \sigma_a{}^n(t)dt \Big/ 60 \right]^{1/n} \tag{2.14}$$

The probability of failure can be obtained from equations (2.7) and (2.14) with the two interdependent surface crack coefficients m and k. Although the general procedure to obtain failure probability in GFPM and Load Duration Theory is the same, they differ significantly. Namely, as mentioned above, equation (2.7) predicts the *instantaneous* failure probability. In order to use equation (2.7), Brown converted time-varying stress into rapid ramp stress using damage accumulation. Beason, however, used the equivalent 60-sec constant stress in equation (2.7), which can hardly be recognized as instantaneous. Therefore, GFPM ignores the effects of any stress corrosion which may occur within 60

sec of failure (Fisher-Cripps & Collins 1995). Current ASTM E 1300-07 utilizes reference load duration of 3 sec instead of 60 sec for NFL calculated by GFPM. Since the load duration is shortened to 3 sec, this effect should become insignificant. However, the detailed explanation of how this change of reference load duration was implemented in the calculation of GFPM in the recent standard has not been found by the author. Reid (1991) uncovered a further apparent defects in the GFPM, which are about the modelling of the time-dependence nature of glass strength and the surface crack coefficient, m. In addition, since the two interdependent surface crack coefficients, m and k, are impossible to directly measure, they are estimated from visual determination of critical crack location of glass plates broken in tests and by repeating a complex iterative process (Haldimann et al. 2008). Since this process is in practice quite clumsy and results tend to vary significantly, only one representative value for each m and k, which represent the surface strength of weathered glass, is given in ASTM E 1300-07 and CAN/CGSB-12.20-M89.

Ishizaki et al. (1972, 1975) studied the cumulative effect of fatigue caused by fluctuating wind, based on the stress corrosion theory, but without using Brown's integral. In their research, an empirical formula widely used in Japan was modified to contain the load duration effect as:

$$p(t_f) = f' B' \frac{h}{a}\left(1 + 70\frac{h}{b}\log_{10}\frac{10^7}{t_f}\right) \tag{2.15}$$

where f' is the strength factor, B' is constant, a and b are lengths of the glass plate. The cumulative effect of wind loading was calculated with the idea of the relative remaining

strength suggested by Shand (1954). It was concluded that high peak wind pressure is dominant in glass plate failure, and that the cumulative effect of wind pressures lower than the peak is about 10 % in total.

2.3.2 Empirical mathematical model of crack growth

In contrast to the stress corrosion theory, many researchers have described crack growth using an empirical mathematical equation of crack velocity, i.e., the rate of sub-critical crack growth on a glass plate, which has been developed using crack velocity data. The following equation is generally accepted (Paris & Erdogan 1963):

$$v = \frac{\delta c}{\delta t} = A'' \cdot K_I^{n'}(t) \tag{2.16}$$

where A'' and n' are constants which depend on the environment (surrounding gas, temperature, humidity, ph) (Reed 1993; Dill et al. 1997; Haldimann 2006), loading rate (Haldimann 2006) and materials (Evans & Wiederhorn 1974; Dill et al. 1997). n' generally displays a value between 15 to 50 for glass (Evans & Wiederhorn 1974).

According to equation (2.16), the relationship between the stress intensity factor K_I and crack velocity v has three distinct regions as shown in Figure 2.3. According to Evans (1974), the rate of reaction at the crack tip in region I controls crack motion and a general relationship of $v \propto \exp(\gamma' \cdot K)$ emerges where γ' is constant. In region II, the crack velocity is essentially constant and crack motion is controlled by diffusion of the corrosive species. In region III, the crack velocity increases very rapidly with an increase

in K_I, and therefore it is reasonable to consider that rapid crack propagation begins at the end of region II.

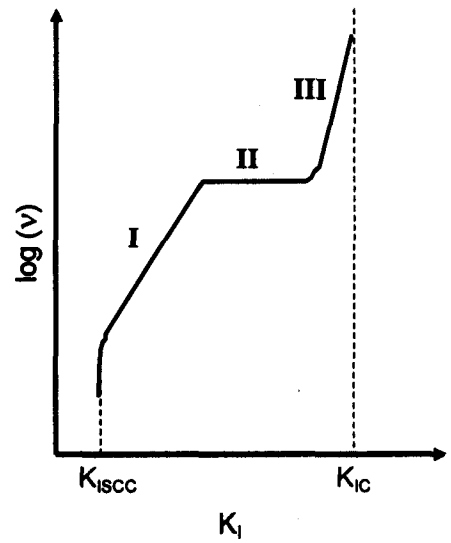

Figure 2.3 A schematic representation of a typical K_I-v curve (Fischer-Cripps 2007)

The relationship between K_I and σ_a is expressed as equation (2.5). Using equations (2.5) and (2.16), the basic relation between stress action and crack growth is obtained as:

$$\int_0^{t_f} {\sigma_a}^{n'}(t) = \frac{2}{(n'-2)A''Y^{n'}}\left[\left(\frac{1}{c_i}\right)^{(n'-2)/2} - \left(\frac{1}{c}\right)^{(n'-2)/2}\right] \tag{2.17}$$

where c_i is the initial crack length. By employing coefficients unique for glass (A'', n', Y) and c_i, equation (2.17) makes it possible to determine the time at which a crack reaches its critical value t_f. This equation has been adopted by many researchers with some modifications and additional assumptions, as explained below.

Wiederhorn and Evans (Wiederhorn 1974; Evans & Wiederhorn 1974) suggested a method based on fracture mechanics and the proof test results. This is the so-called "Crack Growth Model (CGM)", which combines equations (2.7) and (2.17) using linear elastic fracture mechanics. According to this method, the minimum time to failure under constant stress σ_a is expressed as:

$$t_f = \frac{2}{(n'-2)A''\cdot Y^2\cdot \sigma_a{}^2}\left(\frac{K_{IC}\cdot\sigma_a}{\sigma_P}\right)^{2-n'} \tag{2.18}$$

where σ_P is the proof stress. Rapid loading proof tests and constant load proof tests were carried out as verification of this prediction method. In both cases, they found that the measured time lies above the predicted failure time using equation (2.18), meaning that the predictions are conservative. However, if the comparison is made on a probability basis, the accuracy of prediction at the probability of weakest specimen is good. Fischer-Cripps and Collins (1995) subsequently commented that this method ignores the static fatigue limit K_{ISCC}, and suggested the Modified Crack Growth Model. Further, Overend (2002) and Overend et al. (2007b) extended this method by covering the variation of the principal stress ratio on a plate and made it possible to apply for heat strengthened and fully tempered glass. This is called the General Crack Growth Model and its verification was made by comparing results from ring-on-ring tests and full-scale ramp loading test. However, this is applicable only to monotonically-increasing loads (Haldimann 2006).

Evans and Fuller (1974) expanded the CGM in order to predict failure time under cyclic loading utilizing proof test results. Based on equation (2.17), the predicted failure

time of cyclic loading, t_{cyclic}, characterized by the average stress, σ_{ave}, the amplitude, σ_0, and the period of cycle, λ, is obtained as:

$$t_{cyclic} \cong t_{const} \cdot (\sigma_{const}/\sigma_{ave})^{n'} \cdot g(n', \xi)^{-1} \tag{2.19}$$

where t_{const} is the failure time under constant loading, σ_{const} is the applied constant stress, ξ is the ratio of amplitude of cyclic loading ($\xi = \sigma_0 / \sigma_{ave}$), and $g(n', \xi)$ is the dimensionless damage function which is expressed as:

$$g(n', \xi) = \frac{1}{\lambda} \int_0^{\lambda} [\sigma_a(t)/\sigma_{ave}]^{n'} dt \tag{2.20}$$

where $\sigma_a(t)$ is the applied stress time history of cyclic loading. $g(n', \xi)$ is quite useful to examine the strength reduction in glass in relation to the stress amplitude - average stress ratio, ξ, and as a consequence this formulation has been utilized by many researchers (Mencik 1992; Reed 1993).

Simiu and Reed (1983, 1984), differently from others, conducted numerical simulations of glass panel failures. Equation (2.17) is used for the time-dependent strength of glass in their simulation, and is expressed as:

$$S(M_j, \alpha_k, t) = \left[S_i (M_j, \alpha_k)^{n'-2} - \frac{n'-2}{2} A'' Y^2 K_{IC}^{n'-2} \int_0^{t_f} \sigma_a^{n'}(M_j, \alpha_k, t) dt \right]^{\frac{1}{n'-2}} \tag{2.21}$$

where S_i (M_j, α_k) is the initial strength and M_j is a location of an element on glass surface which contains a crack oriented normal to α_k. The Monte-Carlo technique is used to generate fluctuating wind load time history based on statistical data (spectral information or longitudinal fluctuating components of wind speed) and the initial glass strength,

which randomizes the occurrence of glass failure. Given the strength time history, $S(t)$, and the induced stress time history, $\sigma_a(t)$, failure is identified when:

$$\sigma_a(t) \geq S(t) \tag{2.22}$$

The benefit of this method is that it requires a relatively small glass specimen to obtain the basic information for glass initial strength (ring-on-ring test). As a result, it is possible to conduct the glass panel failure simulation under fluctuating wind condition properly and with relative ease. Furthermore, the validity of this numerical simulation under ramp loading was proven experimentally by Kawabata (1996) who conducted full-scale glass breakage tests using monolithic annealed glass plates.

Kawabata (1996) also advanced Simiu and Reed's method by utilizing the actual time history of wind loading from wind tunnel tests instead of simulated wind loading. In addition, the following relationship was obtained by assuming that the relationship of equation (2.17) holds for the applied pressure:

$$DA_{crit} = \int_0^{t_f} [p(t)]^{m'} dt \tag{2.23}$$

where m' of 10 -11 was found from the numerical simulation results, which considers the random failure locations/directions. It is interesting to note that this equation has basically the same meaning as Brown's integral (equation (1.1)), and a modification of Brown's integral (equation (1.2)), but its derivation is altogether different. Moreover, Kawabata confirmed that the value of m' is constant, regardless the glass geometry at least among the glass specimens used in his experiments, which is a different observation from others (Brown 1974; Dalgliesh & Taylor 1990; Calderone 1999).

More recently, Haldimann (2006) established a Lifetime Prediction Model for structural glass elements based on fracture mechanics and probability theory. Using equation (2.17), the time-dependent failure probability of a general glass element was established with cautious consideration of important aspect for glass design (surface condition, crack growth condition, K_{ISCC}, etc), which are sometimes ambiguous in other methods. The comparisons between predicted failure probability and full-scale ramp loading test results (Johar 1981, 1982) were shown as the validity of model.

2.4 Summary and conclusions

There are two main theories to deal with the time-dependent glass strength, both of which originated from fracture mechanics and, interestingly, reached the similar concept of damage accumulation. This can be seen in equations (1.1) and (2.17). Bearing in mind that these two theories both arrived at the same concept, the parameters on which the value of n (or n') and the critical damage accumulation seems to be mainly dependent are material and environment. However, other parameters such as loading rate (Haldimann 2006), glass type (Abbiassi 1981), glass geometry, and boundary stiffness (Daligliesh 1979) are also mentioned as possibilities. Through this literature review, it also becomes clear that most of the suggested methods are using equation (1.1) or the idea of damage accumulation assuming that they are valid for any type of loading. However, these suggested methods have not been experimentally validated, and if they have, then only for simplified loading patterns or for small specimen sizes.

It is not the purpose of this chapter to judge which method is superior to the other, but the numerical simulation of glass panel failures originally suggested by Simiu and Reed and modified by Kawabata appears to be the best for the purposes of present study, based on the following reasons. First, it is likely to be applicable to any type of loading patterns. Second, this method has been validated by full-scale glass breakage tests. Third, not only the failure probability, but various information regarding a glass panel failure which are helpful to analyse failure mechanics in detail and are easily compared with full-scale glass breakage test results, e.g., failure pressure, time, stress, location and direction of critical crack, etc. can be obtained.

3.0 Full-scale testing

3.1 Test methodology

3.1.1 Experimental setup

Full-scale glass breakage tests were conducted at the Boundary Layer Wind Tunnel Laboratory of the University of Western Ontario. The glass specimens used in all of the tests are of the same geometry (1 x 1 x 0.006 m) and glass type (monolithic annealed, soda-lime silicate glass plate). This geometry and glass type were chosen because they have been used in previously conducted tests by other researchers. In order to reduce the variation in glass strength, all glass specimens were purchased from the same supplier, and were transported and stored before testing with methods, and in conditions, as similar as possible. A minimum of twenty glass specimens were broken in each test series in order to achieve a balance between statistically-reliable data and a reasonable amount of testing time, consistent with the recommendation of Dalgliesh and Taylor (1990) (Note that one test configuration used for the verification of methodology has only fifteen glass specimens). In addition, the temperature and humidity were relatively well controlled in this lab and these variables were recorded in each test.

In advance of the tests, all glass specimens were examined by exposing them to ultraviolet radiation in order to determine the 'air' and 'tin' sides. The tin side of the glass plate was always oriented towards the inside of the pressure box, so that negative pressure (suction) was applied to this side, resulting in the least favourable condition for

the plate (Kanabolo & Norville 1985). Also, the thickness of each plate was measured after each test for the record and in order to ensure that it conformed to the dimensional tolerance for a nominal 6 mm glass plate defined in ASTM C 1036-01 (2001), which is 5.56 to 6.2 mm.

Pressure Loading Actuators (PLAs), specifically developed for the "Three Little Pigs" Project at the University of Western Ontario, were employed to apply the pressure loading. This device is able to replicate realistic wind induced pressure traces as well as static (step-up), ramp and cyclic loading patterns. For details, the reader is referred to Kopp et al. (2008).

Each glass specimen was mounted in a pressure box, shown in Figure 3.1, constructed primarily from steel. On the front face of this box, a plywood panel fastened with several bolts acts as the support for the aluminum frames which hold the glass specimen in place. The glass specimen itself is directly supported by rubber tubes affixed to the aluminum frames in order to create a simply-support boundary condition. Further details concerning the pressure box can be found in Appendix A.

The hose from the PLA is connected to the side of the pressure box, allowing both positive and negative (suction) pressures to be applied inside the pressure box. Note that only negative pressures were applied for the tests in question, for safety reasons.

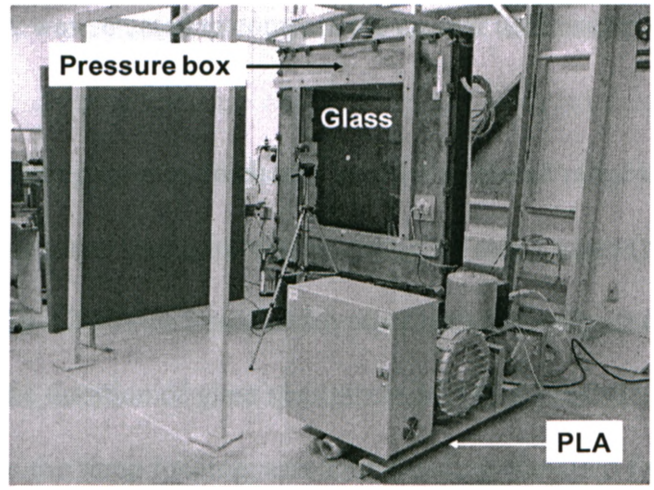

Figure 3.1 Pressure box with PLA

It is quite possible that the differences in physical conditions, at manufacture and in handling, between batches of glass are significant, and that this can cause significant variations in the initial strength based on the preliminary tests (refer to Appendix B for details). Therefore, in order to ensure that the variations of initial glass strength are randomly distributed, the testing of each specimen within the various configurations, was conducted in a randomized order. Testing was repeated until twenty pieces of glass plate were tested for each configuration.

3.1.2 Test configurations

Table 3.1 lists a summary of the test configurations in the present study. Three types of pressure trace were applied, viz., ramp, saw-tooth and realistic fluctuating loads.

Ramp loading 0, R0, was selected to compare the current test results with those of Kawabata (1996).

Two ramp loading rates were chosen in order to span a range of failure times, from 60 sec, which is a load duration reference time for many years (prior to ASTM E 1300-02; CAN/CGSB-12.20), to 3 sec, which represents typical gust durations, and is the current reference time duration of glass strength in ASTM E 1300-07.

In addition to the ramp loading, saw-tooth loading was used for the following reasons. First, saw-tooth loading creates a situation in some ways similar to realistic wind loading but which also retains some similarity to ramp loading, so that the effects due to constrained loading amplitude are characterized. Second, it is possible to decide the pressure level (amplitude) of saw-tooth loading with a certain probability of glass failure in the first cycle based on the results obtained from ramp loading tests. Third, a possible model for realistic fluctuating load is a combination of pulses, which is similar to saw-tooth loading but each pulse with different loading rates and amplitudes.

Regarding the choice of saw-tooth loading configuration, it is known that loading rate has a significant impact on the strength of glass under ramp loading (Brown 1972; Ishizaki et al. 1972; Kanabolo & Norville 1985; Dalgliesh & Taylor 1990), so this must also apply to saw-tooth and realistic wind loads. One of the large differences between ramp loading and saw-tooth loading is that the applied pressure is constrained at a certain maximum or minimum pressure level and, this pressure range has a notable effect on damage accumulation when one considers Brown's integral, i.e., the larger the applied pressure, the more it contributes to the damage accumulation, thereby causing earlier

failure. Hence, these two items needed to be investigated in the saw-tooth loading tests. Three configurations were selected to cover two variations on each item, which are loading rates of 6500 Pa/sec and 230 Pa/sec, with 14.9 kPa and 12.5 kPa for the maximum pressure amplitude. As for the amplitude, it is undesirable to have too many failures in the first cycle, but it is equally undesirable to define too small amplitude which would result in glass plates breaking only after excessive testing time. Hence, the pressure close to the minimum failure pressure of R2 (14.9 kPa) was selected after several trials with different amplitudes. At this pressure the cumulative distribution function (CDF) of the loading rate of 6500 Pa/sec is roughly equal to 0.26 based on the results of R2. For the second amplitude choice, a maximum amplitude larger than 14.9 kPa was rejected in order to avoid more failures in the first cycle. We chose 12.5 kPa so that 2.4 kPa difference would result in a large enough difference to see the effect, but not to cause a significantly longer time duration until failure (12.5 kPa corresponds to CDF of 0.4 and 0.1 of the loading rate of 230 Pa/esc and 6500 Pa/sec, respectively, based on the ramp loading test results).

Table 3.1 Summary of load configurations

Configuration label	Loading rate (Pa/sec)	Pressure range (kPa)
Ramp loading 0 (R0)	16.4	n/a
Ramp loading 1 (R1)	230	n/a
Ramp loading 2 (R2)	6500	n/a
Saw-tooth loading 1 (S1)	6500	0 ~ 14.9 ~ 0
Saw-tooth loading 2 (S2)	6500	0 ~ 12.5 ~ 0
Saw-tooth loading 3 (S3)	230	0 ~ 12.5 ~ 0
Fluctuating loading 1 (F1)	Scaled up wall pressure trace	

Figure 3.2 shows the time history of the pressure applied to a glass plate by the PLA under S2. In the figure "Demand" and "Achieved" represent the pressure trace which the PLA is asked to apply and the pressure history which the PLA actually replicates, respectively. As can be observed, the two traces overlap almost perfectly. In this particular example, the glass plate broke after two hours without any pauses to the load application. The graph makes it quite apparent just how accurately the PLA can apply loading, even over such long durations.

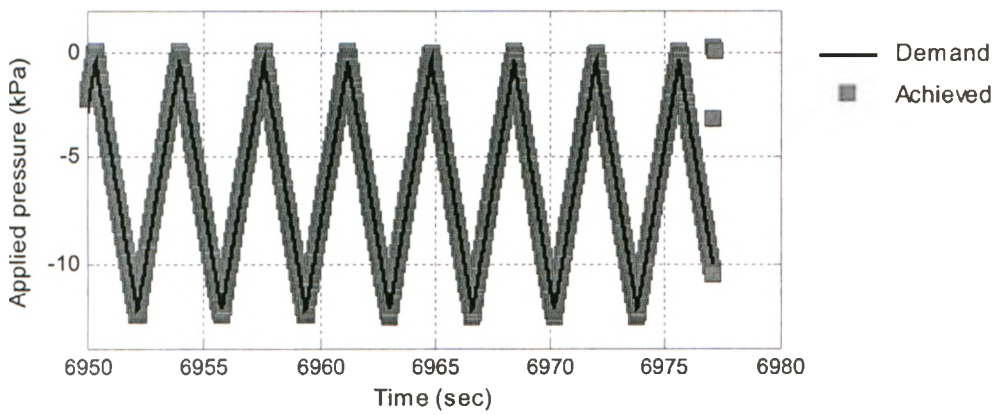

Figure 3.2 PLA pressure trace for S2

For fluctuating load, wind tunnel measured pressure traces from the wall of a 1:50 two-story house model—explained in detail in Kopp et al. (2008)—were used. The area averaged pressure coefficient referenced to the model roof height, $C_{p\_area\_averaged}$, whose tributary area is the same as the test glass specimen in full-scale ($1m^2$) on the windward wall, was calculated over its entire wall area, and the location which experiences the largest $C_{p\_area\_averaged}$ was selected. In order to convert from $C_{p\_area\_averaged}$ to area averaged pressure in full-scale, the time scale and pressure scale for a 150 mph 3-sec gust

speed were selected to create category 5 hurricane conditions. However, the pressure scale was adjusted upwards in order to obtain sufficient loads to fail the 6 mm annealed glass plate. Thus, this time history has realistic spectral content, but should not be considered to be directly to the house's wind loads. Out of the whole length of the trace, a 6-min portion in full-scale containing three significant peaks was chosen, and was repeated continuously until failure. This loading pattern is called F1 in this study (Figure 1.1).

3.1.3 Verification of test rig

Figure 3.3 shows the comparison in CDF of failure pressure between the present test results (R0) and those of Kawabata (1996), who used the same ramp loading with the same size and type of glass. Here, "*F*" stands for the CDF of failure pressure expressed as $F=i/(N+1)$, where i is the rank of specimen when they are in ascendant order and N is the total number of specimens. Even though the number of glass specimens in the present test is fifteen, compared to Kawabata's twenty, the present test results correspond quite well, implying that the current setup is appropriate to conduct further tests.

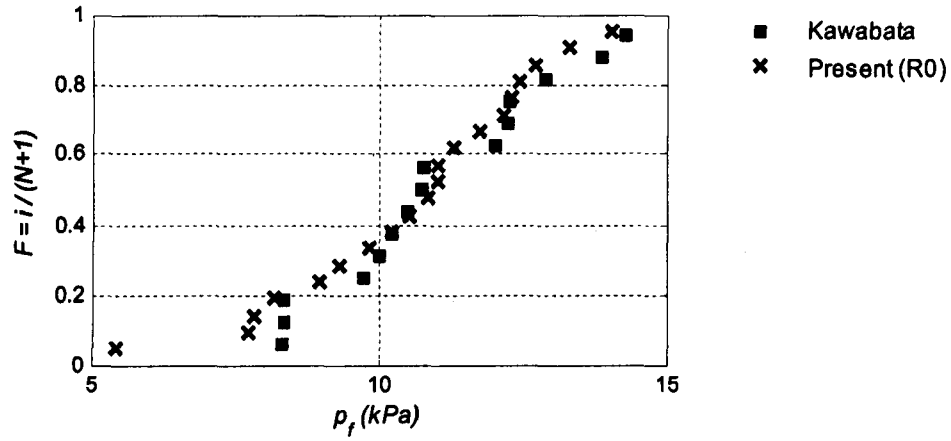

Figure 3.3 Comparison between present and Kawabata's test results

3.2 General test results

Table 3.2 gives some of the basic statistics for all test results; Appendix C provides further details. By way of explanation, failure pressure, p_f, is the pressure applied at the moment of failure, as measured by a pressure transducer attached to the pressure box. Failure time, t_f, is the time duration recorded from the instant the PLA begins to apply pressure until the moment of failure. The symbols, $-$, $\cap$, $\cup$, $\sim$ denote simple mean, maximum, minimum and standard deviation, respectively. The testing environment (temperature and humidity) were steady while the tests were conducted. The coefficient of variation of the test results (p_{f_cov}, t_{f_cov}) for ramp loading is in the range 0.20~0.24, which falls within of those from previously conducted tests (e.g., 0.17~0.24 from Johar 1982), and also from the known variation of glass strength, namely 0.2 ~ 0.25 (Dalgliesh & Taylor 1990). This indicates that the repeatability of the tests is

reasonable and consistent with previously published research, and, as well, that the results are statistically reliable.

Interestingly, one of the plates in both the S3 and F1 series did not break after 20 hours of load application. Since 20 hours duration is longer than most windstorms at a particular location, the test was terminated without glass failure and this result is excluded from the statistics in Table 3.2 and set to the largest failure time when F is calculated, as discussed further below.

Although the testing environment (temperature and humidity) was similar for all tests, the failure pressure and failure time statistics in saw-tooth fluctuating loads show quite distinct results when compared to those from the ramp loading tests. Whereas the variation of the failure pressure becomes smaller, the variation of the failure time becomes much larger for the saw-tooth and fluctuating load tests, as might be expected.

Table 3.2 Statistics from the current tests

		R1	R2	F1
Loading rate	(Pa/sec)	230	6500	n/a
Pressure range	(kPa)	n/a	n/a	1.77 to 16.46
Temperature range	(° C)	19 – 23	18 – 23	19 - 24
Humidity range	(%)	45 - 75	49 – 73	44 – 72.5
$\bar{p}_f$	(kPa)	13.6	17.2	12.74
$\hat{p}_f$	(kPa)	19.2	24.6	16.82
$\breve{p}_f$	(kPa)	8.6	9.7	10.04
$\tilde{p}_f$	(kPa)	3.2	3.5	2.13
p_{f_cov}	(-)	0.24	0.20	0.17
$\bar{t}_f$	(sec)	58.9	2.6	2227.24
$\hat{t}_f$	(sec)	83.7	4.1	37480
$\breve{t}_f$	(sec)	37.5	1.4	7.71
$\tilde{t}_f$	(sec)	14.0	0.59	8547.77
t_{f_cov}	(-)	0.24	0.22	3.84
		S1	S2	S3
Loading rate	(Pa/sec)	6500	6500	230
Pressure range	(kPa)	0 to 14.9 to 0	0 to 12.5 to 0	0 to 12.5 to 0
Temperature range	(° C)	19 - 23	18 - 24	18.5 - 24
Humidity range	(%)	49 – 75	46 - 75	45 - 75
$\bar{p}_f$	(kPa)	13.4	12.0	11.5
$\hat{p}_f$	(kPa)	15.0	13.1	12.5
$\breve{p}_f$	(kPa)	11.6	10.5	9.4
$\tilde{p}_f$	(kPa)	1.1	0.85	1.0
p_{f_cov}	(-)	0.08	0.07	0.09
$\bar{t}_f$	(sec)	695	958	2440
$\hat{t}_f$	(sec)	7530	6977	23072
$\breve{t}_f$	(sec)	1.6	1.6	40.2
$\tilde{t}_f$	(sec)	1749	2085	5542
t_{f_cov}	(-)	2.5	2.2	2.3
Number of cycles	(-)	1 - 1711	1 - 1936	1 - 672

3.3 Discussion

3.3.1 Validity of Brown's integral

Brown's integral, and its modification, have been widely used for both the load resistance (*LR*) and the design load (*DL*) for glass design:

$$DA_{crit} = \int_0^{t_f} [\sigma_a(t)]^n dt \tag{1.1}$$

$$DA_{crit} = \int_0^{t_f} [p(t)]^s dt \tag{1.2}$$

As mentioned in Chapter 1, equations (1.1) and (1.2) have been validated only for limited loading cases. Since the current study examined full-scale glass specimens both under saw-tooth loading with several different parameters as well as fluctuating wind load, the validity of the relationship is re-examined herein among the same glass type and geometry.

Since the magnitude of damage accumulation becomes too large to evaluate with ease, this figure was converted into an equivalent load, which is historically used to examine load resistance capacities (i.e., the critical damage accumulation), to simplify the comparison (Holmes 1985; Kanabolo & Norville 1985; Reed 1993; Li et al. 1999; Ko et al. 2005). Thus, a reference time of 3 sec was selected for this study.

3.3.1.1 Brown's integral coefficient *n*

With respect to the coefficient *n*, a value of 16 for soda-lime silicate glass has been generally accepted by many researchers regardless of the other contributing factors

mentioned in Chapter 2 (e.g. environment, etc), and hence, this value was used for the purposes of the present study. On the other hand, the value of s is known to vary depending on glass type, glass geometry, critical crack location as well as other factors (Allen & Dalgliesh 1973, 12; Brown 1974, 12.3; Dalgliesh 1979, 10~20; Davenport 1983, 15; Dalgliesh & Taylor 1990, 13.6~16.2; Kawabata 1996, 10~11; Calderone 1999, 4.8~20.9). Thus, it was necessary to determine s from the current test results. From equation (1.2), the following two equations are obtained for the case of ramp loading:

$$p_{f,1}/p_{f,2} = (p'_1/p'_2)^{\frac{1}{s+1}} \tag{3.1}$$

$$p_{f,1}/p_{f,2} = (t_{f,2}/t_{f,1})^{\frac{1}{s}} \tag{3.2}$$

One is the relationship between failure pressure, p_f, and loading rate, p', while the other is the relationship between failure pressure and failure time, t_f (Dalgliesh & Taylor 1990; Kawabata 1996; Calderone 1999). In the case of saw-tooth, since it is difficult to obtain a simple converted equation as in the above example, the same value for s, obtained from the ramp loading results, is used. Figure 3.4 shows the relationship of equations (3.1) and (3.2), using the simple mean value, $\bar{p}_f$, within the context of the current ramp load test results, and the coefficient s for both cases was obtained to be about 13. Two loading cases are not likely to be sufficient to determine the coefficient s statistically, and when compared to the approach taken by other researchers (5-7 different loading cases were used according to Brown 1974; Dalgliesh & Taylor 1990; Kawabata 1996). However, the purpose of this calculation is not to determine an accurate value for the coefficient s, but rather to calculate the equivalent load, and the obtained value s =13 seems

appropriate when compared with values obtained by other researchers. For these reasons, s =13 will be used for the discussion below.

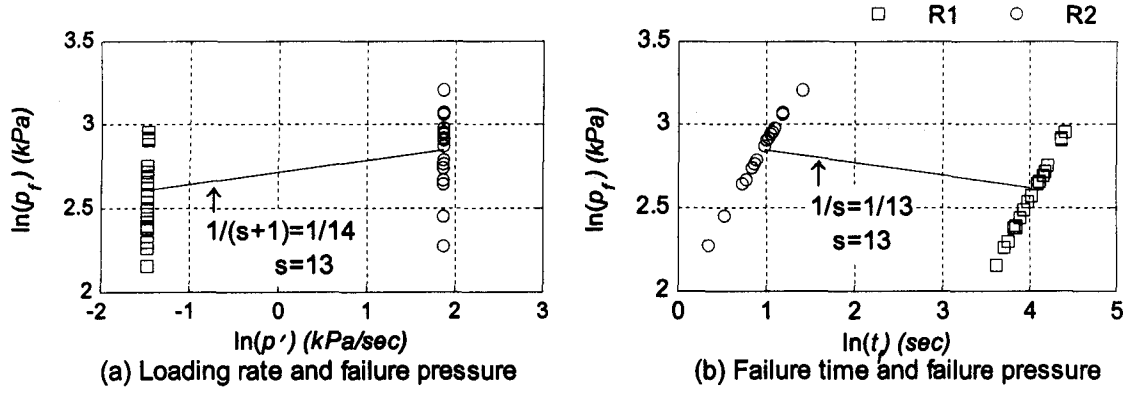

Figure 3.4 Determination of the exponent coefficient s

3.3.1.2 Equivalent load

An equivalent 3-sec load based on a modification of Brown's integral can be calculated from equation (1.2) as

$$p_{3\_pressure} = \left[\int_0^{t_f} p^s(t)dt \Big/ 3 \right]^{1/s} \tag{3.3}$$

where $p_{3\_pressure}$ is an equivalent static pressure of 3-sec duration.

The applicability of equation (1.1) is limited by the fact that it holds true only at the critical crack that causes the failure. Since it was impossible to find the exact failure location by using the current test setup,[6] the following calculation was conducted to overcome this limitation.

---

[6] Determination of the failure location was attempted both by putting masking tape on the glass specimen and by recording the failure moment with a high-speed camera. However, neither of the two methods were successful.

Stress time histories at the crack oriented in the direction normal to α_k at location M_j on a glass plate, were estimated using a finite element analysis (FEA) model (for details, see Appendix D), and an equivalent 3-sec stress at each location and direction σ_3 (M_j, α_k) was obtained based on equation (1.1):

$$\sigma_3(M_j,\alpha_k)=\left[\int_0^{t_f}\sigma_a{}^n(t,M_j,\alpha_k)dt\Big/3\right]^{1/n} \tag{3.4}$$

From the same FEA model, the corresponding applied load to σ_3 (M_j, α_k) was obtained, which is denoted as p_3 (M_j, α_k). The statistics of critical crack locations/directions were obtained from the numerical simulation (explained in detail in Appendix E for each loading case) and an average of p_3 (M_j, α_k) was taken for the sake of comparison based on these statistics. p_3 calculated in this way is expressed as p_{3_stress} in order to distinguish it from $p_{3\_pressure}$.

Figure 3.5 shows the CDF of $p_{3\_pressure}$ and p_{3_stress} for all ramp, saw-tooth and fluctuating loads. Although a 3-sec equivalent load from S2 shows a different trend from others at around F = 0.5 ~ 0.7, the trends of each plot for the different loading cases correspond reasonably well. Even though the presented results in Figure 3.5 may not suffice to validate Brown's integral in and of themselves, the test results and the subsequent observations within the present study are entirely consistent with this concept as you can be seen in the following sections. Therefore, we can conclude, at least, that results which disagree with the applicability of Brown's integral to ramp, saw-tooth and fluctuating loads have not been found in the current study.

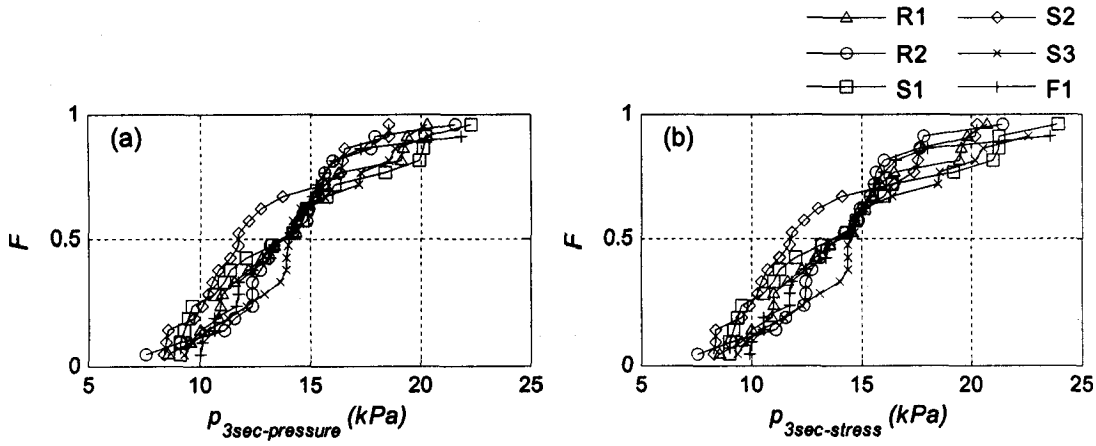

Figure 3.5 CDF of (a) $p_{3\_pressure}$ and (b) p_{3_stress}

3.3.2 Loading rate effect in ramp loading

The relationship between failure pressure and failure time from ramp loading test results is shown in Figure 3.6 with statistical data in Table 3.2. This figure, and the statistics, clearly describes the often-observed effect of a change in loading rate on glass; that is to say, the faster the load is applied, the larger the failure pressure becomes.

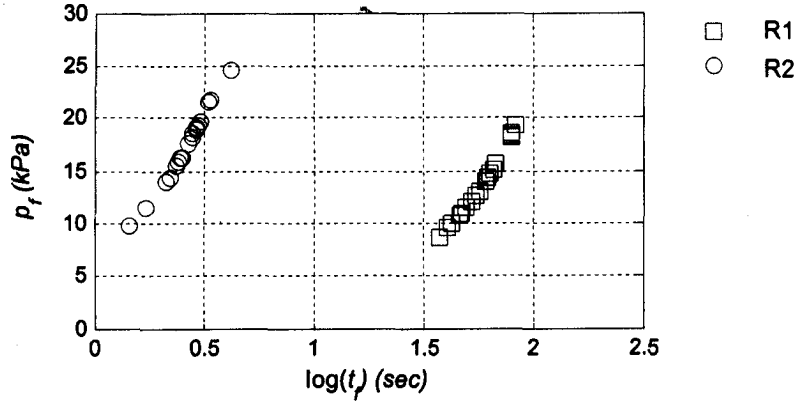

Figure 3.6 Effect of loading rate

3.3.3 Failure pressure in saw-tooth and fluctuating loads

Unlike for ramp loading, where failure eventually occurs due to increasing applied pressure, the relevant failure pressure range seems to be fixed for saw-tooth loading. Figure 3.7 shows the respective failure pressures for those glass plates which remained intact (beyond the first peak) in all three saw-tooth loading cases. In each case, there were five to eight plates which broke before reaching the first peak. It may be plainly observed that a plate always breaks close to its peak pressure, p_{peak} (14.9 kPa, 12.5 kPa. 12.5 kPa) as long as it passes the first peak, regardless of how many cycles it takes to break thereafter.

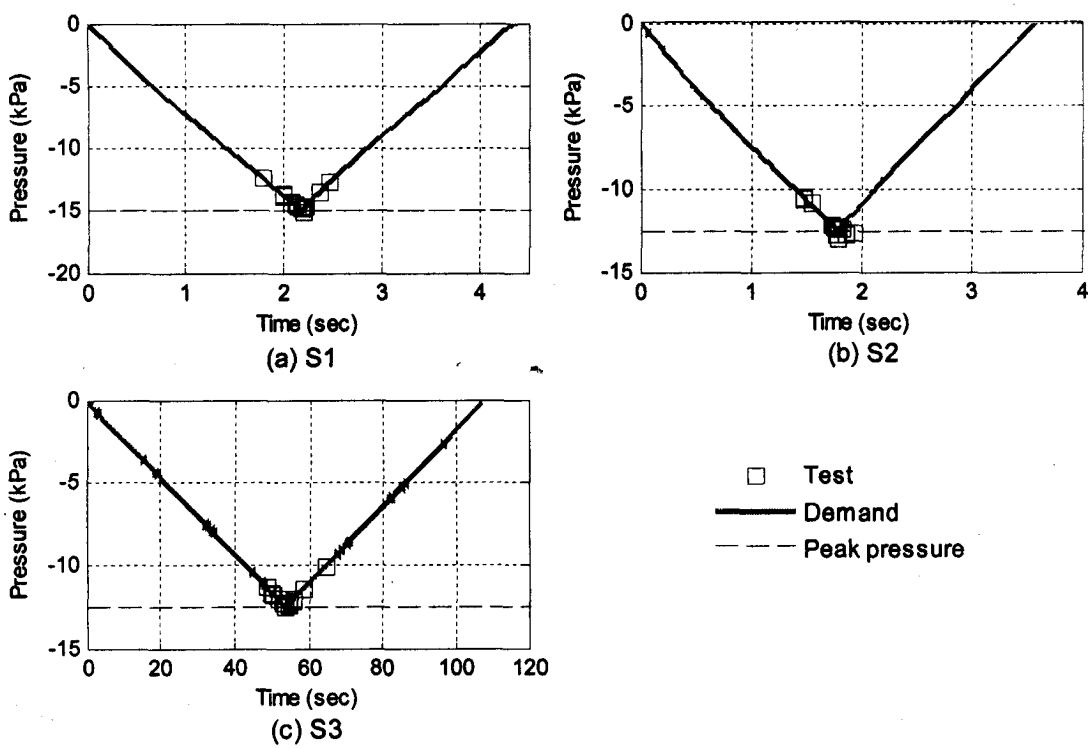

Figure 3.7 Failure pressure level in a cycle of saw-tooth loading

This observation may be understood by considering the differing damage accumulation (DA) contributions of the various parts in one saw-tooth cycle using equation (1.1). Table 3.3 shows the DA contribution of a certain pressure range to the DA of one cycle under S1. Almost half of the contribution is made within the pressure range of $0.95p_{peak}$ to p_{peak} while the proportion of time that the pressure is in this range is 5 %. Moreover, the pressure range above the lowest failure pressure for S1 is 11.59/14.9 ~ 14.9/14.9 = 0.78 $p_{peak} \sim p_{peak}$. According to Table 3.3, this pressure range causes almost 95% ($\approx 0.06 + 0.14 + 0.26 + 0.48$) of the total DA induced in one cycle. This result is to be expected on account of the considerable bearing of the exponent n in Brown's integral, and explains why failure pressure levels tend to be strongly concentrated towards the peak, p_{peak}. This is also the case for the other two saw-tooth loadings.

Table 3.3 Damage integral contribution within a certain pressure range

Pressure range (p_{peak}=1)	0.7 - 0.75	0.75 – 0.8	0.8 – 0.85	0.85 – 0.9	0.9 – 0.95	0.95 - 1
DA contribution (%)	0.02	0.03	0.06	0.14	0.26	0.48

Unlike in the saw-tooth loading results, the failure pressure level is not constant for F1. This can be seen clearly in Figure 1.1, which shows the failure pressure level of each glass plate during one round of the pressure trace (~ 6 min). Almost all the failures occurred close to a peak, like for the saw-tooth loading, but the amplitudes of the various pulses causing failure are quite diverse. Moreover, failure did not necessary occur at one of three large pulses where it may have been expected. This figure validates what Holmes commented on damage accumulated for a glass pane under fluctuating load;

namely that most of the damage is caused by large pressure or suction peaks occurring at infrequent intervals due to the fluctuating nature of wind pressures. However, as can be seen in Figure 1.1, it is difficult to define the threshold of "large" pressure, and failure does not necessary occur even if the applied pressure is larger than the threshold value. Therefore, presuming that a reference time duration for evaluating the DA in his work is appropriate, what Holmes (1985) sequentially mentioned seems true; which is that the use in design of the measured extreme peak pressure from a wind tunnel test, which is the worst among the possible pressure failure levels, as DL is likely to be appropriate, although the duration remains to be evaluated.

Moreover, based on Figure 3.7 and Table 3.3, it is observed that in saw-tooth loading the failure pressure range seems to be concentrated around peak pressures, based on the DA. However, in the case of fluctuating load, all pulses have different sizes. In other words, the DA contribution of each pulse to the critical damage accumulation is different. Therefore, based on our understanding of the DA, this fixed pressure range is merely one where damage accumulation increases noticeably under fluctuating load. Therefore, the failure pressure range cannot be specified as narrowly as in saw-tooth loading.

In Figure 1.1, four glass plates which did not break in the first round of pressure trace are indicated with a circle. Each of them broke at different pulses, and did not necessarily break at those failure pulses where glass plates broke in the first round. Based on these observations, there appears to be no perceptible correlation between failure pressure and failure time.

3.3.4 Cumulative distribution function

Although researchers have sometimes differed on how best to present the results, a CDF plot has generally been favoured, with some researchers choosing to fit data to various models. For example, Kawabata (1996) utilized the Weibull distribution in order to approximate failure pressure. Dalgliesh and Taylor (1990) adapted failure pressure and failure time to a log –log least squares fit. Simiu and Reed (1983) did not conduct full-scale glass breakage tests, but a 60-sec equivalent failure pressure from their numerical simulation was represented by the Weibull distribution.

The probability distribution fitting of p_f and t_f was carried out using these common probability distributions. Since no particular distribution has been used for (statistically) modeling p_f and t_f in past studies, the three different probability distributions, namely the normal distribution, the lognormal distribution, and the Weibull distribution were tested. Figure 3.8 depicts the results for R1 and F1[7]. These three distributions were chosen because they have been used in the past to represent the failure stress of glass (Brown 1972; Kawabata 1996; Calderone 1999; Haldimann 2006). All the parameters were obtained by the method of maximum likelihood. Overall, characteristics of the failure pressure results are captured reasonably well by either the lognormal distribution or the Weibull distribution, although the correspondence becomes poor at small failure probability for F1. A similar tendency is shown in the results for the other test configurations (see Appendix F for details).

---

[7] Failure pressures from saw-tooth loading are not presented since they are governed by the peak pressure, based on the discussion at section 3.3.3.

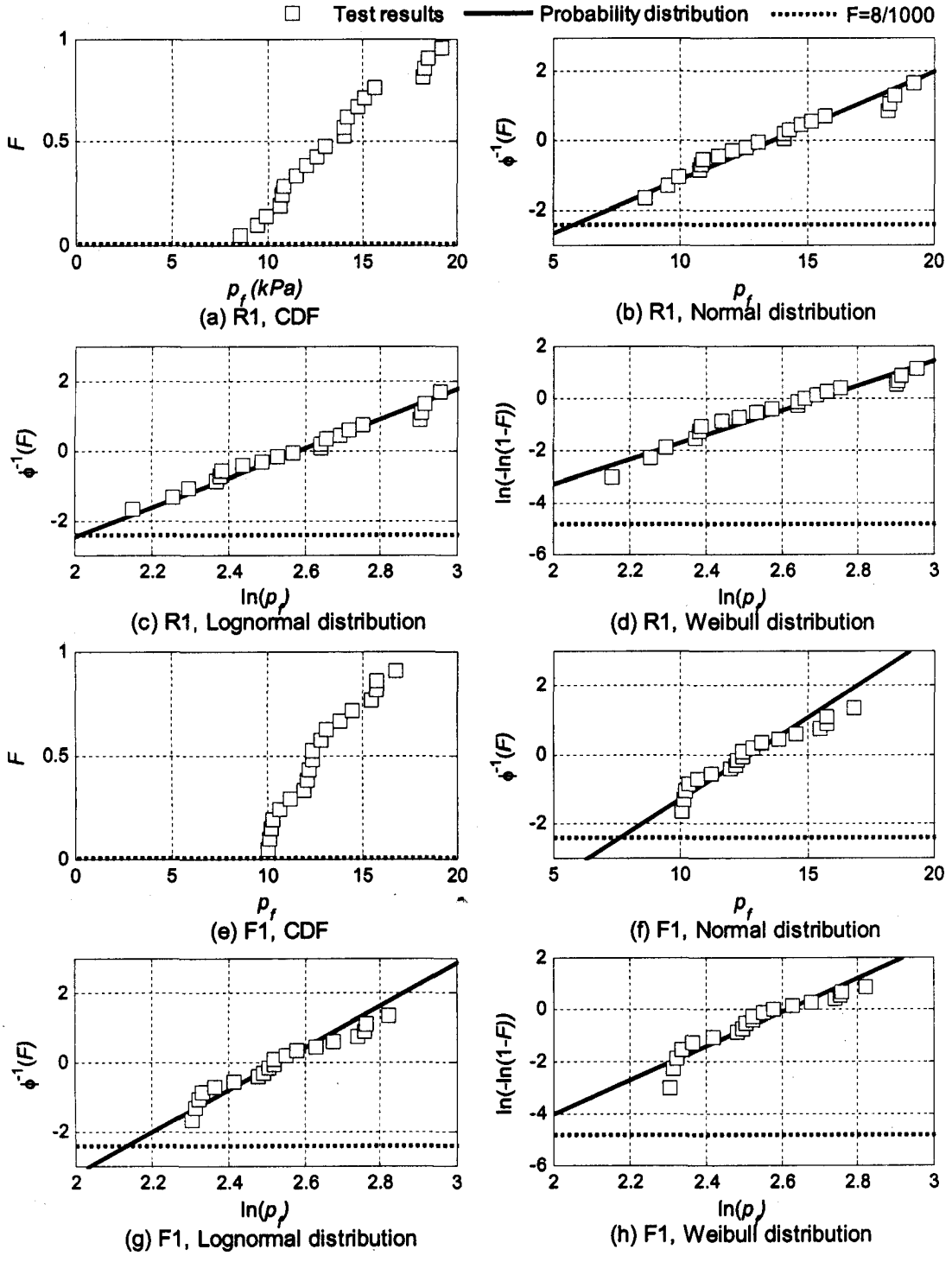

Figure 3.8 CDF of failure pressure (R1, F1)

The CDF figures for failure time are given in Figure 3.9 as a semi-log plot[8]. It is apparent that none of the loading cases would be captured by a single straight line but rather are characterized by two straight lines, which situation differs from the case of failure pressure. For saw-tooth loading cases particularly, it seems necessary to treat the failure time results separately. Hence, the data were divided into those cases which break before and after the first peak pressure (called Group 1 and Group 2, respectively).

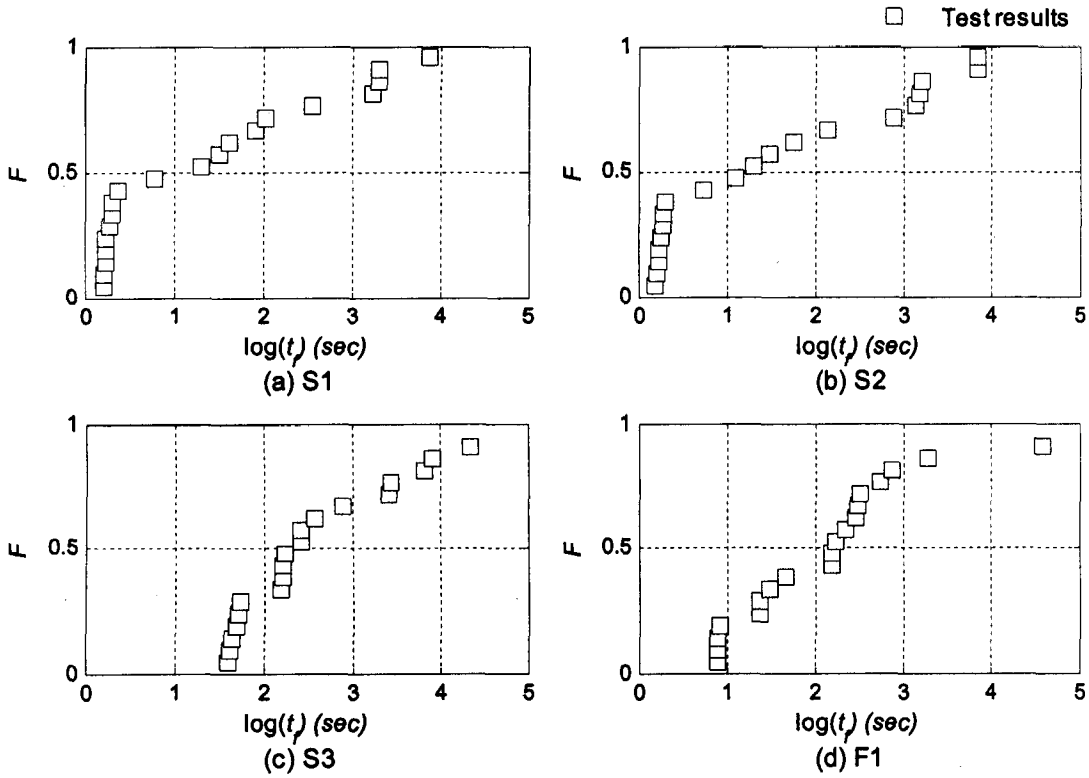

Figure 3.9 CDF of failure time for saw-tooth and fluctuating loads

The test results, as well as the fitted probability distributions for Groups 1 and 2 of S1 are given in Figure 3.10. For both groups, the model parameters for each

[8] The figure for ramp loading is not presented since it has the same trend as failure pressure.

probability distribution were calculated using only those test results which belong to each respective group. In addition, the calculation of the plotting position was maintained separate for each group in order to ensure that the test results would correspond to the model. From the Weibull and lognormal probability papers in particular, it is apparent that data of both groups are approximated well by these probability distributions.

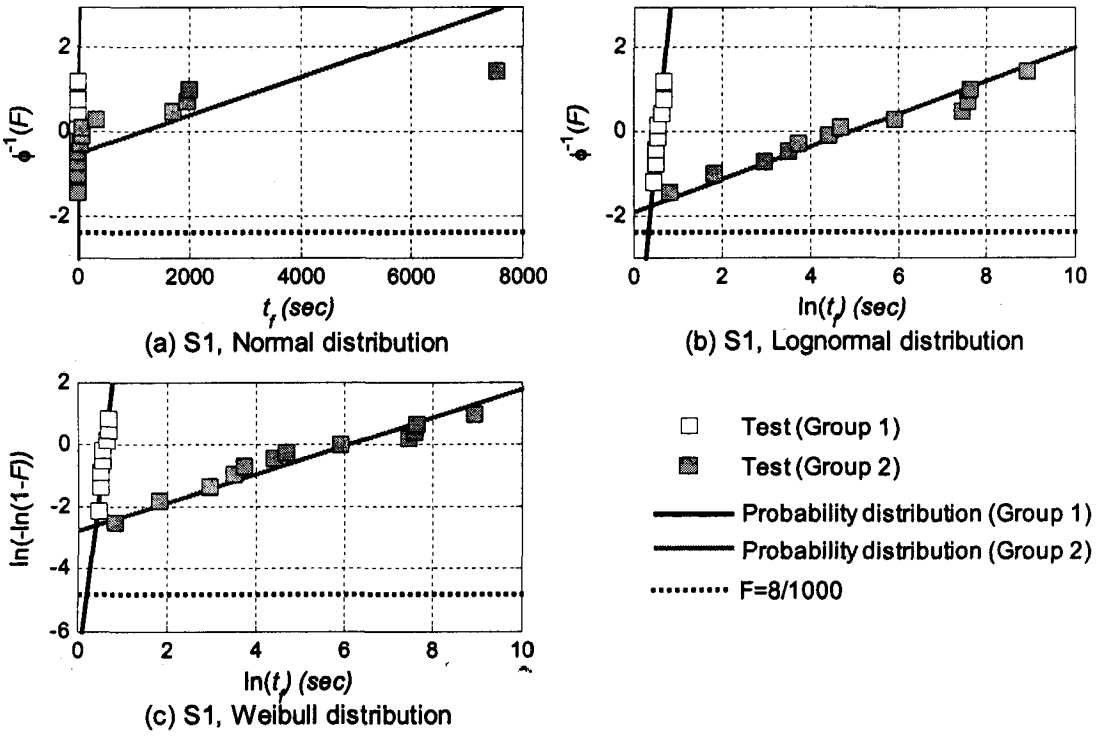

Figure 3.10 CDF of failure time (S1)

These graphs clearly indicate that glass failure is divided into two different groups under saw-tooth loading, which can be characterized fairly well by existing probability models. The reason that grouped failure times are better suited to probability models may be explained by Brown's integral. As mentioned in section 3.3.2, DA depends upon the stress induced at the critical crack on the glass surface and the duration of the load

application. Under ramp loading, the degree of each variable's DA contribution to the critical damage accumulation changes depending on the loading rate. However, since in the case of saw-tooth loading, the applicable stress range is already fixed, contribution to DA is more dependent on time duration. Moreover, due to the lack of the exponent *n* modifying time duration in equation (1.1), the increase of DA in saw-tooth loading is much slower than in ramp loading. In other words, since the pressure range in one cycle of saw-tooth loading which does not contribute to damage accumulation is rather large (Table 3.3), failure time under saw-tooth loading tends to be much longer than under in ramp loading. Thus, there is a distinct difference in failure times between glass plates belonging to Group 1 and those belonging to Group 2. The nature by which glass failure is influenced is likely to be the DA contribution ratio of stress and time duration. Again, the results of S2 and S3 display the same tendency (Appendix F). For both failure pressure and time, it is neither possible nor useful to conclude at this point which distribution model is best used to represent all results. However, at present it seems appropriate to examine all three distributions for probability distribution fitting.

In the current design method, glass failure probability is set to 8/1000, which falls within Group 1 for the saw-tooth loading cases examined here. Note that glass plates in Group1 are essentially the same as those glass plates broken under ramp loading before applied pressure reaching to the first peak pressure of saw-tooth loading traces. Hence, ramp loading tests may prove to be enough to obtain the necessary information even for saw-tooth loading for design purposes. However, this is not the case for fluctuating load. Based on Figure 3.9 (d), drawing a line at a failure time of 7-8 sec—which corresponds to

the point where the first pulse approaches 12 kPa within the entire trace of F1 in Figure1.1—seems to be an appropriate way to categorize the results into two groups for the present case. However, this border, or more precisely stated, the ramp loading which can represent the pressure trace up to this border, may obviously change, depending on the characteristics of fluctuating load. For this reason, ramp loading results seem ill suited to obtaining design pressure levels for fluctuating load.

3.3.5 Conversion to equivalent static load

Based on the discussions in sections 3.3.3 and 3.3.4, on account of the pressure range which does not contribute significantly to the critical damage accumulation, failure time tends to become quite long in saw-tooth (and fluctuating) loading, and this makes the evaluation of the critical damage accumulation complicated. The elimination of time duration which does not affect the critical damage accumulation can be carried out by calculating the ratio g' of one cycle (period λ) DA of saw-tooth loading, whose peak pressure is $p_{peak,}$ to DA of the static loading p_{peak} for time duration of λ :

$$g' = \int_0^{\lambda} \sigma_a(t)^n dt \Big/ \lambda \cdot \sigma_{peak}{}^n \tag{3.5}$$

where σ_{peak} is the stress corresponding to p_{peak}. By using g', the approximate failure time range where the damage integral notably increases can be obtained as $g' \cdot \lambda$ (Figure 3.11), and these values are shown in Table 3.4. It seems that the value g' is constant regardless of saw-tooth loading type. In the case where the stress induced on a glass plate increases

and decreases linearly with the same amplitude (Figure 3.11, left), the value g' is equal to $1/(n+1)$, regardless of p_{peak} and the loading rate based on Brown's integral. $1/(n+1)$ is 0.06 when n=16, which is smaller than the value g' in Table 3.4. This phenomenon occurs because of the non-linear relationship between applied pressure and the induced stress in the present test situation, namely, that the induced stress does not increase nor decrease linearly. Considering this fact, the hypothesis that g' is constant seems appropriate. Note that g' expressed in equation (3.5) is essentially the same as g in equation (2.20).

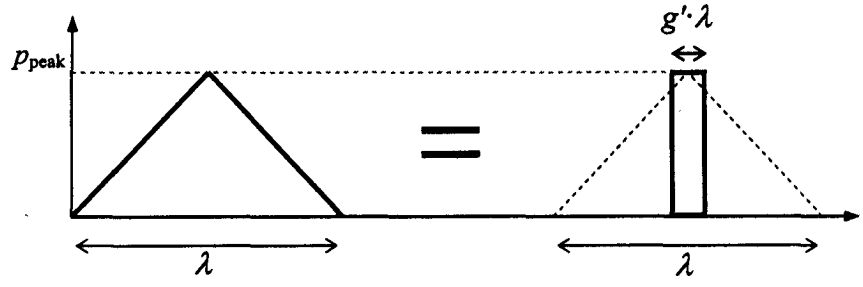

Figure 3.11 Equivalent static loading

Table 3.4 Values of g' and other related numbers for equivalent static loading

	g'	λ (sec)	$g' \cdot \lambda$ (sec)
S1	0.0771	4.60	0.36
S2	0.0788	3.85	0.30
S3	0.0790	108.98	8.61

As for $g' \cdot \lambda$, since the total failure time of saw-tooth loading is the sum of λ, the equivalent failure time t_{eq_sta} under static loading whose pressure level is p_{peak} can be obtained by multiplying g' to the total failure time t_f under saw-tooth loading.

$$t_{eq\_sta} = g' \cdot t_f \tag{3.6}$$

Since S2 and S3 have the same p_{peak} and their t_{eq_sta} should be the same, and hence their failure time t_f should be equal based on this concept, regardless of their loading rates. Figure 3.12 shows the CDF of the failure time of glass plates belonging to Group 2 in S2 and S3. Their correspondence is not good enough to validate this concept. However, since it becomes better as F approaches 1, a larger number of specimens may produce the results necessary to confirm this concept.

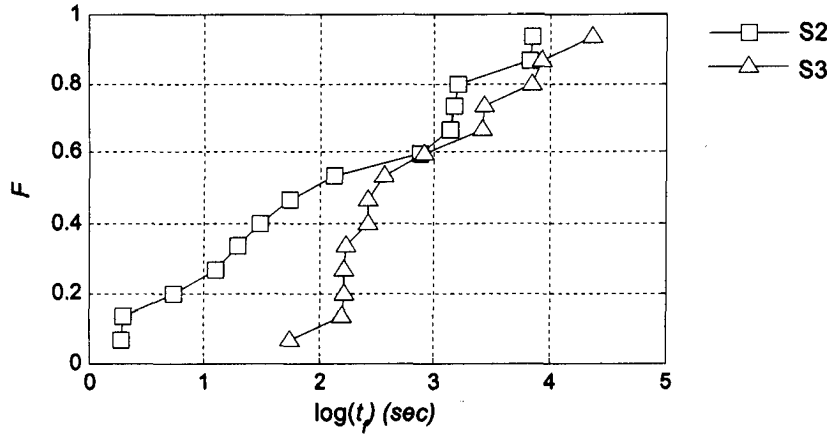

Figure 3.12 Failure time comparison in S2 and S3

Equivalent failure time has the benefit of being able to determine the critical damage integral and the lifetime of glass under saw-tooth loading from experimental results under static loading, which are relatively easier to conduct. According to Mencik (1982), this approach can be extended to the other loading types. Mencik defined g' as a coefficient characterizing the type of loading, which is applicable to any stresses. Moreover, he indicated the possibility of critical damage accumulation prediction using g' under fluctuating load conditional upon treating the fluctuating load as a combination of

different saw-tooth pulses. According to this method, the damage accumulation under the each pulse will be easily obtained using equation (3.5) with its peak pressure and time duration assuming that g' is already known, and a sum of the damage accumulation from each pulse is the total damage accumulation under the fluctuating load. The problem here is that, peak pressure level and time duration for each pulse are different for each pulse. Therefore, this method could be clumsy in practice unless a loading is expressed as a repetition of same pulse. Thanks to currently available technology, it will be simpler merely to calculate damage accumulation using Brown's integral itself for fluctuating load (equations (1.1) and (1.2)).

3.3.6 Fluctuating load

Based on the discussions thus far, it should now be apparent that there are characteristics which can help to predict failure pressure and time with relative ease under ramp and saw-tooth loadings. For example, loading rate effect, which is the inverse correlation between failure pressure and time, is always present under ramp loading. Similarly, for saw-tooth loading, failure pressure is likely to be close to the peak pressure level, and the value g' can predict failure time using static loading test results. The key point is that all these characteristics originate from the damage accumulation theory.

Trying to apply these characteristics or to single out new characteristics for the purposes of prediction under fluctuating load, we soon realize that this task is impossible

due to its recurrence and combination of different pulses, thus damage accumulation itself, needs to be properly understood and applied in order to predict failure pressure and time. Although a method to predict failure pressure and time does exist for certain loading cases, it is also true that these variables can fluctuate depending on the loading case and its parameters, so that they cannot be used as representative values for glass generally, that is to say, for the purposes of design. The only value which is independent of loading patterns and their parameters is critical damage accumulation, and this value should be the starting point for dependable glass design.

3.4 Summary and conclusions

By conducting full-scale glass breakage tests under different loading types, this study has further substantiated that glass failure is defined and controlled by damage accumulation, and that failure occurs when damage accumulation reaches a critical value. To simplify matters however, depending on the loading type, a method to predict failure based on damage accumulation is available, and indeed easier to use compared to dealing with damage accumulation itself. For ramp loading, glass failure is predictable based on the loading rate effect (section 3.3.2).

For saw-tooth loading, the failure pressure range is predictable based on its peak pressure and damage accumulation(section 3.3.3). Compared to ramp loading, glass plate failure under saw-tooth loading is likely to occur accompanied by a relatively longer failure time. Saw-tooth loading also tends to produce a larger variation within failure

times, which makes the glass failure mechanism appear more complicated. Fortunately however, since saw-tooth loading is merely a repetition of the same pulse, the variation of damage accumulation can be easily handled, and the prediction of failure time is readily obtainable through the application of conversion to an equivalent load (section 3.3.5).

When the test configurations were selected, the key items to define saw-tooth loading were loading rate and peak pressure. Based on the discussion in sections 3.3.3 and 3.3.5, peak pressure is undoubtedly an important factor in determining failure pressure. The loading rate effect, however, does not appear to have bearing on saw-tooth loading at all.

Finally, in the case of fluctuating load, all the relatively easier methods that may be used to predict failure pressure and time for ramp and saw-tooth loadings are unsuitable on account of the recurrence and combination of different pulses. It seems that the only way to approach prediction under fluctuating load would be to deal with damage accumulation itself. Moreover, when it comes to glass design, neither failure pressure nor failure time are the correct values to use for determining code values. Instead, the code would ideally reference critical damage accumulation, which is always independent of loading patterns and their parameters.

4.0 Glass failure prediction models

4.1 Theoretical background

As mentioned in Chapter 2, Kawabata (1996) conducted the numerical simulation originally suggested by Simiu and Reed (1983, 1984), and verified its results by comparing them to full-scale glass breakage data obtained using monolithic, annealed glass plates under ramp loading. In this simulation, Simiu and Reed used fracture mechanics in order to obtain time-dependent glass strength.

Using equation (2.17), the time-dependent glass strength of an element at location M_j, which contains a crack oriented normal to α_k after t sec of load application is described as

$$S(M_j,\alpha_k,t)=\left[\left\{S_i\left(M_j,\alpha_k\right)\frac{K_{IC}}{K_{Ii}}\right\}^{n'-2}-\frac{n'-2}{2}A''Y^2K_{IC}^{n'-2}\int_0^{t_f}\sigma_a^{n'}(M_j,\alpha_k,t)dt\right]^{\frac{1}{n'-2}} \tag{4.1}$$

where $K_{Ii}=Y\cdot S_i\cdot(c_i)^{0.5}$ being the initial stress intensity factor. Simiu and Reed's simulation assumes the highest value of K_{Ii} placing the results from this method firmly on the safer side of design ($K_{Ii}=K_{IC}$). Consequently, Simiu and Reed's assumption modifies $S(M_j, \alpha_k, t)$ into the following equation:

$$S(M_j,\alpha_k,t)=\left[S_i\left(M_j,\alpha_k\right)^{n'-2}-\frac{n'-2}{2}A''Y^2K_{IC}^{n'-2}\int_0^{t_f}\sigma_a^{n'}(M_j,\alpha_k,t)dt\right]^{\frac{1}{n'-2}} \tag{2.21}$$

S_i (M_j, α_k) is the initial strength of an element at point M_j that contains a crack having an orientation angle of $\alpha_1 < \alpha < \alpha_2$ in the direction normal to α_k. This reflects the unpredictability of the severity of cracks existing on a glass panel. The value of S_i (M_j, α_k) can be obtained by the Monte-Carlo technique as follows. S_i (M_j, α_k) is assumed to follow the Weibull distribution:

$$P(S_i, A, \alpha_1 < \alpha < \alpha_2) = 1 - \exp\left\{-\left(\frac{S_i(M_j, \alpha_k)}{S_0(A, \alpha_1 < \alpha < \alpha_2)}\right)^m\right\} \tag{4.2}$$

where P (S_i, A, $\alpha_1 < \alpha < \alpha_2$) is the probability of the initial strength of an element whose area is A and which contains a crack having an orientation angle of $\alpha_1 < \alpha < \alpha_2$; S_0 is a scale parameter; and m is a shape parameter[9]. $S_0(A, \alpha_1 < \alpha < \alpha_2)$ at each element located at M_j on a plate can be deduced:

$$S_0(A, \alpha_1 < \alpha < \alpha_2) = S_0(A, 0 < \alpha < 2\pi)\left(\frac{\pi}{\alpha_2 - \alpha_1}\right)^{\frac{1}{m}} = S_0(A_0)\left(\frac{A_0}{A}\right)^{\frac{1}{m}}\left(\frac{\pi}{\alpha_2 - \alpha_1}\right)^{\frac{1}{m}} \tag{4.3}$$

where A_0 is a reference element area. This relationship reflects the dependence of strength on the element size. Otherwise put, the larger the element area, the smaller strength becomes. Since S_0 and m represent the surface crack characteristics, it is important that these values be obtained in conditions as close as possible to those of "in-service" plates. Furthermore, they must be obtained through the use of loading that will not cause subcritical crack growth (inert condition), which would otherwise influence

---

[9] Equation (4.2) is merely a different form of equation (2.7) in Chapter 2. Therefore, S_0 here has the same meaning as k in equation (2.7). k is already fixed regardless surface area, while S_0 in equation (4.2) varies with surface area.

surface crack coefficients. From a practical point of view, concentric ring-on-ring tests might be the easiest method by which to obtain $S_0(A, 0< \alpha< 2\pi)$ and m. Finally, by using $S_0(A, \alpha_1< \alpha< \alpha_2)$ and m from equation (4.3), $S_i(M_j, \alpha_k)$ is obtained by inserting uniformly distributed random numbers between 0 and 1 into $P(S_i, A, \alpha_1< \alpha< \alpha_2)$ in equation (4.2). The foregoing can be conceptualized by imagining a glass panel having uniformly distributed cracks on its surface, and these cracks having different lengths, which randomizes the occurrence of glass failure.

The failure of the glass element can be assumed to have been initiated by a crack oriented in the direction normal to α_k, at point M_j; and bearing this in mind, failure is defined as the moment when the relationship expressed in equation (4.4) is achieved:

$$\sigma_a(M_j,\alpha_k,t) \geq S(M_j,\alpha_k,t) \tag{4.4}$$

where $\sigma_a(M_j, \alpha_k, t)$ is expressed as

$$\sigma_a(M_j,\alpha_k,t) = \sigma_x(M_j,t)\cos^2\alpha_k + \sigma_y(M_j,t)\sin^2\alpha_k + 2\tau_{xy}(M_j,t)\sin\alpha_k\cos\alpha_k \tag{4.5}$$

where σ_x and σ_y are normal stresses in x-direction and y-direction respectively, and τ_{xy} is shear stress as shown in Figure 4.1 at each point M_j induced by the applied load $p(t)$. Note that $\sigma_a(M_j, \alpha_k, t)$ from equation (4.5) is also used for stress integral term in equation (4.1).

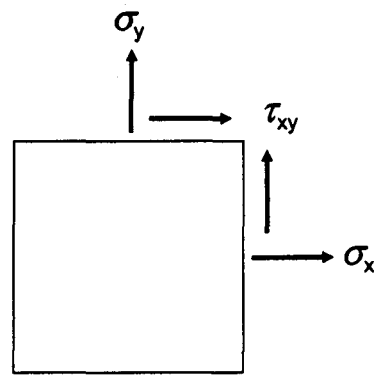

Figure 4.1 Stress acting at location M_j

The relationship between stress and strength is monitored at each location and each direction on the glass panel at time t. In this scenario, the shortest time at which stress exceeds strength (as described by equation (4.4)) will be recorded as the failure time. Once this variable is determined, it will subsequently allow us to infer the applied pressure, stress on the glass plate, initial strength, as well as location and direction at failure.

Figure 4.2 shows the diagram of the numerical simulation procedure. The numerical simulation was implemented in the programming language C++.

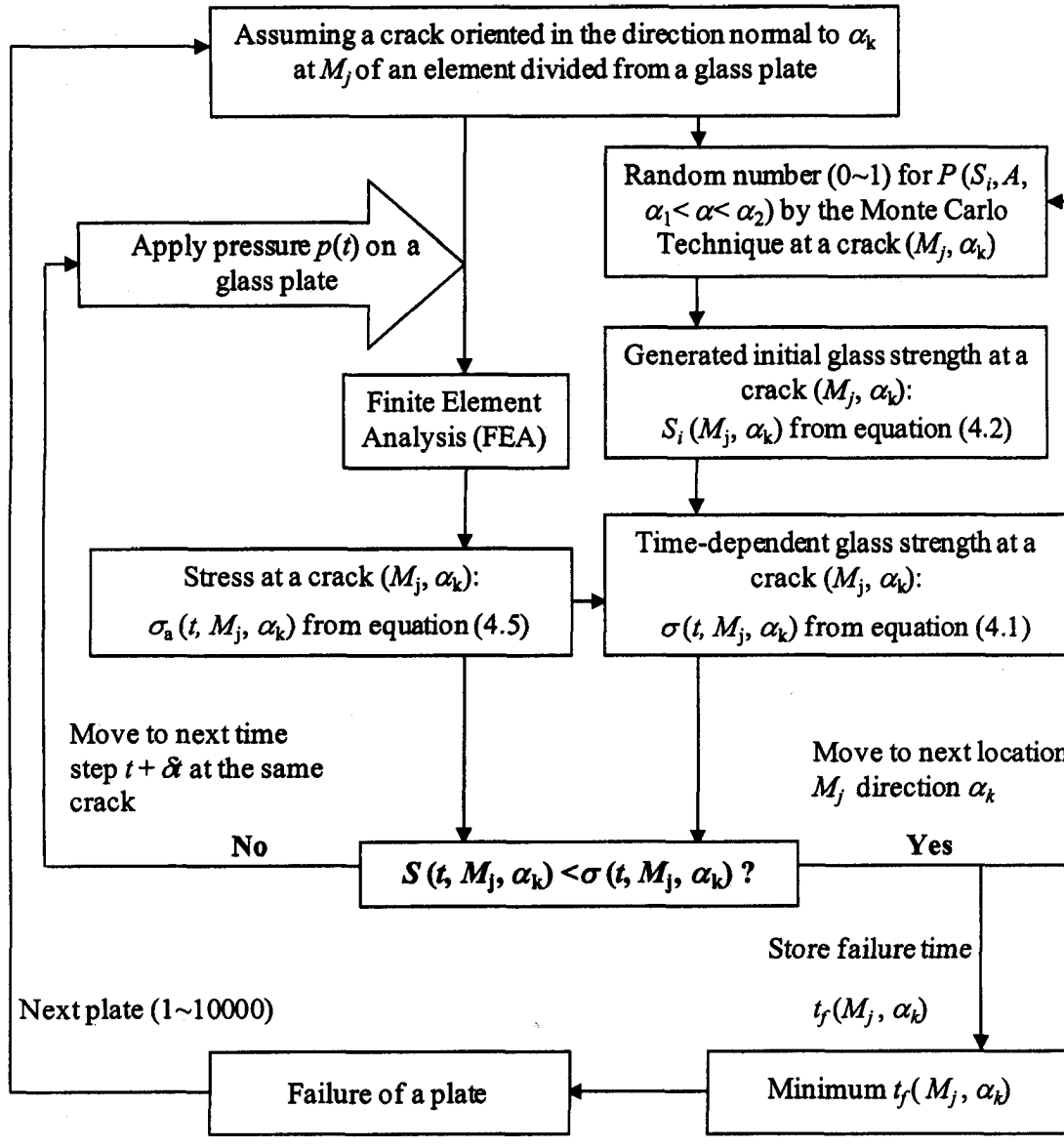

Figure 4.2 Numerical simulation flow chart

4.2 Setup in numerical simulation

The general procedure of the numerical simulation followed Kawabata's method. The input data σ_x, σ_y and τ_{xy} to obtain $\sigma_a(M_j, \alpha_k, t)$ on the glass panel (equation (4.5))

were obtained via commercial finite element analysis (FEA) software, SAP 2000. For details, the reader is referred to Appendix D. In order to save computational time, only one quarter of the glass panel was taken into account for this analysis, and expanded to the whole panel based on symmetry. The entire panel was divided into 225 elements (M_1~ M_{225}) and each element contains a crack having 10 different directions with increments of $\pi/10$ ($\alpha_1 \sim \alpha_{10}$) as shown in Figure 4.3. The grid independence with respect to the numerical simulation results has been confirmed, as shown in Appendix D.

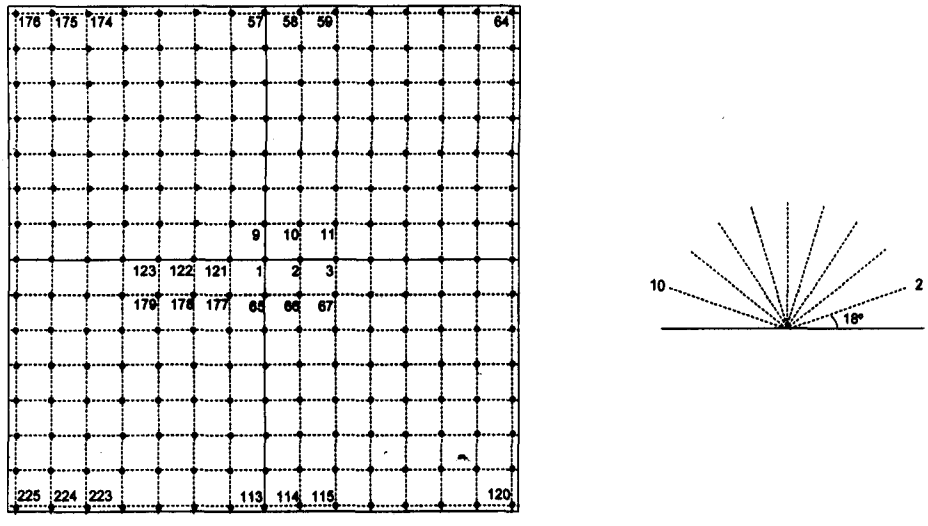

Figure 4.3 Graphical explanation of M_j and α_k

4.3 Input data

4.3.1 Y and K_{IC}

Several of the input parameters in the numerical simulation are shown in Table 4.1. For a detailed explanation of each parameter, refer to Chapter 2. Amongst these, Y

and K_{IC} report quite consistent values when utilized by researchers (including Kawabata) where Y corresponds to the value of a long single-ended crack in a semi-infinite solid, 1.12, and K_{IC} corresponds to the value of a soda-lime silicate glass, 0.75.

$$Y = 1.12, \quad K_{IC} = 0.75 \text{ [MPa·m}^{1/2}\text{]}$$

Table 4.1 Input parameters

S_0, m	Surface crack coefficients
A'', n'	Crack growth coefficients
Y	Geometrical shape factor
K_{Ii}	Initial stress intensity factor
K_{IC}	Fracture toughness

4.3.2 Surface crack coefficients S_0 and m

The initial glass strength S_i used in this numerical simulation is expressed in the form of the Weibull distribution (equation (4.2)). As shown in Chapter 2, the surface crack coefficients in equation (4.2) take different values depending on the researcher. Even though the surface condition has significant effects on glass strength, there is not much experimental and quantitative information available concerning the surface damage caused by various scenarios (Haldimann 2006). In order to conduct their numerical simulation, Simiu and Reed (1983, 1984) used coefficients from the literature (Fuller et al. 1980), while Kawabata conducted ring-on-ring tests with small glass specimen to obtain these values. It would have been ideal to conduct the test with glass specimens which are from the same glass manufacturer since the surface crack coefficients tend to vary significantly. In the current study, however, we did not have the opportunity to

conduct such tests. Hence, it was necessary to follow an alternative method, and the prediction was made using full-scale glass breakage test results.

Haldimann (2006), who validated his prediction method (lifetime prediction model), utilized full-scale glass breakage test results under ramp loading, published by the Ontario Research Foundation (Johar 1981, 1982). The test results whose loading rate is 15 kPa/sec were selected. This loading rate is the minimum ramp loading necessary to create the inert condition in their test setup, namely, a glass size of 3.721 m^2 and a simply-support condition without lateral displacement. Subsequently, a goodness of fit between the CDF of borrowed test results and the predicted CDF of the lifetime prediction model constructed using the various surface coefficients was checked by performing the maximum log-likelihood fitting. The best estimate of surface coefficients through this approach was determined to be the surface crack coefficients of the glass panel. The same method was used in the present research and they were determined as follows:

$$S_0(A_0=1\text{m}^2) = 69(MPa), \qquad m = 6$$

For detailed calculations, the reader is referred to Appendix G.

4.3.3 Crack growth coefficients A'' and n'

The rate of sub-critical crack growth on a glass plate may be described by equation (2.17). Crack propagation data have been collected for many types of brittle materials in different test environments in order to obtain the crack growth coefficients

A'' and n'. As was mentioned in Chapter 2, these coefficients seem to vary depending on several parameters. However, detailed information on these parameters to obtain crack propagation data is not always available. Therefore, unless the crack growth coefficients, which have sufficient accuracy and are stable for the design condition, are obtained, it is difficult to carry out numerical simulations precisely. Simiu and Reed (1983) used coefficients for soda-lime silicate glass from the literature (Wiederhorn 1974) which correspond to 50% relative humidity (RH) and 20° C temperature (T), but an unknown loading type. Kawabata (1996) utilized the same value for A''as Simiu and Reed, but obtained n' from his concentric ring-on-ring tests.

Only a few sets of data with enough information are available. Table 4.2 shows a summary of these available data with the corresponding crack growth coefficients, obtained by linear regression under conditions similar to those used for the current research: RH=50~100%, room temperature and glass type (Soda-lime silicate glass). The data from Evans and Fuller (1974), which are missing both relative humidity and temperature, are included because these are the only ones from cyclic loading tests.

Table 4.2 Crack growth coefficients

	Evans (1974)	Evans & Fuller (1974)		Wiederhorn & Bolz (1970)		Simiu & Reed (1983)	Kawabata (1996)
Loading type	Static loading	Static loading	Cyclic loading	Static step-up loading		n/a	n/a
RH (%)	100	n/a		100		50	n/a
T (° C)	25	n/a		25		20	n/a
A''	3.46	30.45	558.44	0.70	2.13	1.08	1.08
n'	16.64	25.15	25.379	14.98	17.84	19.69	16

Figure 4.4 shows the $v - K_I$ curves for the coefficients listed in Table 4.2. Even though both A'' and n' in Table 4.2 take quite different values, all the $v - K_I$ curves follow the same basic outline with small deviations. In order to know the effect of the different crack growth coefficients on the numerical simulation results, numerical simulations were carried out for R1 and S3 cases used in the full-scale glass breakage test. Figure 4.5 shows the numerical simulation results of failure time at a lower failure probability. Of the loading cases in question, the results of crack growth coefficients from Simiu & Reed take the longest failure time and the ones from Evans take the shortest at F= 8/1000, which is the failure breakage probability specified in ASTM E1300-07 (ASTM 2007). The difference in failure time of these cases is not trivial at this failure probability level (21-25%). Since it is unknown which crack growth coefficients were measured in the closest condition to present test setup, it was decided to carry out the numerical simulation using both the coefficients of Simiu & Reed and Evans to show the possible range that simulation results could take.[10]

---

[10] Note that the surface crack coefficients S_0 and m obtained in the previous section was based on n'=16, which is generally recognized as valid. It was confirmed that similar values for S_0 and m were obtained based on n' =16.64 for Evans' data and n'=19.69 for Simiu & Reed's data.

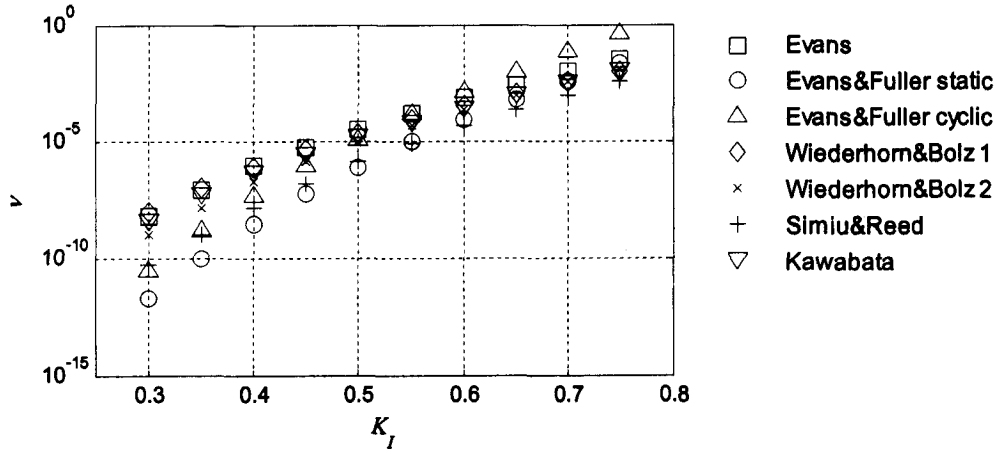

Figure 4.4 $v - K_I$ curves

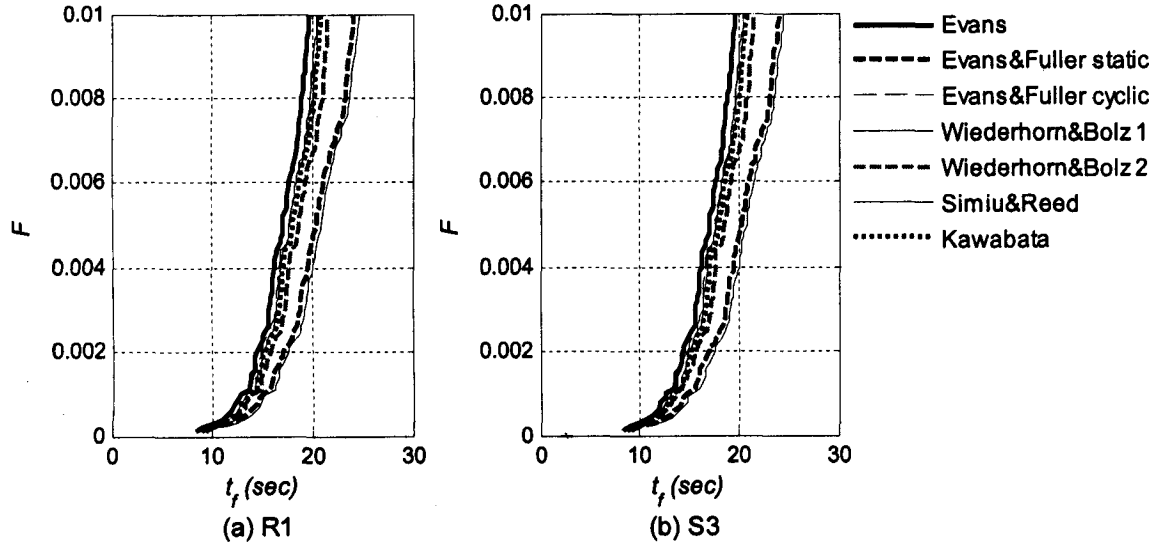

Figure 4.5 Numerical simulation results with different crack growth coefficients

4.4 Convergence of numerical simulation results

In his thesis, Kawabata (1996) confirmed that 1000 repetitions of a numerical simulation for one case were satisfactory to obtain an adequate predicted value at lower

failure probability as long as the surface crack coefficients S_0 and m were properly chosen. As was explained, S_0 and m were estimated in the current study instead of being obtained from tests. Hence, Kawabata's number of repetitions would have fallen short of prudence, and it was likely necessary to increase the repetition number in order to achieve more reliable predicted values. In order to determine the adequate number of repetitions, respective numerical simulations of 1000, 5000, and 10000 pieces of glass under the R1 trace with constant input coefficients were repeated 10 times each. The results at a lower probability level are shown in Figure 4.6. The variation of simulation results at F=8/1000 noticeably changes by increasing the number of glass plates in the simulation. Since the variation at F=8/1000 for 10000 pieces of glass plates is less than the variation caused by a difference in crack growth coefficients, 10000 glass plates to be simulated is deemed sufficient in order to obtain a reliable predicted value at a lower failure probability.

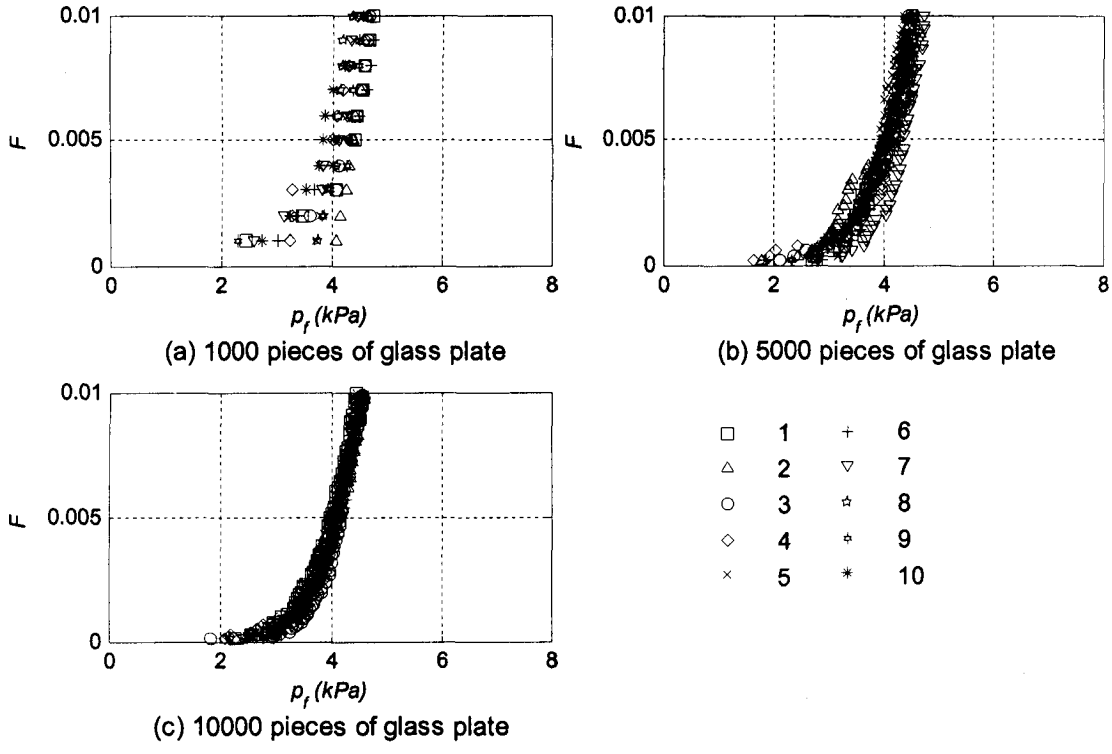

Figure 4.6 Numerical simulation results with different repetition number

4.5 Comparison of test and numerical simulation results

4.5.1 Ramp loading

A numerical simulation was conducted for the ramp loading tested in the present study (R1, R2). All of the input data for the simulations were explained previously, but are summarized for completeness in Table 4.3.

Table 4.3 Input data for numerical simulation

		Evans	Simiu &Reed
$S_0(A_0=1m^2)$	(MPa)	69	69
m	(-)	6	6
A''	$(MPa^{-n'}m^{1-n'/2}sec^{-1})$	3.46	1.08
n'	(-)	16.64	19.96
Y	(-)	1.12	1.12
K_{Ii}	$(MPa\cdot m^{1/2})$	$K_{Ii}=K_{IC}$	$K_{Ii}=K_{IC}$
K_{IC}	$(MPa\cdot m^{1/2})$	0.75	0.75

Figure 4.7 shows the comparison of failure time[11] between the test results and the numerical simulation results in CDF form. Generally, the test results are closer to the numerical simulation results when using the crack growth coefficients of Simiu & Reed, than those of Evans. The numerical simulation results under R1 correspond well at lower probability levels, but not at higher probability levels. With respect to R2, the numerical simulation results show that glass strength is much smaller than the test results at all probability levels, even though the general shape of the curves is similar. From these figures, the significant effect of different crack growth coefficients on glass failure can also be seen, and it increases as glass panels become stronger.

[11] Comparison in failure pressure was not presented since it has a similar trend as failure time for ramp loading.

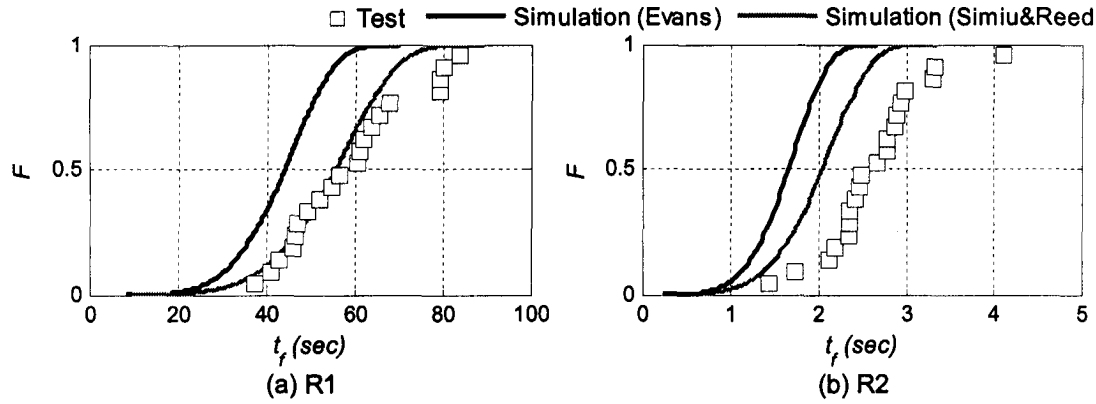

Figure 4.7 Comparison of test and simulation results for ramp loading

4.5.2 Saw-tooth loading

A numerical simulation for saw-tooth loading was conducted using the same input coefficients as ramp loading, and the comparisons on failure pressure (left side) and failure time (right side) are given in Figure 4.8. Test results are categorized into two groups, Group 1 and Group 2, as was explained in Chapter 3. However, failure probably F was calculated by the plotting position without considering this categorization. As for failure pressure, the simulation results using Simiu & Reed's coefficients correspond generally well with test results in all cases. Regarding the comparison of failure time, the simulation results using Simiu & Reed's coefficients for S1 and S3 match with test results very well at lower probability levels, but as the failure time becomes longer, the deviation becomes larger. However, test results of S2 match well with the simulation results using Evan's coefficients at lower probability levels and begin to correspond with the simulation results using Simiu & Reed as probability levels become higher. Overall, the Simiu & Reed coefficients bring a better match for these experiments.

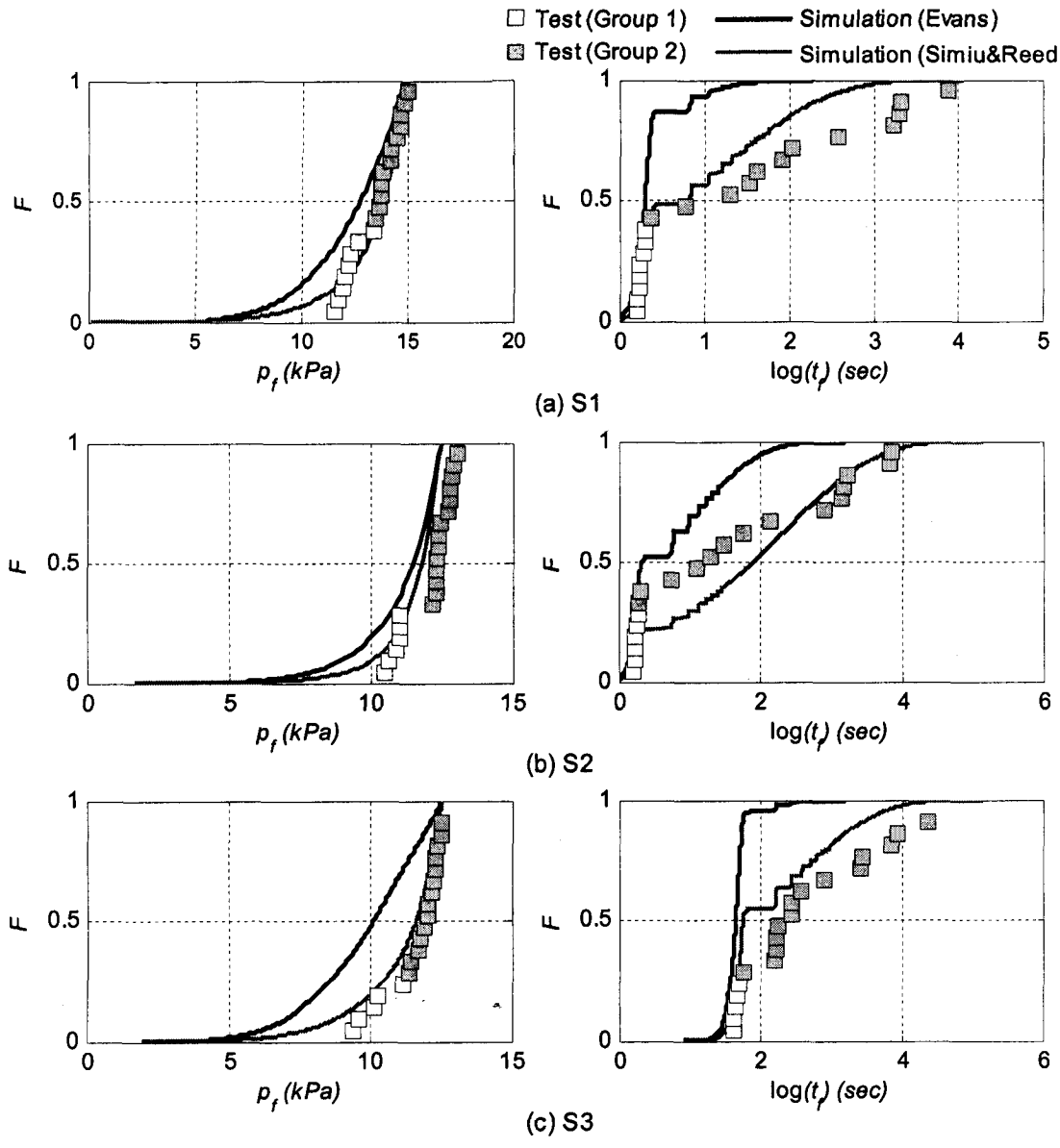

Figure 4.8 Comparison of test and simulation results for saw-tooth loading

Figure 4.9 represents the CDF plot of failure time. The results demonstrate that failure probability F increases forming a stair-like shape as failure time increases. The

enlarged failure time CDF plot for S1[12] is shown in Figure 4.9 (above) along with the input pressure trace used in the numerical simulation (below). As mentioned in Chapter 3, failure occurs only at the pressure level which contributes significantly to critical damage accumulation –peak pressure— under saw-tooth loading. This figure clearly demonstrates this phenomena occurring under the numerical simulation. In other words, F increases only at the pressure levels close to peak pressure (14.9 kPa for S1), resulting in a stair-like shape.

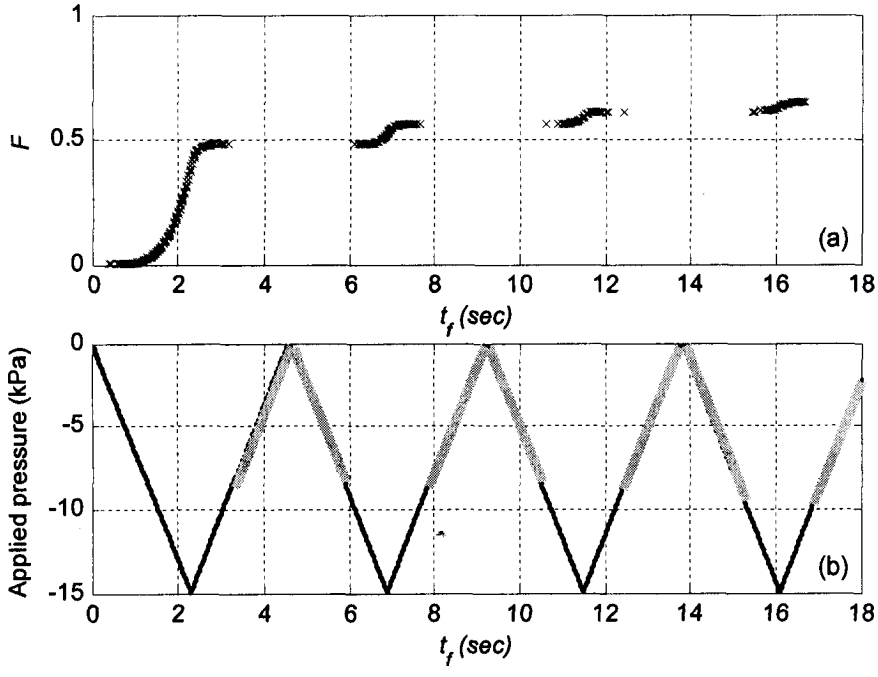

Figure 4.9 Comparison of test and simulation results for S1 (enlarged, (a)) and input pressure trace of S1 used in the numerical simulation (b)

[12] Note that the horizontal axis here is linear, not lognormal.

4.5.3 Fluctuating loading

Figure 4.10 shows the same comparison for F1 using the initial input given in Table 4.3. Failure pressures from test locate somewhere between the simulation results using Evans coefficients and Simiu & Reed's coefficients. However for failure time, test results correspond generally well with the simulation results using Simiu & Reed's coefficients. This correspondence, while not "perfect", but is surprisingly satisfactory.

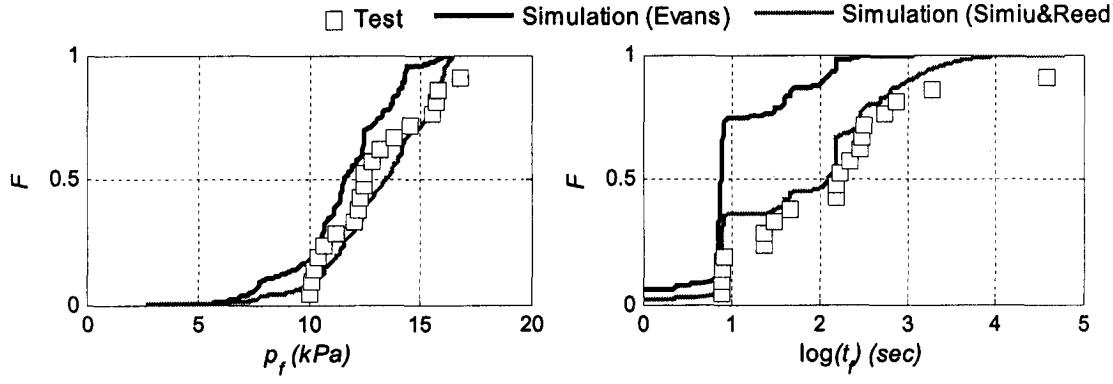

Figure 4.10 Comparison of test and simulation results for fluctuating loading

4.6 Discussion

4.6.1 Observations from comparisons

As seen in previous sections, the numerical simulation results generally capture the test results well, not only for ramp loading, which was verified by Kawabata, but also for saw-tooth and fluctuating loads. However, the simulation's accuracy may allow room

for improvement in order to hone it to a precise prediction tool. Common features found in the comparisons are

1. Failure pressure is predicted more accurately than failure time;
2. A better correspondence can be found at lower probability levels in failure time, but it becomes less accurate as the probability level becomes large, especially for saw-tooth loading;
3. The general shape of the curves of numerical simulation and that of test results are similar;
4. When results do not correspond well, the numerical simulation results report more conservative values than the test results;
5. Different crack growth coefficients change numerical simulation results notably.

Based on these observations, the principal of numerical simulation is unlikely to be flawed, and the input coefficients used in the present calculations (Table 4.3) also seem to be satisfactory. The only exception is the surface crack coefficients, S_0 and m which determine initial glass strength, and seem to vary depending on the specific loading case. Also, failures in weak glass and strong glass seem different based on the variation in discrepancies between test and numerical simulation results at lower and higher probability levels, respectively, and this hypothesis is actually consistent with what was found in Chapter 3. Proceeding from these results, a modification of the current numerical simulation is pursued.

4.6.2 Variation of strength and stress in numerical simulation

Since failure in this numerical simulation is determined by the relative magnitude of strength and stress at failure (equation (4.4)), the initial strength S_i which is given by the Monte-Carlo technique and the non-linear relationship between applied pressure $p(t)$ and induced stress $\sigma_a(t)$ play an important role. Considering the issues raised in the preceding section, it is necessary to understand the variation of this relationship in the numerical simulation in order to modify the current simulation method.

Figure 4.11 shows the variation of strength and stress towards failure of a panel where the failure location and direction are the same under R1 and S3, both having the same loading rate of 230Pa/sec. On the one hand, for those glass panels that break under ramp loading and those belonging to Group 1 under saw-tooth loading, stress increases until it exceeds strength, which is relatively constant but is suddenly reduced just before failure due to damage accumulation. In other words, the increase of stress is more dominant in glass failure than the reduction of strength. Therefore, a small variation of initial strength will have little effect on failure pressure and time.

On the other hand, for glass that breaks under saw-tooth loading after a considerable time (Group 2), since the variation range of stress is fixed, the reduction of strength due to damage accumulation is the only possible cause of failure. In this case, the reduction of strength during each cycle is quite small relative to the total time that pressure is applied; hence, the small variation of initial strength and the shape of stress variation can cause a large difference in a failure time.

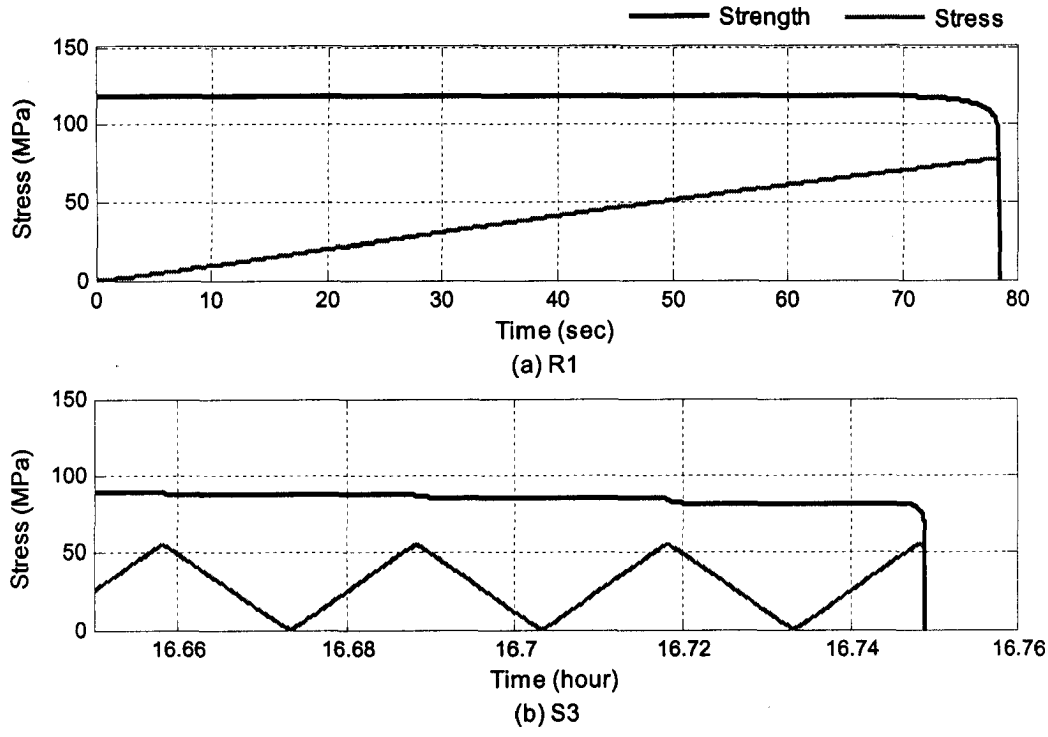

Figure 4.11 Variation of stress and strength

4.7 Modification of numerical simulation

4.7.1 Initial stress intensity factor K_{Ii}

The relationship between K_I, crack length, c, and induced stress, σ_a, is expressed as

$$K_I = \sigma_a(t) \cdot Y \cdot \sqrt{c(t)} \tag{2.5}$$

This relation is illustrated in Figure 4.12. As was explained in section 4.1, the current simulation assumes that K_{Ii} is equal to the highest value of K_{IC} in equation (4.1), which means that the rapid crack growth process begins immediately in the glass panel at the moment of load application. The range that K_{Ii} actually takes is from 0.25, which is the

static fatigue limit, K_{SCC}, where slow crack growth begins, to 0.75, which is K_{IC}. Bearing this in mind, alongside the observation in section 4.6.1 and the finding in section 4.6.2, it seems possible to reach an agreement between failure time in the test results and in the numerical simulation results at high probability levels by implementing the variation of K_{Ii}.

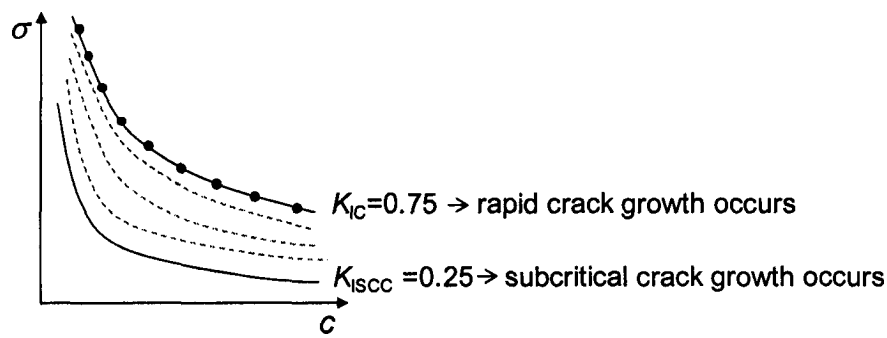

Figure 4.12 Relationship between K_I, c and σ

This implementation may make sense if we consider the situation created in the numerical simulation. The variation of K_{Ii} in this range may be regarded as an initial strength of a glass plate which differs from batch to batch, or differs on account of manufacture on different production lines. The Monte-Carlo technique used in equation (4.2) also represents a variation of initial strength (severity), but this is simply the initial strength variation of *an element* of a panel, and may be understood as the variation of c on the curve of $K_I = K_{IC}$ in Figure 4.12. In practice, this means that the simulation reproduces a setup comprising 10000 glass panels from the same batch/production line, which produces the weakest glass panels ($K_{Ii} = K_{IC}$) compared to other

batches/production lines. Subsequently, the variation of initial strength of an element of each glass panel is considered.

Moreover, regarding the discussion in section 4.6, both the small variation in the initial glass strength and the shape of stress variation were found to affect the failure time of the glass panels which break after a considerable time under saw-tooth loading. Since the shape of stress variation, which is the output of FEA using SAP 2000, had been validated (Appendix D), this does not need to be re-examined for the purpose of a modification of the numerical simulation.

4.7.2 Variation of K_{IC}/K_{Ii}

In order to consider the variation of K_{Ii}, the Monte-Carlo technique was used to induce 10000 random numbers in the range of 1~3 for the term K_{IC}/K_{Ii} in equation (4.1), which corresponds to the K_{Ii} range of 0.25~ 0.75. First, the random numbers for K_{IC}/K_{Ii} were generated from the standard uniform distribution. Since the statistics of variation of K_{Ii} in real circumstances are unknown, different probability models (the normal distribution, the lognormal distribution, the Gumbel distribution and the Weibull distribution) were also taken into account, besides the standard uniform distribution. In this case, the random numbers for K_{IC}/K_{Ii} were generated by the inverse transformation method. The mean and standard deviation (SD) of K_{IC}/K_{Ii} needed in order to use this method were also assumed in order to make the simulation results fit to test results. Since a random number which is less than 1 or more than 3 can also be induced by this

method, the following two procedures were subsequently used to obtain 10000 random numbers in the range of 1~3. One is to set the induced random number less than 1 to 1 and more than 3 to 3 (Procedure 1). The other is to disregard any induced random number less than 1 or more than 3, and to keep generating the random number until 10000 random numbers in the range of 1 ~ 3 are obtained (Procedure 2).

Figure 4.13 shows the graphical image of these methods.

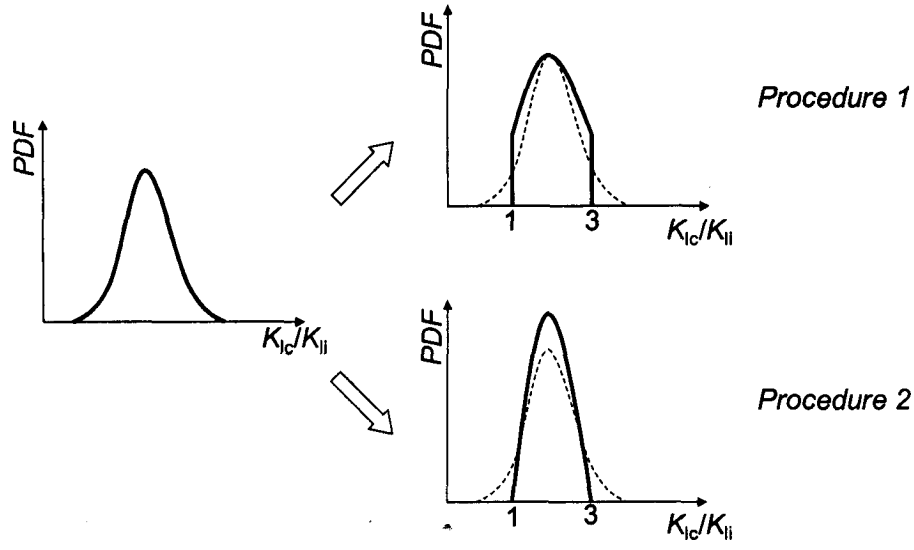

Figure 4.13 Graphical explanation of methods to induce K_{IC}/K_{Ii}

Figure 4.14 shows the CDF of generated random numbers of K_{IC}/K_{Ii} for different probability distribution models, based on mean =1.1 and SD = 0.3. Although the shapes of CDF between Procedure 1 and 2 are different as expected, the difference between different probabilistic models is generally not significant (Figure 4.14 above). However, as the initial glass strength becomes stronger (K_{IC}/K_{Ii} becomes larger), this difference

becomes apparent (Figure 4.14 below). Since it is unknown which distribution best represents K_{IC}/K_{Ii}, the normal distribution and the Gumbel distribution were selected for use in this study, to show the possible range that simulation results can take.

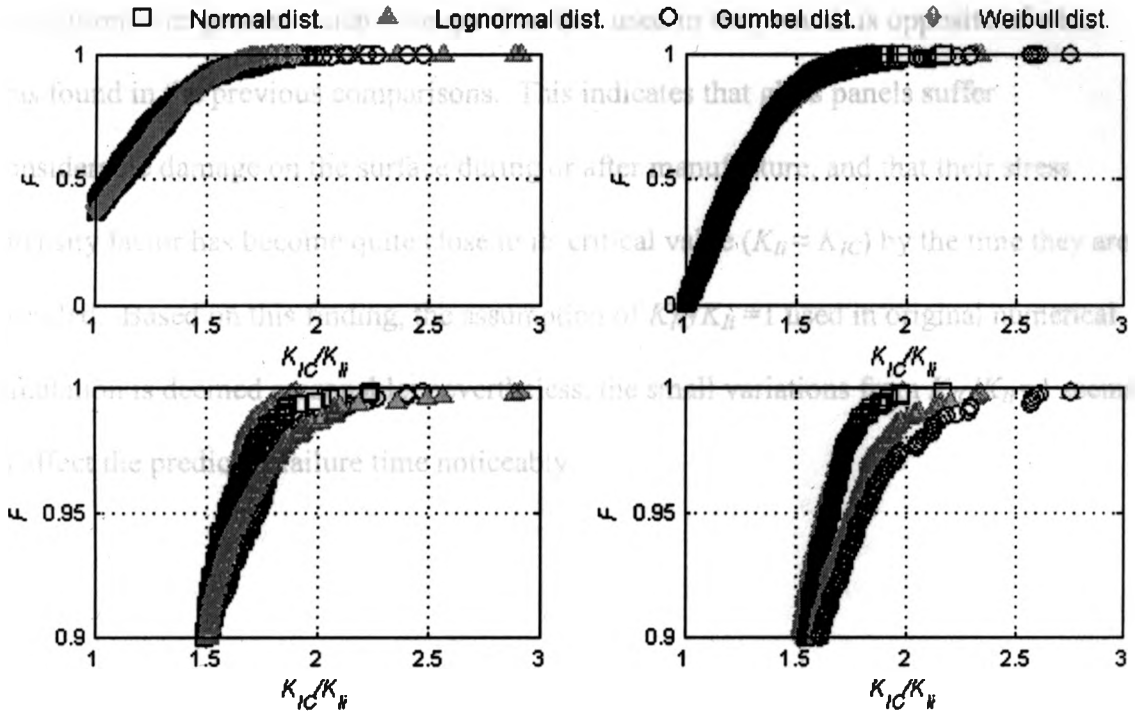

Figure 4.14 CDF of random numbers for K_{IC}/K_{Ii}

4.8 Comparison of test and modified numerical simulation results

4.8.1 K_{IC} / K_{Ii} generated from standard uniform distribution

Figure 4.15 shows the comparison of failure time between test results and the numerical simulation results that use K_{IC}/K_{Ii} generated from the standard uniform distribution and use the crack growth coefficients of Evans (n'=16.64, A''=3.46) and those

of Simiu & Reed (n'=19.69, A''=1.08). In all loading cases, the correspondence becomes worse than the one shown in section 4.5, except at the lower probability levels. Moreover, the numerical simulation results show that glass strength used in the simulation is in general much stronger than that used in test, which is opposite of what was found in the previous comparisons. This indicates that glass panels suffer considerable damage on the surface during or after manufacture, and that their stress intensity factor has become quite close to its critical value ($K_{Ii} \approx K_{IC}$) by the time they are installed. Based on this finding, the assumption of K_{IC}/K_{Ii} =1 used in original numerical simulation is deemed reasonable; nevertheless, the small variations from K_{IC}/K_{Ii} =1 seems to affect the predicted failure time noticeably.

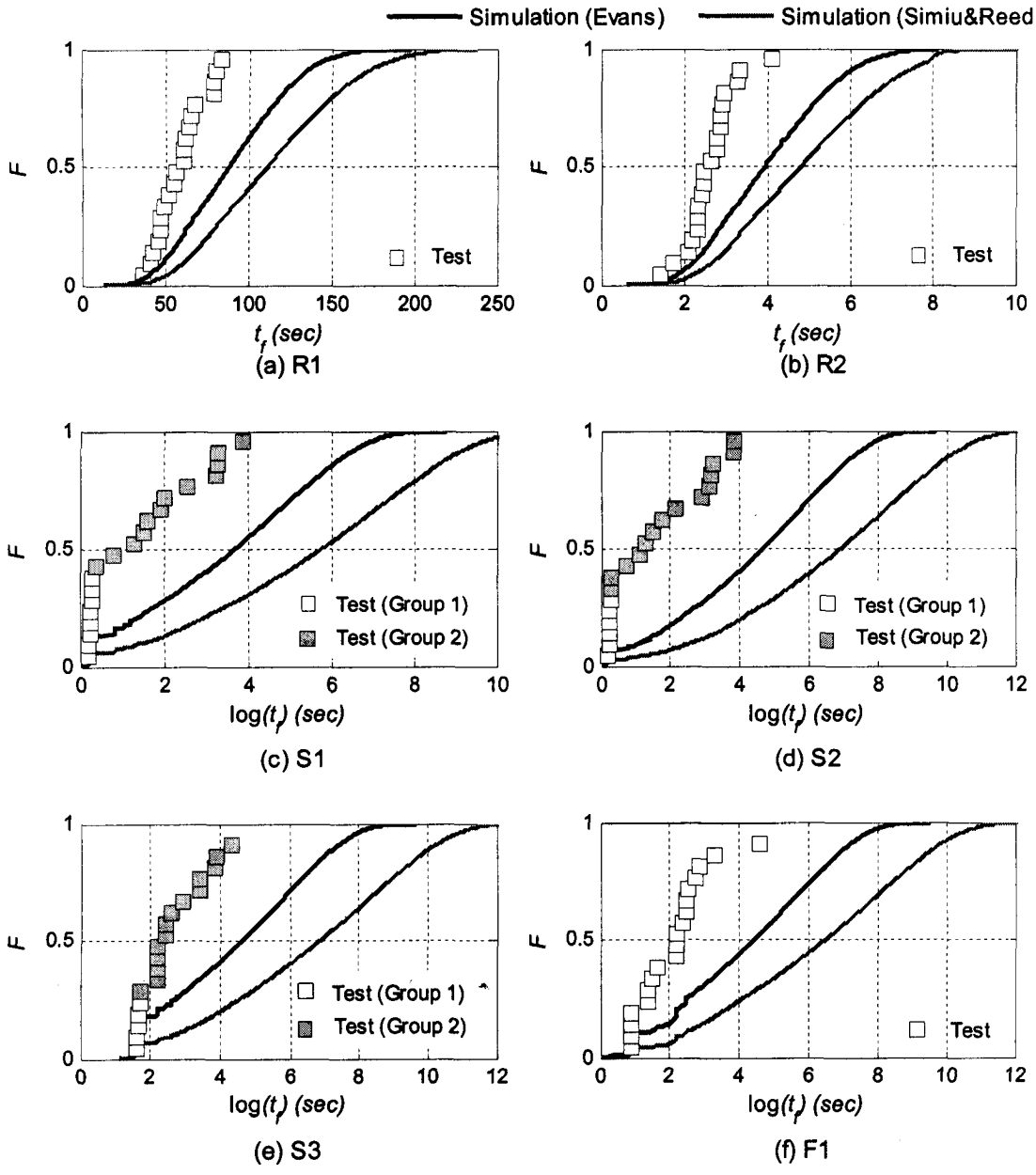

Figure 4.15 Comparison of test and modified numerical simulation results when K_{IC}/K_{Ii} generated from standard uniform distribution

4.8.2 K_{IC} / K_{Ii} generated by the normal and Weibull distributions

The mean and SD values needed to generate K_{IC}/K_{Ii} using the inverse transformation method were selected for each loading type so that the simulation results

match the test results. Figure 4.16 shows the numerical simulation results using K_{IC}/K_{Ii} generated by the method mentioned earlier for S1. The ranges of mean and SD to generate K_{IC}/K_{Ii} which give the best correspondence with the test results for each crack growth coefficient were used to obtain these figures. On the one hand, a change in the values for mean and SD does not change the simulation results at lower probability levels, but it does so quite notably at relatively higher probability levels. On the other hand, a change in the procedure used to generate K_{IC}/K_{Ii} results in the opposite tendency; that is to say, a larger difference at lower probability levels, and a smaller difference at higher probability levels. Using different crack growth coefficients (Evans, Simiu & Reed) also changes the shapes of the plots substantially. However, this effect will not be as apparent in this figure because a change of mean and SD used to generate K_{IC}/K_{Ii} accompanies any modification of the crack growth coefficients in order to obtain the best matching of the numerical simulations with the test results. Finally, the discrepancy due to different distributions (the normal distribution, the Gumble distribution) does not significantly affect the numerical simulation results.

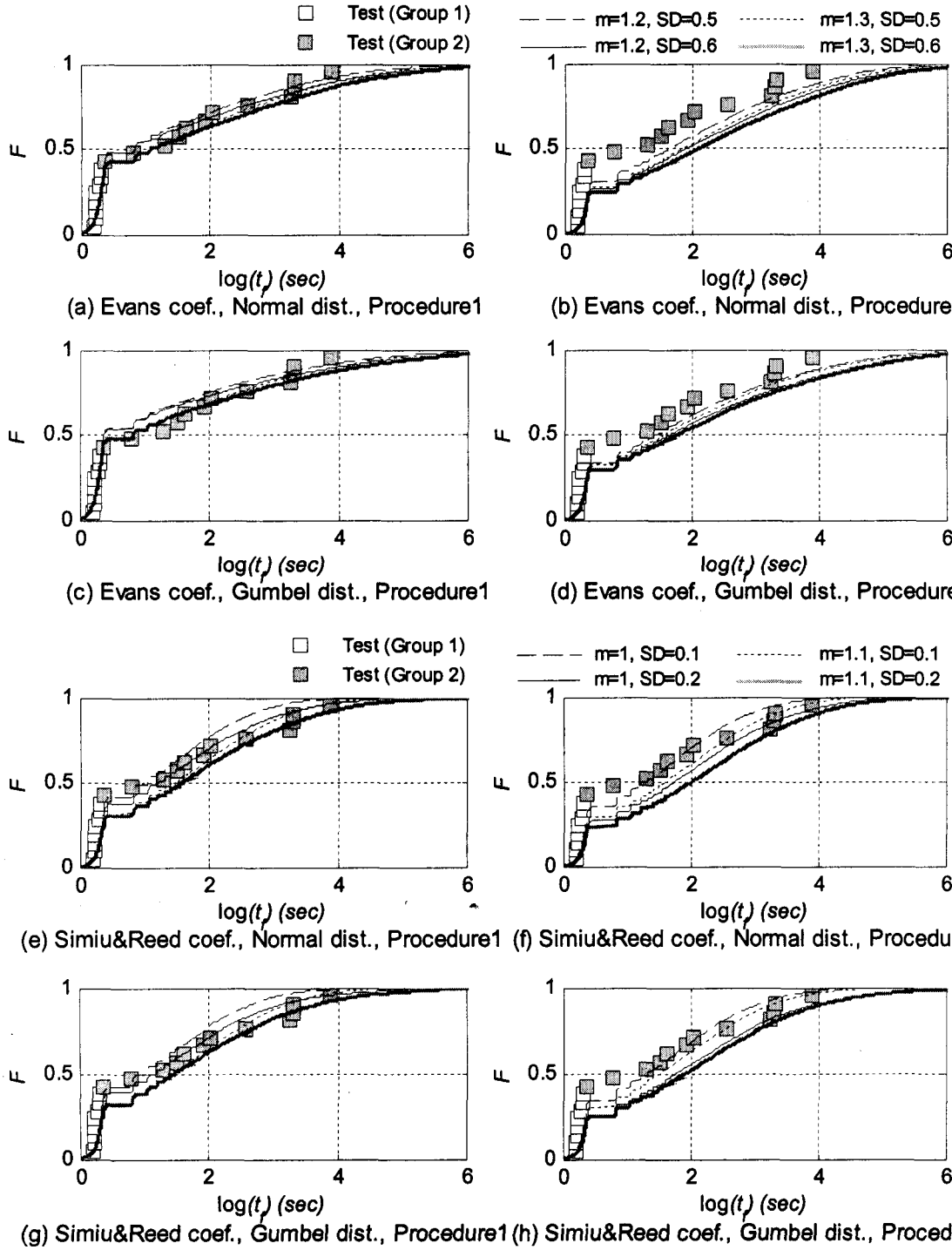

(a) Evans coef., Normal dist., Procedure1 (b) Evans coef., Normal dist., Procedure2

(c) Evans coef., Gumbel dist., Procedure1 (d) Evans coef., Gumbel dist., Procedure2

(e) Simiu&Reed coef., Normal dist., Procedure1 (f) Simiu&Reed coef., Normal dist., Procedure2

(g) Simiu&Reed coef., Gumbel dist., Procedure1 (h) Simiu&Reed coef., Gumbel dist., Procedure2

Figure 4.16 Comparison of test and modified numerical simulation results when K_{IC}/K_{Ii} generated from normal and the Weibull distributions (S1)

Corresponding to the observations from the previous section, the simulation results obtained by using K_{IC}/K_{Ii}, generated by the best combination of probability distribution, procedure, mean and SD were pursued for each loading case with different crack growth coefficients. The degree of correspondence between test results and the numerical simulation results were measured by performing the least square method, and the "best" correspondence was set to be the sum of the square error of around 0.05. Figure 4.17 shows these comparisons on failure pressure and failure time. As you may notice, the best mean and SD to generate K_{IC}/K_{Ii} vary among the different loading cases. However, only one set of these values are supposed to be obtained since the difference in the initial glass strength among difference batches were minimized by randomizing glass panels in the full-scale glass breakage tests (Chapter 3). This may indicate that the modified numerical simulation is not *perfect* to capture the glass failure. However, overall, the match between the test results and the numerical simulation is improved compared to that of the original numerical simulation method for all loading cases, especially at higher probability levels which we were aiming at. Thus, it is concluded that the current modified numerical simulation has enough accuracy to be used for the further examination.

The simulation results obtained using Evans' coefficients tend to fit well with a larger mean value for K_{IC}/K_{Ii} when compared to those of Simiu & Reed. This is because the use of Evans' coefficients yields simulation results typical of relatively weaker glass panels, compared to the results obtained using Simiu & Reed's coefficients. Therefore, a

larger mean value for K_{IC}/K_{Ii} is necessary in order to adjust the simulation results using Evans' coefficients to the test results in Figure 4.17.

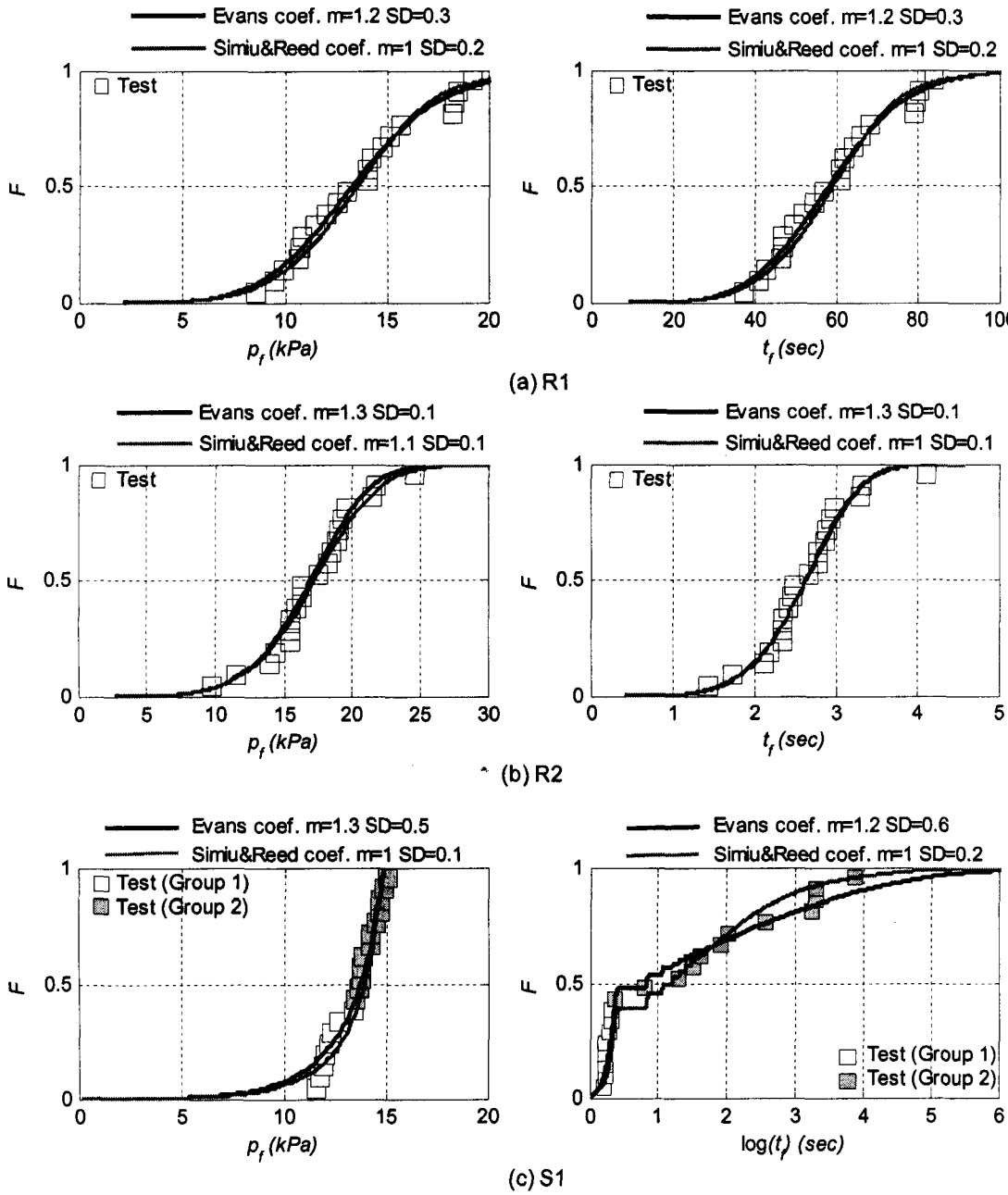

Figure 4.17 Comparison of test and modified numerical simulation results

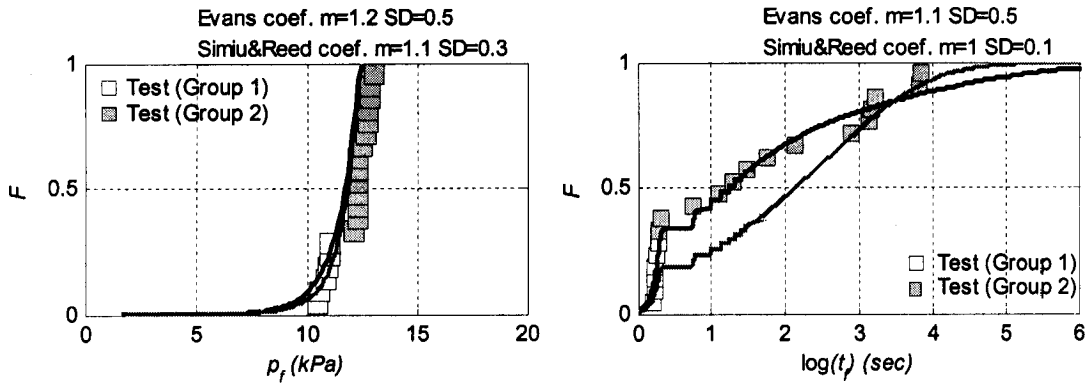

(d) S2

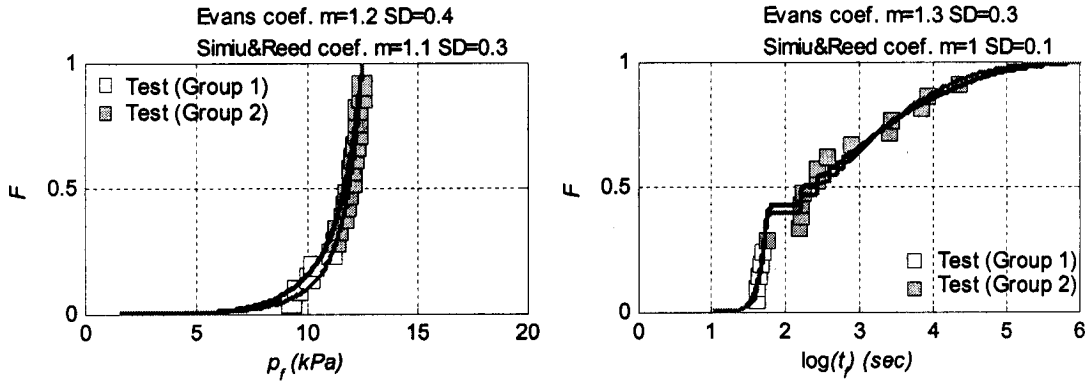

(e) S3

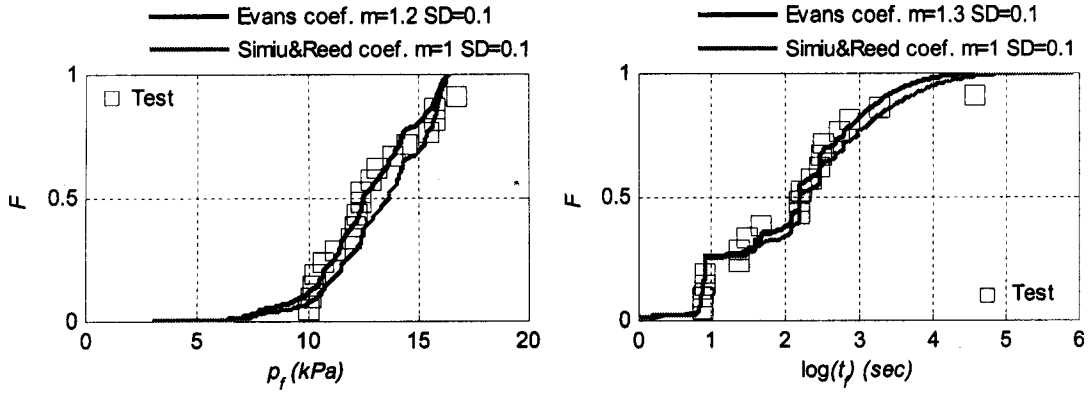

(f) F1

Figure 4.17 Cont.

4.9 Summary and conclusions

The numerical simulation originally suggested by Simiu and Reed, further developed by Kawabata was replicated, and the results from the numerical simulation were compared with the results from full-scale glass breakage tests which used 1 x 1 x 0.006 m, monolithic, annealed glass plates. Since the correspondence in failure pressure and time was not as well modeled for stronger glass, the variation of K_{Ii}, which influences the initial glass strength, was implemented in order to obtain a more precise prediction method. The comparison between test results and the results from the modified numerical simulation indicate that not only the variation of initial strength of an element of each glass panel, but the variation of K_{Ii} considerably affects the distribution of glass failures. In addition, since the shape parameter, S_0, shifts the CDF plots of failure pressure and time horizontally, this is also an important factor affecting the numerical simulation results. In summary, the modified numerical simulation seems to be a more accurate method whereby to predict design loading and lifetime of glass panels than the original numerical simulation. However, it is not possible to conduct the completed prediction without accurate information describing the initial strength of glass (surface crack coefficients, crack growth coefficients, K_{Ii}).

5.0 Glass design method for wind pressure loading

5.1 A proposal of glass design method for wind pressure loading

Based on the findings from Chapters 3 and 4, it can be concluded that, unlike for other materials where definite loads are sufficient to define failure, critical damage accumulation is the only quantity able to define failure for glass. Thus, an ideal glass design method would be as follows:

- First, extreme wind pressure time histories, which may occur for the specific design situation (site/building), need to be obtained.
- Second, a modeling method (such as the numerical simulation in Chapter 4), which can predict failures for a particular glass geometry and type, is applied, using the wind pressure time histories.
- Third, the glass geometry and type, which can provide sufficient lifetime (e.g., return period specified in design codes) with a certain failure probability level (e.g. F=8/1000 from ASTM E 1300-07) calculated by the modeling method, are selected.

In order to implement this method, it would be necessary to obtain representative input coefficients to define the initial glass strength for each glass type—which in Chapter 4 were found to be critical for the prediction of failure—and input stress values from FEA for the various glass types and geometries. Once these input data are obtained and tabulated in advance, this method gives the most accurate information about the

behaviour of the selected glass panels in a realistic wind pressure loading situation. Furthermore, the usefulness of these results is not confined to the purposes of design, but they can yield the maximum lifetime of the selected glass, which may be used for other analysis (e.g., risk assessment such as HAZUS (Vickery et al. 2006)).

However, for the case of design specifications set by building codes, only the minimum requirement for glass design is demanded. In this case, the design code—which specifies Load Resistance (*LR*) as the capacity that a certain glass can take, and Design Load (*DL*) as the extreme wind pressure becomes important, and the specified *LR* and *DL* must be sufficiently reliable to cover the range of design situations allowed by the code. As has been abundantly repeated, glass failure is governed by the damage accumulation (DA); thus, the required *LR* and *DL* should reflect the critical damage accumulation which the selected glass panel can accommodate and the DA caused by the appropriate wind loads for the specific design situation, respectively. In addition, since Brown's integral holds true, a given dynamic load can be converted into the corresponding static load, thereby simplifying the representation of the load and its analysis, based on the results obtained in Chapter 3. Therefore, this equivalent static load can be used for glass design, instead of DA itself.

As for the conversion to static load, the reference pressure magnitude and reference time duration need to be specified. Since the current design codes specify the design pressure, it will be easier to fix this and to determine a reference time duration for the calculation of an equivalent static load. The actual value of the reference time duration is irrelevant as long as the same time duration is used for the calculation of both

LR and *DL*. For example, if the reference time duration is chosen to be t_{ref} sec, extreme wind pressure time histories for the specific design situation that last *T* hours would need to be converted into a t_{ref} –sec equivalent static load, $p_{eq}(t_{ref})$,

$$p_{eq}(t_{ref}) = \left(\int_0^T p^s(t)dt \Big/ t_{ref} \right)^{1/s} \tag{5.1}$$

This $p_{eq}(t_{ref})$ corresponds to *DL*, and should be available in the design code. On the other hand, failure pressure at a certain failure probability P_f under static load whose time duration is t_{ref} is obtained using existing failure models and expressed as $p_f(t_{ref}, P_f)$. Thus, $p_f(t_{ref}, P_f)$ becomes *LR* which would be tabulated for different glass geometries and types in the code. A glass geometry and type which satisfy the following relationship is the appropriate selection of glass:

$$p_{eq}(t_{ref}) < p_f(t_{ref}, P_f) \tag{5.2}$$

A similar methodology was suggested by Kawabata (1996).

5.2 Examination of current glass design method

Based on the suggested method using design codes, the current state of window glass design in North America is examined.

5.2.1 Load resistance

In the United States and Canada, load resistance, *LR* is specified as a 3-sec static load (ASTM E 1300-07) and a 60-sec static load (CAN/CGSB-12.20-M89), both at a

failure probability of 8/1000. The calculation of *LR* is based on the GFPM in both codes. Hence, the current codes already contain the appropriate procedure to obtain *LR*. However as mentioned in Chapters 1 and 2, during the application of the GFPM and the drafting of the code, several cautious assumptions were made in order to obtain a safe value for *LR*, and there is a possibility that these assumptions may have produced overly-conservative numbers for *LR*, as pointed out by Minor and Norville (2006), and discussed in section 1.2. In addition, several defects in the application of the GFPM have been pointed out by Reid (1991) and Fisher-Cripps & Collins (1995); these possible flaws in the calculation of *LR* in both codes will be examined below.

5.2.2 Comparison in *LR*

The modified numerical simulation presented in Chapter 4 can serve as an alternative to the current method for obtaining *LR*. Figure 5.1compares *LR*s for 1 x 1 x 0.006 m, monolithic, annealed glass plate with a simply-supported condition, whose respective reference load durations t_{ref} of 3 sec, 1 min, and 1 hour, obtained from ASTM E 1300-07, CAN/CGSB-12.20-M89, and *LR*s from the numerical simulation at a failure pressure of *F*=8/1000. In order to adjust t_{ref}, Table X6.1 from ASTM E 1300-07 Appendix 6, and equation (2) of CAN/CGSB-12.20-M89 Appendix B, expressed in the following form from CAN/CGSB-12.20-M89, were used:

$$R_t = R_{ref} \cdot t^{-1/n''} \tag{5.3}$$

where R_t is the average resistance under a constant pressure sustained for t min, n'' is the coefficient (=15 for annealed glass), and R_{ref} is the reference resistance under a pressure sustained for 1 min.

The numerical simulation results under static loading given in Figure 5.1 were obtained as follows: A constant pressure of 0.05 kPa is applied to a glass panel for the time duration t_{ref} (=3 sec, 1 min, 1 hour). If failure does not occur, the applied pressure is increased by 0.05 kPa. This process is repeated until glass failure does occur.

In addition, a common set of inputs (probability distributions, procedure, mean, SD), used to generate the values of K_{IC}/K_{Ii}, which is applicable to all loading cases (R1, R2, S1, S2, S3, F1) in order to match the simulation results closely to test results was not determined in Chapter 4. Since the best set of input values were rather different for each loading case. Therefore, all the "best sets" for each loading case used in Figure 4.17 were employed in this calculation, and their results are presented as a possible range. The ranges of output at F=8/1000 are shown as LR in Figure 5.1. The rest of the procedure, and other initial input coefficients are the same as those used in Chapter 4. As for LR at F = 8/1000, the CDF of failure pressure is obtained by the plotting position from 10000 failure pressure values derived from the numerical simulations. Subsequently, instead of fitting the simulation results to probability models, the failure pressure whose F value is closest to 8/1000 was selected.

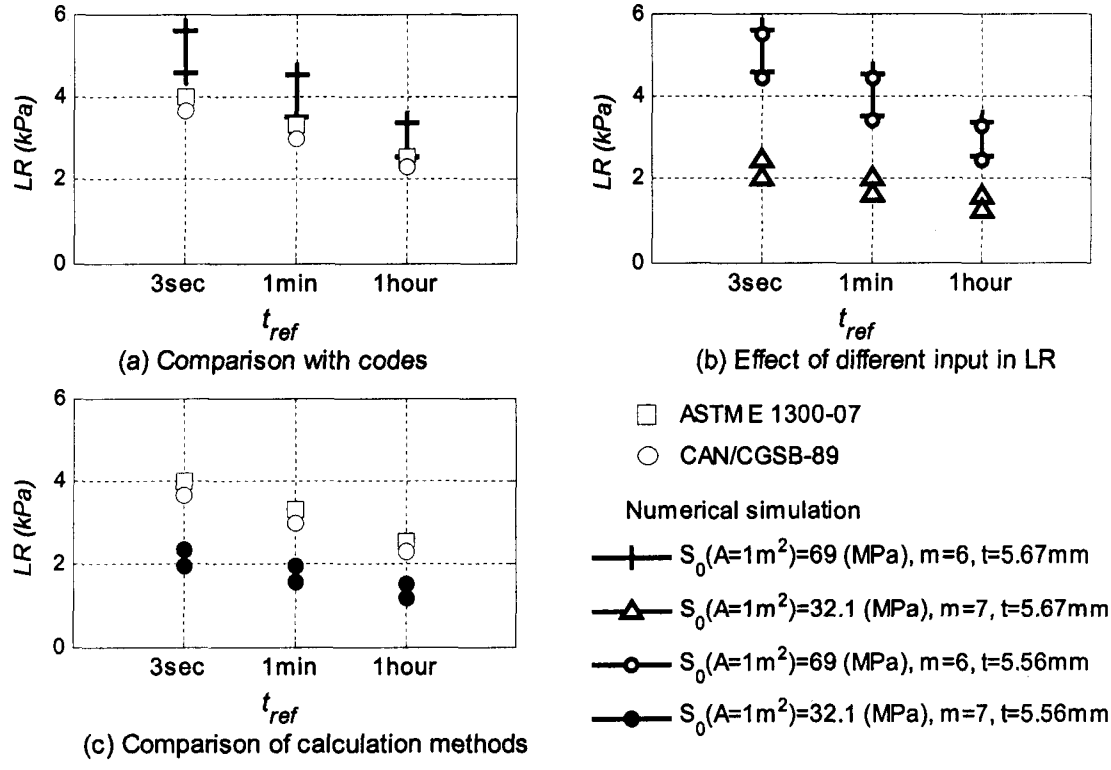

Figure 5.1 Comparison of *LR* between the codes and the numerical simulation

For all t_{ref}, *LR* values from both codes are smaller than the results of the numerical simulation (Figure 5.1 (a)). These smaller values from codes are likely to be produced by the use of conservative values for several parameters because of their uncertainty; namely, (1) the assumption of minimum glass thickness; and (2) the assumption of weathered window glass in the calculation of glass surface crack coefficients ($S_0(A_0=1\text{m}^2)$ =32.1 (MPa), m =7) for this particular calculation. In the numerical simulation, a glass thickness of 5.67 mm (which was the average thickness of glass plates (nominal thickness of 6 mm) used in full-scale tests), and the surface crack coefficients $S_0(A_0=1\text{m}^2)$ =69 (MPa) and m =6, respectively, were used.

In order to examine the difference in *LR* due to each assumption made in the parameters (i.e., the effects of thickness, weathering, etc), the numerical simulations were conducted with weathered glass surface crack coefficients of $S_0(A_0=1m^2)$ =32.1 (MPa), m =7, which are used in both codes, and a glass thickness of 5.56 mm which is the minimum glass thickness for nominal 6 mm glass (ASTM C 1036-01, ASTM 2001). The results are given in Figure 5.1 (b). The numerical simulation results based on t =5.56 mm (circle) and t =5.67 mm (cross) in Figure 5.1 (b) show that the use of minimum glass thickness reduces *LR* only a small amount. On the other hand, the numerical simulation results based on $S_0(A_0=1m^2)$ =69 (MPa), m =6 and $S_0(A_0=1m^2)$ =32.1 (MPa), m =7 (triangle) show that the use of surface crack coefficients from weathered window glass lowers the *LR* significantly.

Bearing in mind that the effect of minimum glass thickness is minor on *LR*, consider Figure 5.1 (a) again. For new glass, with $S_0(A_0=1m^2)$ =69 (MPa) and m=6, the code yields a conservative (i.e., smaller) *LR*. However, the code considers weathered glass, so the effects of using coefficients appropriate for weathered glass must be examined. Thus, numerical simulation using the same input parameters as employed in the design code (viz., $S_0(A_0=1m^2)$ =32.1 (MPa), m =7, thickness of 5.56 mm) was performed. Figure 5.1 (c) shows the results. Contrary to the results observed in Figure 5.1 (a), the design codes now yield larger values of the *LR* when compared to the numerical simulation results for all t_{ref}. Although the assumed input parameters for $S_0(A_0=1m^2)$ =32.1 (MPa), m =7 is a choice made in the process of codification, it is actually quite difficult to obtain such information. For example, only a few studies on the

reduction of glass strength in weathered glass can be found in Table 1.1. Since the current numerical simulation methodology is able to closely replicate the experimental results[13], these simulated values are likely better estimates of the true *LR* values. Hence, the current comparison result calls the code values into question for weathered glass, considering the substantial differences.

Another feature found in Figure 5.1 (a) is that *LR* from CAN/CGSB-12.20-M89 are slightly more conservative in all t_{ref} than ASTM E 1300-07. This discrepancy exists despite the fact that the calculations of NFL and R_{ref} are based on the same method (CFPM), and the coefficients used to multiply NFL for ASTM E 1300-07 and R_{ref} for CAN/CGSB-89 in order to obtain *LR* (*R*) are also identical for this particular case (1 x 1 x 0.006 m monolithic annealed glass). Based on these observations, although the methods whereby Table X6.1 in ASTM E 1300-07 and equation (2) in CAN/CGSB-12.20-M89 were obtained are nowhere made explicit, they most likely differ. In addition, the discrepancy in *LR* between the two codes collectively and the numerical simulation—which should remain constant—becomes slightly larger as t_{ref} becomes shorter. These facts indicate that the reference time conversion in design codes may be the potential cause of these inconsistencies. An inappropriate use of n'' was identified by Haldimann et al. (2008) in equation (2) in CAN/CGSB-12.20-M89, which fixed n'' at a single value of 15. The coefficient n'' is the same as the exponential coefficient s in the modification

---

[13] Note that full-scale glass breakage tests used for the validation of the current numerical simulation were conducted using the worst combination of glass surface side and loading (e..g. combination of tin side and suction pressure). Hence, this numerical simulation outputs the worst true *LR* values among those produced from possible combinations of glass surface side and loading.

of Brown's integral reproduced in equation (1.2), which generally takes a smaller value than the coefficient n used in Brown's integral (n =16 in equation (1.1)). Since s was found to vary depending on glass geometry and support conditions by several researchers, as discussed in Chapter 2, providing a single value of n'' for all glass geometries seems to be inappropriate and hence, this criticism is likely to be correct.

5.2.3 Design load

The main source for *DL* in the United States is ASCE 7-05, which specifies the acceptable wind load coefficients for the structural system and cladding components. The *DL* obtained from ASCE 7-05 is essentially a peak pressure normalized by a 3-sec gust wind speed with a return period of 50 years. Note that the time duration of 3 sec used in ASCE 7-05 is based on the capacity (frequency response) of an anemometer to measure the velocity and the duration of gust in wind, while the pressure coefficients are of much shorter duration. According to the suggested method, *DL* needs to be an equivalent static load for the time duration of t_{ref} which has the same damage accumulation as the extreme wind pressure time history in the specific design situation. In addition, the reference time duration t_{ref} for the conversion to $p_{eq}(t_{ref})$ must be the same as the one used for *LR*. Since the *LR* defined in ASTM E 1300-07 uses a reference time duration of 3 sec, unless $p_{eq}(t_{ref}$=3 sec) is equal to the peak pressure specified in ASCE 7-05 under the same design situation, the use of peak pressures from ASCE 7-05 is not adequate to compare the *LR* from ASTM E 1300-07. In the case that $p_{eq}(t_{ref}$=3 sec) is

less than the peak pressure specified in ASCE 7-05—that is to say, the load duration of an equivalent static load whose pressure is the same as the peak pressure from ASCE 7-05 is less than 3 sec—the current *DL* would be overestimated; hence, the design would err on the side of safety. However, if the case is opposite, the peak pressure from ASCE 7-05 will be underestimated for the use as *DL*, and the current glass design method would err on the side of danger.

The practice of using peak pressures from ASCE 7-05 as values for *DL* in glass design is examined herein, in light of the above considerations. Instead of a direct comparison with the peak pressures drawn from ASCE 7-05 (which would involve a large database of many buildings), a peak wind pressure p_{mean_peak} was calculated in the same way as the wind load in ASCE 7-05 for a particular building model (see, e.g., Kopp et al. 2005). Then, t_{ref}–sec equivalent static load whose pressure level is p_{mean_peak} was calculated by Brown's integral for the same building model, as discussed further detail, below.

5.2.3.1 Design cyclone

In order to create a pressure time history for the purpose of this analysis and realistic with respect to natural windstorms, the "design" cyclone generation method, developed by Jancauskas et al. (1994), was employed. A "design" cyclone (DC) is a pressure time history which considers the variation of wind speed and direction during the passage of cyclone. The length of this cyclone is assumed to be five hours.

Figure 5.2 shows the variations of a 10-min mean wind speed at a height of 10 m in open country terrain, $V_{10m,\,o.c,\,10min}$, and of a wind direction. In the current analysis, the peak wind speed, occurring at around 2.5 hours of the cyclone duration, coincided with the most severe design wind speed specified in ASCE 7-05, which is a 3-sec gust wind speed of 150 mph ($=V_{10m,o.c,\,3sec}$). Thus, the 10 min peak wind speed ($=V_{10m,o.c,\,10min}$) in Figure 5.2 becomes 47 (m/sec), using peak to mean gust factor of 1.41. In order to preserve the simplicity of the calculation, the 5 hour wind speed and wind direction variations were divided into 10-min segments, which create thirty 10-min means of wind speed and wind direction data, assuming that they are constant during these time intervals.

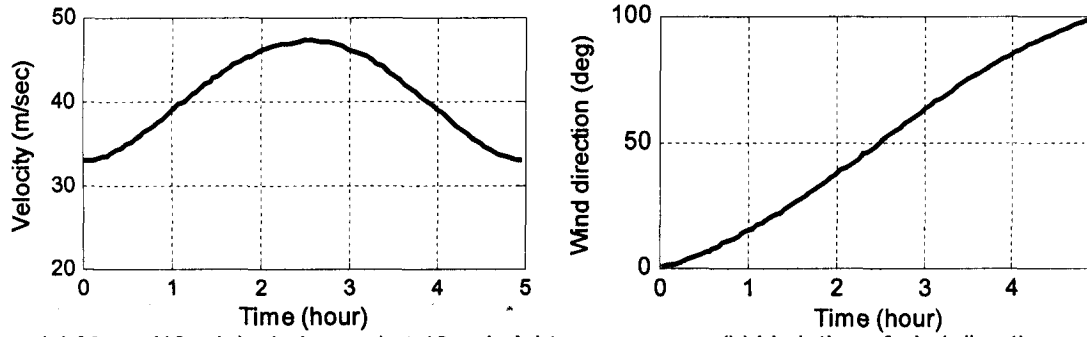

(a) Mean (10 min) wind speed at 10 m height (b) Variation of wind direction

Figure 5.2 Variation of mean wind speed and direction

The wind pressure experienced on part of a building during the passage of the DC was determined by combining the variations of wind speed and wind direction obtained above with pressure coefficients, C_p, measured in a wind tunnel. Time series from the NIST aerodynamic database were employed for this purpose. The building model configuration chosen for this analysis has full-scale plan dimensions of 38.1 m x 24.4 m;

a building height of 9.75 m; a roof slope of 1:12; and a surrounding exposure of open country terrain. All the parameters necessary for this analysis are summarized in Table 5.1, and the reader is referred to Ho et al. (2005) for details. The obtained C_p time series in the NIST aerodynamic database were referenced to the mean hourly wind speed measured at model roof height H in the open exposure, $V_{H,\text{o.c, meanhrly}}$.

Table 5.1 Wind tunnel test parameters

Model scale	1:100
Model sampling rate	500 Hz
Sampling period	100 sec
Test angles	180° to 360° with increment of 5°
Mean wind tunnel speed at 10 m (full-scale equivalent)	8.8 (m/sec)

Area-averaged pressure coefficients, referenced to the model roof height, $C_{p\_area\_averaged}$, with a tributary area of 1m^2 (in full-scale) were obtained for all possible areas on the gable end wall (i.e., the windward wall when wind direction $\theta = 0^\circ$). The location with the largest mean value for $C_{p\_area\_averaged}$ was selected (Figure 5.3) for analysis. Three different building orientations, relative to the DC, were selected, as follows (Figure 5.4):

- BO1 : The "target area" experiences positive $C_{p\_area\_averaged}$ for nearly the entire passage of the DC, and that the wind direction which causes the largest positive wind pressure to the target area coincides with the time of the peak wind speed (at around 2.5 hours)
- BO2 : The "target area" experiences negative $C_{p\_area\_averaged}$ for nearly the entire passage of the DC, and that the wind direction which causes the largest negative

wind pressure to the target area coincides with the time of the peak wind speed (at around 2.5 hours)

- BO3 : The "target area" experiences both positive and negative $C_{p\_area\_averaged}$ for almost the same time duration during the passage of the DC.

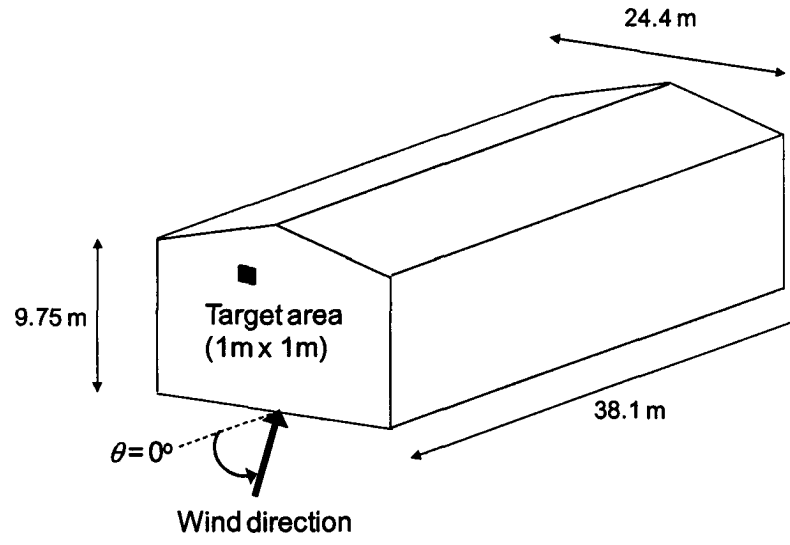

Figure 5.3 Full-scale dimension and target area location on wind tunnel model building

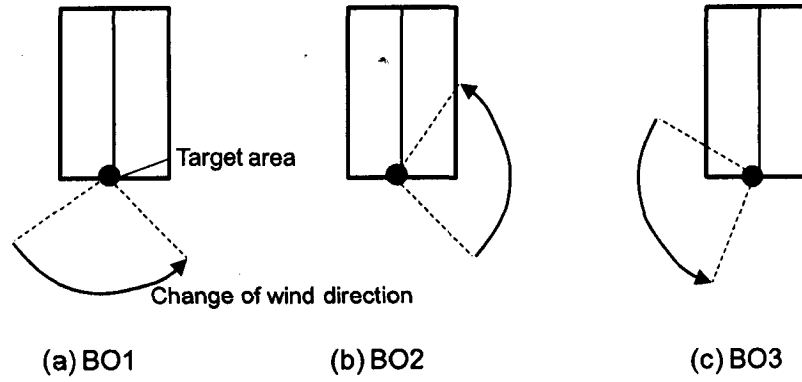

Figure 5.4 Wind direction change for each building orientation

A sensitivity check was performed to determine the degree of variation within the final results of this analysis (i.e., the equivalent static load), which may result from using different portions of the $C_{p\_area\_averaged}$ time series to create the DC. For this sensitivity check, the following three approaches were used to obtain the relevant portion of the $C_{p\_area\_averaged}$ time series:

- Approach 1: Consider the 10-min portion of the DC which experiences the i^{th} (i =1~30) largest 10-min mean wind speed during the entire cyclone. The $C_{p\_area\_averaged}$ time series corresponding to the wind direction for this 10-min portion was divided into 30 equal segments. The 30 peak $C_{p\_area\_averaged}$, $\hat{C}_{p\_area\_averaged}$ from each segment were obtained and the part of the $C_{p\_area\_averaged}$ time series whose length is 10 min in full-scale[14] and which contains the i^{th} largest peak $\hat{C}_{p\_area\_averaged}$ in its middle was utilized;
- Approach 2: The $C_{p\_area\_averaged}$ time series corresponding to the wind direction for a certain 10-min portion was divided into 30 segments and the 30 $\hat{C}_{p\_area\_averaged}$ from each segment were obtained. The part of the $C_{p\_area\_averaged}$ time series whose length is 10 min in full-scale and which contains the largest peak $\hat{C}_{p\_area\_averaged}$ in its middle was utilized for each 10-min portion of the DC;
- Approach 3: For each 10-min portion of the DC, a randomly selected part of the $C_{p\_area\_averaged}$ time series corresponding to the wind direction for a certain 10-min portion, was utilized.

---

[14] The number of data points corresponding to 10-min in full-scale changes depending on the wind speed in the 10-min portion of "design" cyclone.

For all three approaches mentioned above, the part of the $C_{p\_area\_averaged}$ time series for a particular 10-min portion of the DC was multiplied by pressure velocity ($0.5\rho V_{H,\,\text{o.c.,}\,\text{meanhrly}}$ where ρ is the air density and $V_{H,\text{o.c, meanhrly}}$ is the wind speed converted from a 10-min mean of $V_{10\text{m, o.c, 10min}}$ from Figure 5.2 using a value of 1.06) to obtain 10-min portion of the pressure time history. The DC pressure time history was created by combining all thirty 10-min portion of the pressure time histories. The ones calculated by Approach 3, for all three building orientations, are shown in Figure 5.5.

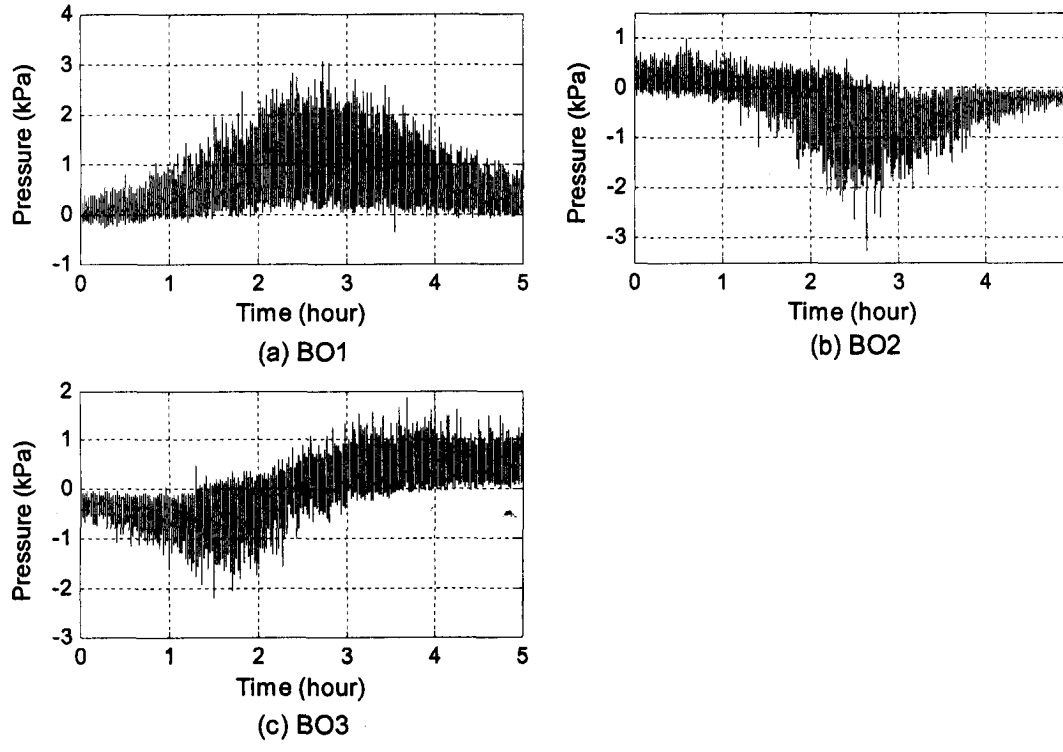

Figure 5.5 "Design" cyclone external pressure time history

5.2.3.2 Peak wind pressure p_{mean_peak}

The peak wind pressure in the interior wall region of this building model was calculated as follows: the pressure time histories at all locations and for all wind directions, part of which are also used for the generation of DC, were divided into 10 equal segments. For each segment, the peak pressure was identified and the Lieblein BLUE formulation (Lieblein 1974) was performed. The outputs of this analysis are the mode and dispersion of the Gumbel distribution. Using these parameters, the mean peak wind pressure for each time history was determined. The worst value among mean peak wind pressures at all locations and for all wind directions was determined to be the mean peak wind pressure for the selected building model, p_{mean_peak}. Researchers recognise this mean peak value of the pressure as a more statistically-reliable value than the actual recorded peak. By taking this approach, p_{mean_peak} may be considered identical to the wind load specified in ASCE 7-05 for a particular design situation (e.g., Kopp et al. 2005). Evaluation of the actual wall pressure coefficients in wind tunnel data and comparing with the ASCE 7-05 is an additional task beyond the scope of the current work. Thus, the present analysis assumes that there is a perfect match between the wind tunnel data utilized herein and the ASCE 7-05 coefficients.

5.2.3.3 Reference time duration of equivalent static load

Using a modification of Brown's integral (equation (1.2))) and the DC pressure time history, $p(t)$, a reference time duration t_{ref} of an equivalent static load whose pressure level is the same as p_{mean_peak} obtained in section 5.2.3.2 was calculated from:

$$t_{ref} = \int_0^T p^s(t)dt \Big/ \left(p_{mean\_peak}\right)^s \tag{5.4}$$

where T is the length of DC, which is 5 hours in the current study.

As mentioned in Chapters 2 and 3, the coefficient s in equation (5.4), for the window glass size in question (1 m^2), varies depending on each researcher's experimental results. In order to show the possible range which t_{ref} could take, depending on s, t_{ref} was calculated using various values of s (10~13) for the current window size (1 m^2). Note that either only positive or only negative pressure, whichever was dominant during the whole pressure trace, was used for this calculation. For example, since positive pressure was dominant in BO1, negative pressure of the DC was set to be zero, i.e., as having no effect on damage accumulation, since only surface tensile stresses are important.

5.2.3.4 Comparison of t_{ref}

The results are shown in Figure 5.6 and, as explained earlier, three different approaches were used to calculate t_{ref}. As expected, the value of t_{ref} calculated by Approach 2 yields the largest value in all building orientations. In general, we may conclude that the different approaches for obtaining the relevant portions of the $C_{p\_area\_averaged}$ time series have significant influence on the calculation of t_{ref} but its degree changes depending on the characteristics of the DC pressure time history.

In terms of the effect of different s values, there is no discernable relationship between t_{ref} and s. Based on equation (5.4), t_{ref} increases as s decreases when the total damage accumulation from the DC and the reference pressure level, p_{mean_peak}, are the

same. However, if the total damage accumulation from the DC changes as a result of different s values, which is the case, the variation of t_{ref} as a function of s depends on the magnitude relationship between total damage accumulation from the DC and p_{mean_peak}. On the one hand, as s becomes larger, the increase of $(p_{mean\_peak})^s$ becomes more rapid than the one of total damage accumulation from the DC in the case of BO2, approach 2, and t_{ref} decreases. On the other hand, the increase of $(p_{mean\_peak})^s$ is slower than that of total damage accumulation from the DC in the case of BO1, approach 2, and hence, t_{ref} increases with s. Thus, although the variation of s certainly has a significant effect on t_{ref}, the variation of t_{ref} as a function of s has no uniform tendency.

In the United State, the reference time of LR is 3 sec. Therefore, if t_{ref} shown in Figure 5.6 is less than 3 sec, the use of peak pressure as DL is regarded as appropriate. In the case of BO1, t_{ref} is larger than 3 sec for all values of s and all approaches, being in the range of 13 to 53 sec, indicating that the use of peak pressure for 3 sec underestimates DL. In the cases of BO2 and BO3, t_{ref} is less than 3 sec at all s values.

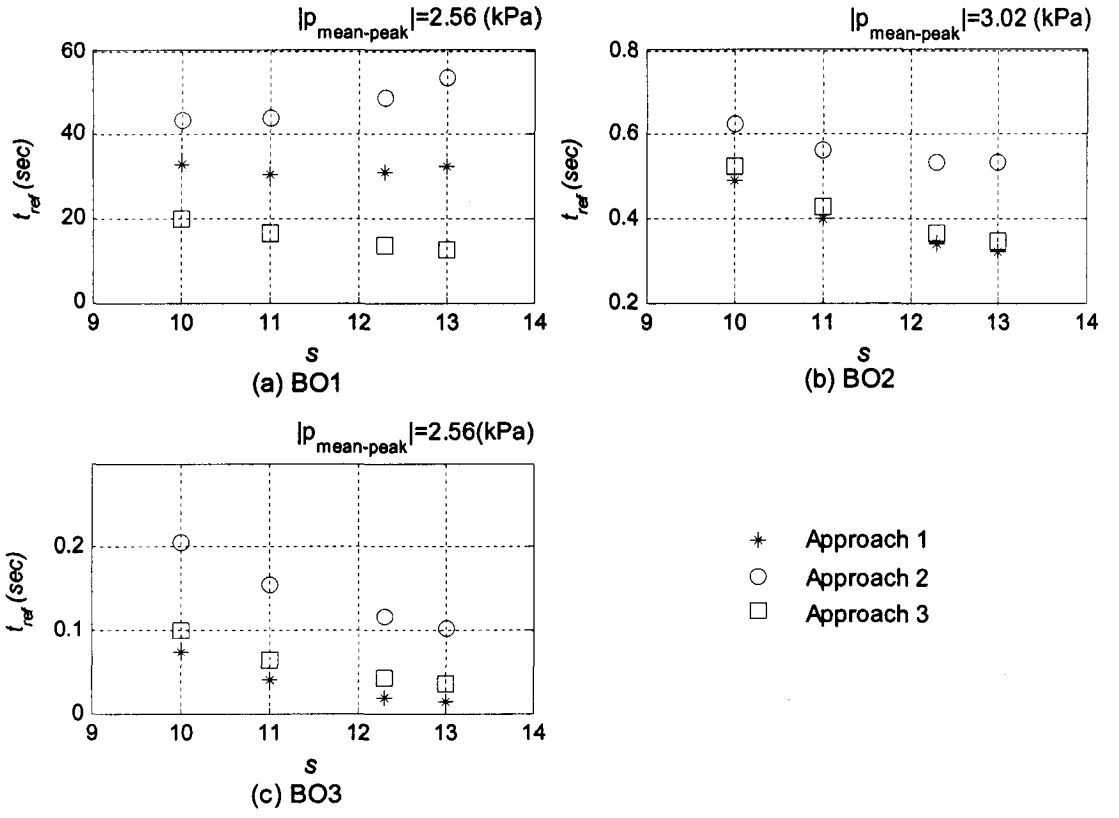

Figure 5.6 Comparison of t_{ref}

However, realistically speaking, window glass should not possibly be designed to survive only one windstorm in its lifetime (or storms can be substantially longer than 5 hours). Moreover, window glass panels on buildings which did not receive any extensive glazing damage but were located in the path of windstorms are unlikely to be replaced even though their strength may have been reduced due to pressure and also "chips" caused by small windborne debris. Hence, the same calculation was conducted considering not merely one 5-hour DC, but rather a longer duration of DC by considering a series of DC's below. Although Dalgliesh has reported that some recovery of strength can occur in glass during sufficiently long intervals between load applications (Dalgliesh

1979), the author has not succeeded in locating a detailed study on this topic. Therefore, we presumed recovery of glass strength to be zero for the purpose of this calculation. Even though the difference between the approaches was not always small, all the calculations were performed using the DC obtained by Approach 3. It is because this approach may be closest to the most common practice, and it delivered the most favourable results to support the use of peak pressures from ASCE 7-05 as *DL* in Figure 5.6.

Figure 5.7 shows t_{ref} for three building orientations which experience 5- to 25-hours of DC. Since t_{ref} and damage accumulation from the DC have a linear relationship in Brown's integral in equation (5.4), t_{ref} increases linearly in proportion to the number of repetitions of the DC. In BO2, although t_{ref} at all s values is still less than 3 sec, the difference between 3 sec and t_{ref} is not longer necessarily large . This indicates that cases may exist where the current practice of calculating *DL* underestimates its value when more severe windstorms are considered than just one 5-hour windstorm or comparable storm. Since the characteristics of windstorms—such as intensity, size and duration—as well as their occurrence frequency vary depending on location and year-to-year variation, it is impossible to draw a definite conclusion from this analysis without further statistics. However at least, this analysis could infer that the use of peak pressures from ASCE7-05 could possibly underestimate the value for *DL* in glass design depending on windstorm characteristics and design situations. Clearly, long duration hurricanes with significant wind speeds could cause serious issues.

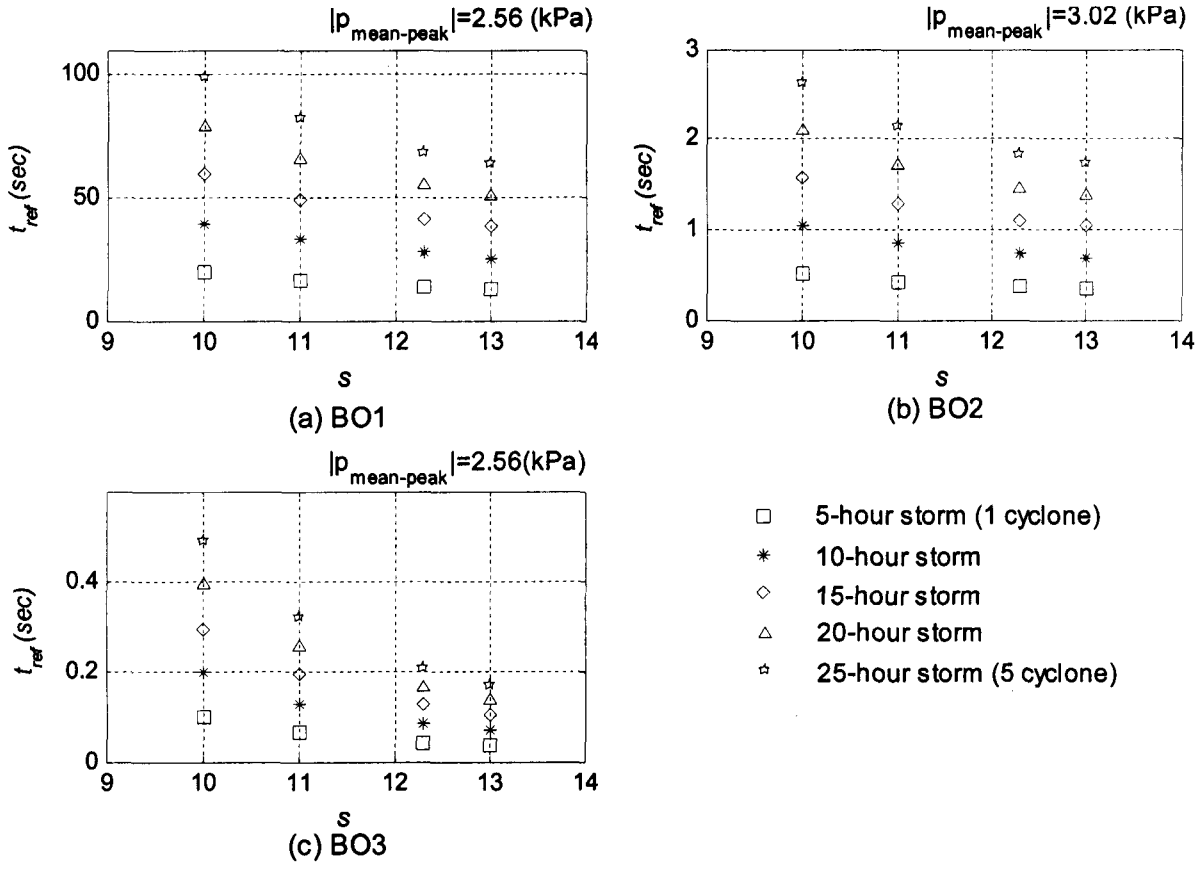

Figure 5.7 Comparison of t_{ref} for numbers of "design" cyclones

5.3 Summary and conclusions

The current North American window glass design method was re-examined in terms of *LR* and *DL*. For *LR*, the value from ASTM E 1300-07, CAN/CGSB-89 and the glass failure numerical simulation developed in Chapter 4 were compared within the same design situation. It was found that both ASTM E 1300-07 and CAN/CGSB-89 produce smaller value for *LR* than the numerical simulation when new window glass coefficients are used. We also note that the use of initial glass strength of weathered

window glass reduces the value of *LR* substantially, much more than the use of minimum glass thickness. If *LR* from the codes is compared with the numerical simulation using the weathered glass initial strength, the codes tend to overestimate this value. Provided that assumed input used in the calculation of *LR* in the codes is the best estimate for the current state of knowledge and technology, this points to potential problems in the code values for the case of weathered glass. In addition, the conversion method for adjusting different reference time durations, t_{ref}, in these codes may require re-examination.

For *DL*, a peak wind pressure (obtained in the same manner as peak pressures in ASCE7-05, p_{mean_peak}), and an equivalent load (whose pressure level is p_{mean_peak} with a reference time of t_{ref} using a modification of Brown's integral), were calculated using the pressure time history wind tunnel data obtained from a low-rise building. The results of t_{ref} indicates that the use of peak pressures from ASCE7-05 as *DL* is approximately adequate when only one 5-hour DC passage is considered with actual reference times, t_{ref}, for positive pressures being 13-53 sec, not 3 sec. However, when different windstorm characteristics and design situations are assumed, the current design practice may underestimate *DL* to an unacceptable degree.

6.0 Conclusions and recommendations

6.1 Conclusions

Recent glazing damage during windstorms, the development of the current window glass design process, and findings from the previously-conducted research have all motivated this study. This research has attempted to examine the behaviour of glass under wind pressure loads by performing full-scale glass breakage tests under several different loading configurations and a numerical simulation which can predict various types of information regarding glass panel failure. The full-scale glass breakage tests revealed that glass failure may only be understood properly through damage accumulation. Glass failure pressure and time can be predicted with relative ease by unique characteristics appearing in certain loading patterns, all of which originate from damage accumulation. However, none of these characteristics are applicable for the prediction under fluctuating wind loads. Although it is altogether possible to predict failure pressure and time under ramp and saw-tooth loadings, these variables are not in and of themselves determinative of glass failure, and therefore improperly used in glass design. Instead, critical damage accumulation, which is invariant for different loading patterns and their parameters, needs to be utilized.

While the full-scale glass breakage tests yielded new findings about glass failure, their results were also used for the validation of the glass failure prediction numerical simulation which was selected to be the most suitable among various existing methods.

Without any modification, the numerical simulation predicts failure pressure and time reasonably well except at larger failure probability levels. In order to hone it to a more precise prediction tool, a modification regarding the initial glass strength was implemented. The modified numerical simulation gives better prediction results than the original one and captures the fact that the initial glass strength plays an important role in glass failure.

Based on the results and knowledge gained from these studies, two glass design methods were suggested in order to overcome the shortcomings found in the current window glass design with the use of an equivalent static load which can represent the critical damage accumulation easily. One is an individual analysis that can output precise information necessary for design, but may be more expensive than the other option. The other design method is the use of design codes. For the purposes of fully considering the second method, a thorough examination of the current North American window glass design code was carried out. Based on this assessment's results, current codes seem to have smaller load resistance (*LR*) value compared to the numerical simulation results for new glass. However, *LR* from the codes is likely to be overestimated compared to the results from numerical simulation when the weathered glass initial strength is used. This result indicates the possible problems in the codes' value. Moreover, a conversion method for a certain reference time duration, t_{ref}, in ASTM E-1300-07 and CAN/CGSB-89 may require an examination. Regarding design load (*DL*), the code accurately sets values for *DL,* but only where one passage of a representative windstorm is considered.

Otherwise or a duration of windstorm is considerably long, it has a possibility of underestimating this value.

6.2 Recommendations

The following subjects must be investigated for the realization of the proposed window glass design method:

- Reliable information regarding parameters which quantify initial glass strength (A'', n', S_0, m, K_{Ii})
- Statistical information of windstorm characteristics (intensity, size and duration)
- Validation of the current failure probability used in design code (8/1000)

The current study selected relatively simple parameters for testing and the numerical simulation (monolithic, annealed, 1 x 1 x 0.006 m glass plate in a simply-support condition) in order to obtain a fundamental understanding of glass failure under pressure loadings. However, it is not necessarily true that findings and modeling methodology from the instant research are applicable to different cases (glass type, glass geometry, support condition).

According to Kawabata (1996), for example, since glass panels installed in buildings are usually supported by materials which may deform, an elastic-support condition may simulate the closest representation of actual support conditions. Fortunately, an elastic-support condition is unlikely to cause a large difference in the induced principal stresses on a glass panel at the design pressure level compared to the

simply-support condition (Kawabata 1996). In order to deepen our knowledge of glass failure under pressure loadings, and to make the output applicable to design, it behoves us to extend this work to other glass types, geometries and support conditions which reflect actual window glass practice and its installation.

Clearly, the most important quantity in this research is critical damage accumulation. Through the present study, it was at least shown that the obtained test results did not present any disagreement with the assumption that the critical damage accumulation is independent of loading patterns and their parameters. As mentioned in Chapter 2, the critical damage accumulation is believed to be dependent on several parameters. However, which particular parameters of these may be has not been conclusively demonstrated. Ideally, further investigation of this matter would yield results which would further assist in improving design practice.

REFERENCES

Abiassi, J.J. (1981). "The strength of weathered window glass using surface characteristics." Inst. for Disaster Res., Texas Tech. University, Lubbock, Tex.

Allen, A.E., Dalgliesh, W.A. (1973). "Dynamic wind loads and cladding design." *Int. Assoc. of Bridge and Structural Engineering Symp. on Resistance and Ultimate Deformability of Structures*, Lisbon, Portugal, 279-285.

ASCE. (2005). "Minimum design loads for buildings and other structures." *ASCE 7-05,* Reston, Va.

ASTM. (1994). "Standard practice for determining the minimum thickness and type of glass required to resist a specific load." *ASTM E 1300-94*, Philadelphia, Pa.

ASTM. (2001). "Standard specification for flat glass." *ASTM C 1036-01*, Westshohocken, Pa.

ASTM. (2002). "Standard practice for determining load resistance of glass in buildings." *ASTM E 1300-02*, West Conshohocken, Pa.

ASTM. (2006). "Standard terminology of building constructions." *ASTM E 631-06*, West Conshohocken, Pa.

ASTM. (2007). "Standard practice for determining load resistance of glass in buildings." *ASTM E 1300-07*, West Conshohocken, Pa.

Beason, W.L. (1980). "A failure prediction model for window glass." Ph.D. Thesis, Texas Tech. University, Lubbock, Texas.

Beason, W.L., Kohutek, T.L., and Bracci, J.M. (1998). "Basic for ASTM E 1300 annealed glass thickness selection charts." *J. Struct. Eng.,* 124 (2), 215-221.

Beason, W.L., Meyers, G.E., and James, R.W. (1984). "Hurricane related window glass damage in Houston." *J. Struct. Eng.*, 110 (12), 2843-2857.

Beason, W.L., and Morgan, J.R. (1984)." Glass failure prediction model." *J. Struct. Eng.,* 110 (2), 197-212.

Block, V. (2002). " New Version of Glass strength Standard is Major Departure." *Glass Magazine*, Glass Association of North America (GANA).

Bowles, R., and Sugarman, B. (1962). "The strength and deflection characteristics of large rectangular glass panels under uniform pressure." *Glass Technol.*, 3(5), 156-170.

Brewick, P., Divel, L., Butler, K., Bashor, R., and Kareem, A. (2009). "Consequence of urban aerodynamics and debris impact in extreme wind events." *11th Americas Conference on Wind Engineering*, American Association for Wind Engineering, San Juan, Puerto Rico.

Brown, W.G. (1972). "A load duration theory for glass design." *Pub. No. NRC* 12354, National Research Council of Canada, Ottawa.

Brown, W.G. (1974). "A practicable formulation for the strength of glass and its special application to large plates." *Pub. No. NRC* 14372, National Research Council Canada, Ottawa.

Caldelone, I.J. (1999). "The equivalent wind loading for window glass design." Ph.D. thesis, Depertment of Mechanical Engineering, Monash University, Clayton, Australia.

Cardano, G. (1954). "Ars Magna", Sive de Regvlis Algebracis Unus, Chapter XXXVII.

Canadian General Standard Board (CAN/CGSB). (1989). "Structural design of Glass for Buildings." *CAN/CGSB-12.20-M89*, National Standard of Canada, Canada.

Charles, R.J. (1958a). "Static fatigue of glass. I." *J. Appl. Phys.*, 29 (11), 1549-1553.

Charles, R.J. (1958b). "Static fatigue of glass. II." *J. Appl. Phys.*, 29 (11), 1554-1560.

Charles, R.J. (1958c). "Dynamic fatigue of glass." *J. Appl. Phys.*, 29 (12), 1657-1662.

Charles, R.J., and Hillg, W.B. (1962). "The kinetics of glass failure by stress corrosion. Proceedings", *Symposium sur la resistance machanique du verre, et les moyens de l'ameliorer*, Union Scientifique Continentale du Verre, Charleroi, Belgium, 511-527.

Dalgliesh, W.A. (1979). "Assessment of wind loads for glazing design." *Symp. on Practical Experiences with Flow-Induced Vibrations*, Karlsruhe, Germany, 696-708.

Dalgliesh, W.A. and Taylor, D.A. (1990). "The strength and testing of window glass." *Can. J. Civ. Eng.*, 17, 752-762.

Dauskardt, R.H. (1993)." A frictional-wear mechanism for fatigue-crack growth in grain bridging ceramics." *Acta metal. matar.*, 41 (9), 2765-2781.

Davenport, A.G. (1975). "Discussion of 'Wind pressures on buildings-probability densities' (complete text)." *Res. report BLWT-4-1975*, The Boundary Layer Wind Tunnel Laboratory, The University of Western Ontario, Canada.

Davenport, A.G. (1983). "Notes on the reliability of glass under wind action." *Res. report BLWT-2-1983*, The Boundary Layer Wind Tunnel Laboratory, The University of Western Ontario, Canada.

Dill, S.J., Bennison, S.J., and Dauskardt, R.H. (1997). "Subcritical crack-growth behavior of borosilicate glass under cyclic loads: Evidence of a mechanics fatigue effect." *J. Am. Ceram. Soc.*, 80 (3), 773-776.

European Committee for Standardisation (CEN). (1999). "Glass in building –Design of glass panes –part1: General basis of design." *prEN 13474-1*, Draft European Standard, Brussels, Belgium.

European Committee for Standardisation (CEN). (2000). "Glass in building –Design of glass panes –part2: Design for uniformly distributed load." *prEN 13474-2*, Draft European Standard, Brussels, Belgium.

Evans, A.G. (1974). "Slow crack growth in brittle materials under dynamic loading." *Int. J. Fract.*, 10 (2), 251-259.

Evans, A.G., and Fuller, E.R. (1974). "Crack propagation in ceramic materials under cyclic loading conditions." *Metallurgical Transactions* 5, 27-33.

Evans, A.G., and Wiederhorn, S.M. (1974). "Proof testing of ceramic materials – an analytical basis for failure prediction." *Int. J. Fract.*, 10 (3), 379-392.

Fischer-Cripps, A.C. (2007). "Introduction to contact mechanics" *Mechanical engineering series*, 2nd edition, Springer.

Fischer-Cripps, A.C., and Collins, R.E. (1995). "Architectural glazings: Design standards and failure models." *Build. Environ.*, 30 (1), 29-40.

Fuller, E., Wiederhorn, S.M., Ritter, J.E., and Oates, P.B. (1980). "Proof testing of ceramics: Part II: Theory." *J. Mater. Sci.* 15, 2275-2281.

Griffith, A.A. (1921). "The phenomena of rupture and flow in solids." *Phil. Trans. Roy. Soc. London*, Ser. A (221), 163-198.

Haldimann, M. (2006). "Fracture strength of structural glass elements – analytical and numerical modeling, testing and design." Ph.D. Thesis, École polytechnique fedérale de Lausanne.

Haldimann, M., Luible, A., and Overend, M. (2008). "Structural Engineering Document 10, Structural Use of Glass." *International Association for Bridge and Structural Engineering*, Zurich, Switzerland.

Hershey, R.L. and Higgins, T.H. (1973). "Statistical prediction model for glass breakage from nominal sonic boom loads." *Report No. FAA-RD-73-79*, Booz-Allen Applied Research, Inc., Bethesda, MD (NTIS Accession No. AD-763-594).

Hillig, W.B., and Charles, R.J. (1965). "Surfaces, stress-dependent surface reactions, and strength." *High strength materials*, Chapter 17, John Wiley & Sons, New York, 682-701.

Ho, T.C.E., Surry, D., Morrish, D., and Kopp, G.A. (2005). "The UWO contribution to the NIST aerodynamic database for wind loads on low buildings: Part 1. Archiving format and basic aerodynamic data. " *J. Wind. Eng. Ind. Aerodyn.* 93, 1-30.

Holmes, J.D. (1985). "Wind action on glass and Brown's integral." *Eng. Struct.*, 7 (4), 226-230.

Inglis, C.E. (1913). "Stress in a plate due to the presence of cracks and sharp corners." *Trans. Inst. Nav. Archit.*, 55, 219-230.

Irwin, G.R. (1948). "Fracture dynamics." *Fracturing Metals*, American Society for Metals, Cleveland, 147-166.

Irwin, G.R. (1957). "Analysis of stress and strain near the end of a crack traversing a plate." *J. Appl. mechanics*, 24, 361-364.

Ishizaki, H., Miyoshi, S., Miura, T., and Ide, M. (1972). "Effect of duration of gusts on wind resistivity of glass panel." *Proc., 2nd Symp. on wind resistance of structure,* 59-65 (in Japanese).

Ishizaki, H., Miyoshi, S., and Miura, T. (1975). "On the design of glass pane against wind loading." *Proc., 4th Int. Conference Wind Effects on Buildings and Structures*, Cambridge University Press, 655-661.

Jancauskas, E.D., Mehendran, M., and Walker, G.R. (1994). "Computer simulation of the fatigue behaviour of roof cladding during the passage of a tropical cyclone." *J. Wind. Eng. Ind. Aerodyn.*, 51, 215-227.

Johar, S. (1981). "Dynamic fatigue of flat glass – Phase II." *Technical Report 67039,* Ontario Research Foundation, Missisauga, Canada.

Johar, S. (1982). "Dynamic fatigue of flat glass – Phase III." *Technical Report 67049*, Ontario Research Foundation, Missisauga, Canada.

Kanabolo, D.C. and Norville, H.S. (1985). "The strength of new window glass plates using surface characteristics." Glass Res. and Testing Lab., Texas Tech. University, Lubbock, Tex.

Kareem, A, and Bashor, R. (2006). "Performance of Glass/Cladding of High-Rise Buildings in Hurricane Katrina." *Newsletter of American Association for Wind Engineering (AAWE)*, AAWE, 1-5.

Kareem, A., and Stevens, J.G. (1985). "Window glass performance and analysis in Hurricane Alicia." *Hurricane Alicia: One Year Later*, ASCE, 178-186.

Kawabata, S. (1996). "Study on wind resistance design of glass plate for cladding." Ph.D. Thesis, Nippon Sheet Glass Co. Ltd., Japan (in Japanese).

Ko, N.H., You, K.P., and Kim, Y.M. (2005). "The effect of non-Gaussian local wind pressures on a side face of a square building." *J. Wind. Eng. Ind. Aerodyn.* 93, 383-397.

Kopp, G.A., Morrison, M.J., Iizumi, E., Henderson, D., and Hong, H.P. (2008)."The 'Three Little Pigs' Project: Hurricane risk mitigation by integrated wind tunnel and full-scale laboratory test." Submitted to *Nat. Haz. Rev.*

Krall, W.R., Siskos, W.R., Steward, R.A., and Spindler, R.G. (1981). "The behavior of float glass under uniform wind loading." *Preprints of 4th U.S. National Conference on Wind Engineering Research*, University of Washington, Seattle, WA, 155-159.

Kropschott, R.H., and Mikesell, J. (1957). "Strength and fatigue of glass at very low temperature." *J. of applied physics* 28 (5), 610-614.

Li, Q.S., Calderone, I.J., and Melbourne, W.H. (1999). "Probabilistic characteristics of pressure fluctuations in separated and reattaching flows for various free-stream turbulence." *J. Wind. Eng. Ind. Aerodyn.* 82, 125-145.

Lieblein, J. (1974). "Efficient methods of extreme-value methodology." *Report No. NBSIR 74-602*, National Bureau of Standards, Washington, DC.

Mencik, J. (1992). "Strength and Fracture of glass and ceramics." *Elsevier*, Amsterdam.

Minor, J.E. (1981). "Window glass design practices: A review." *J. Struct. Div.*, 107(ST1), 1-12.

Minor, J.E. (1984). "Window glass performance and hurricane effects." *Hurricane Alicia: One Year Later*, ASCE, 151-167.

Minor, J.E., and Beason, W.L. (1976). "Window glass failures in windstorms." *J. Struct. Div.*, 102(1), 147-160.

Minor, J.E., and Norville, H.S. (2006). "Design of window glass for lateral pressures." *J. Archit. Eng.*, 12(3), 116-121.

Miyoshi, S. (1964). "Wind pressure test on glass plate." *Summaries of technical paper of annual meeting* 100, Architectural Institute of Japan, 13-18.

Norville, H.S., Bove, P.M. and Sheridan, D.L. (1991). "The strength of new thermally tempered window glass lites." Glass Res. and Testing Lab., Texas Tech. University, Lubbock, Tex.

Norville, H.S., Bove, P.M., Sheridan, D.L. and Lawrence, S.L. (1993). "Strength of new heat treated window glass lites and laminated glass units." *J. Struct. Eng.*, 119 (3), 891-901.

Norville, H.S. and Minor, J. E. (1985). "Strength of Weathered Window Glass." *Am. Ceram. Soc. Bull.*, 64 (11), 1467-1470.

Orowan, E. (1952). "Fundamentals of brittle behaviour of metals." *Fatigue and Fracture of Metals*, Wiley & Sons, New York, 139-167.

Orr, L. (1957). "Engineering properties of glass - Windows and glass in the exterior of buildings." *Publication 478*, Building Research Institute, National Academy of Sciences, National Research Council, Washington, DC, 51-62.

Overend, M. (2002). "The appraisal of structural glass assemblies." Ph. D. Thesis, Univ. of Surrey, Surrey, U.K.

Overend, M., DeGaetano, S., and Haldimann, M. (2007a). "Diagnostic interpretation of glass failure." *Struct. Eng. Int.*, IABSE, 17(2), 151-158.

Overend, M., Parke, G.A.R., and Buhagiar, D. (2007b). "Predicting Failure in Glass – A General Crack Growth Model." *J. Struct. Eng.*, 133(8), 1146-1155.

Paris, P., and Erdogan, F. (1963). "A critical analysis of crack propagation laws." *J. Basic Eng.*, 85, 528-534.

Peterka, J.A. and Cermak, J. E. (1978). "Wind tunnel study of Atlanta office building." *Fluid Mechanics and Wind Engineering Program*, Colorado State University, Fort Collins, CO.

PPG Industries. (1979)." PPG glass thickness recommendations to meet architects' specified 1-minute wind load." *Technical Services/Flat Glass Division*, PPG Industries, Pittsburgh, Pennsylvania.

Reed, D.A., and Simiu, E. (1984). "Wind Loading and strength of cladding glass." *J. Struct. Eng.*, 110 (4), 715-729.

Reed, D.A. (1993). "Influence of non-Gaussian local pressures on cladding glass." *J. Wind. Eng. Ind. Aerodyn.* 48, 51-61.

Reid, S.G. (1991). "Flaws in the failure prediction model of glass strength." *Proc., 6th Int. conference on the Applications of Statistics and Probability in Civil Engineering (ICASP6)*, Mexico City, Mexico, 111-117.

Seaman, L. (1967). "Response of Windows to Sonic Booms." *Technical Report to U.S. Air Force,* Project ETU-5897, Stanford Research Institute.

Shand, E.B. (1954). "Experimental study of fracture of glass: II, Experimental data." *J. Am. Ceram. Soc.*, 37 (12), 559-572.

Shen, X. (1997). "Entwicklung eines Bemessungs- und Sicherheitskonzeptes fur den Glasbau. Ph.D. Thesis, Technische Hochschule Darmstadt.

Siebert, G. (1999). "Beitrag zum Einsatz von Glas als tragendes Bauteil im konstruktiven Ingenieurbau." Ph.D. Thesis, Technische Universitat Munchen (TUM).

Simiu, E., and Reed, D.A. (1983). "Probabilistic design of cladding glass subjected to wind loads." *4th Int. Conference on Applications of Statistics and Probability in Soil and Structural Engineering*, Universita di Firenze, Italy.

Timoshenko, S., Woinowsky-Krieger, T. (1959). "Theory of plates and shells." *McGraw-Hill Book Company*, 2nd edition.

Tsai, C.R., and Steward, R.A. (1976). "Stress analysis of large deflection of glass plates by the finite element method." *J. Am. Ceram. Soc.*, 59 (9-10), 445-448.

Vickery, P.J., Lin, J., Skerli, P.E., Twisdale Jr, L.A., and Huang, K. (2006). "HAZUS-MU Hurricane Model Methodology. I: Hurricane Hazard, Terrain, and Wind Load Modeling." *Nat. Haz. Rev*, 7(2), 82-93.

Weibul, W. (1939). "A statistical theory of the strength of materials." *Ingeniors Vetenskaps Akademiens*, Handlingar (Royal Swedish Institute of Engineering Research), 151, Stockholm.

Werthwein, P., personal communication, 2007-2009.

Wiederhorn, S.M. (1967). "Influence of water vapour on crack propagation in soda-lime glass." *J. Am. Ceram. Soc.*, 50 (8), 407-414.

Wiederhorn, S.M. (1974). "Subcritical crack growth in ceramics." *Fracture Mechanics of Ceramics vol. 2*, R.C. Bradt, D.P.H. Hasselman, F.F. Lange, eds., Plenum Publishing Corp., New York, NY, 613-646.

Wiederhorn, S.M., and Bolz, L.H. (1970). "Stress Corrosion and Static Fatigue of Glass." *J. Ame. Ceram. Soc.*, 53 (10), 543-548.

Wiederhorn, S.M., Fuller, E.R.Jr, and Thomson, R. (1980). "Micromechanisms of crack growth in ceramics and glasses in corrosive environments." *Metal Sci.* 14, Aug.-Sep., 450-458.

Williams, T., and Kareem, A. (2003). "Performance of building cladding in urban environments under extreme winds." *Proc., 11th Int. Conference on Wind Engineering*, Lubbock, Tex.

APPENDIX A Verification of test rig

A.1 Verification of plywood panel stiffness

The purpose of this test was to check the stiffness of a plywood panel mounted on the front of pressure box to ensure that it would not affect the behaviour of glass plate under pressure. In order to increase the stiffness of the plywood panel under suction (positive pressure was not applied in this pressure box for safety reasons), 2 x 4 timbers were placed inside the box. Since the PLA's performance was shown to improve with a decrease in the pressure box's volume, styrofoam was also inserted. This had the added benefit of adding stiffness to the plywood panel (Figure A. 1).

Figure A. 1 Pressure box with timber and Styrofoam inside

The displacement measurement δ was made by a Laser Displacement Transducer (LDT) at four locations of the plywood panel (Figure A. 2). There are two measuring modes in LDT, long range mode, whose measuring range is ± 100 mm, and precision mode, in which the measuring range is ± 250 mm in LDT. For the purposes of this test,

all measurements were made in "precision mode". In order not to damage the pressure box and to allow enough time for constant measurement, the pressure trace which is a combination of ramp loading and constant loading was applied in this testing (Figure A. 3).

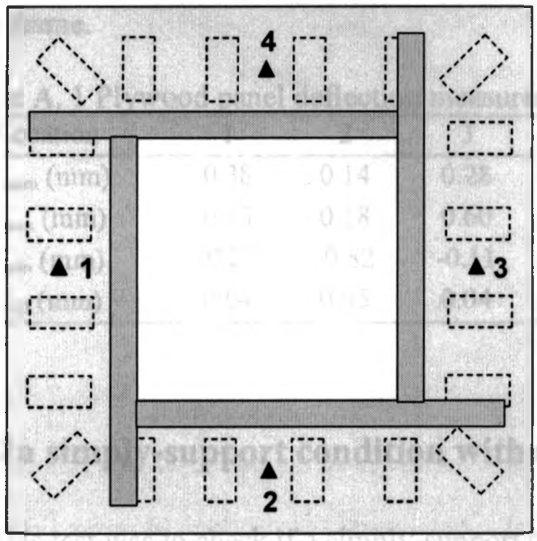

Figure A. 2 Location of plywood panel deflection measurement

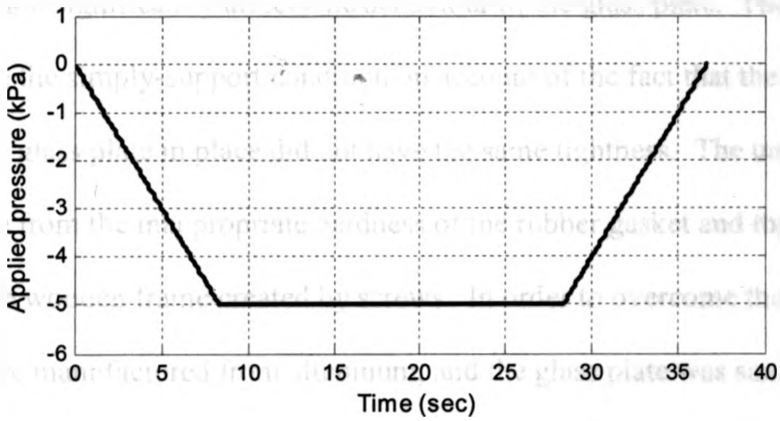

Figure A. 3 PLA pressure trace

Table A. 1 shows the result of this test. The SD of the deflection measurements in all locations is found to be quite small. Although the mean deflection at each location varies slightly, it is less than 1 mm at any given location. Therefore, it is concluded that the plywood panel is rigid enough not to affect the measurements in question on the steel plate and the aluminum frame.

Table A. 1 Plywood panel deflection measurement

Location	1	2	3	4
δ_{mean} (mm)	0.38	0.14	0.28	0.03
δ_{max} (mm)	0.88	0.18	0.60	0.60
δ_{min} (mm)	-0.26	-0.82	-0.11	-0.40
δ_{SD} (mm)	0.04	0.05	0.04	0.04

A.2 Verification of a simply-support condition with steel plate

The purpose of this test was to check if a simply-support condition could be created in the pressure box. The trial tests performed in winter 2007, confirmed that the support condition significantly affects the behaviour of the glass plate. The latter test failed to create the simply-support condition on account of the fact that the four frames which kept the glass plate in place did not have the same tightness. The unequal tightness came from the inappropriate hardness of the rubber gasket and the inconsistent tightness of the wooden frame created by screws. In order to overcome these problems, the frames were manufactured from aluminum, and the glass plate was sandwiched between two aluminum frames with threaded bolts instead of screws. Also, the sides of the glass plate were supported by relatively hard rubber tubes (Figure A. 4).

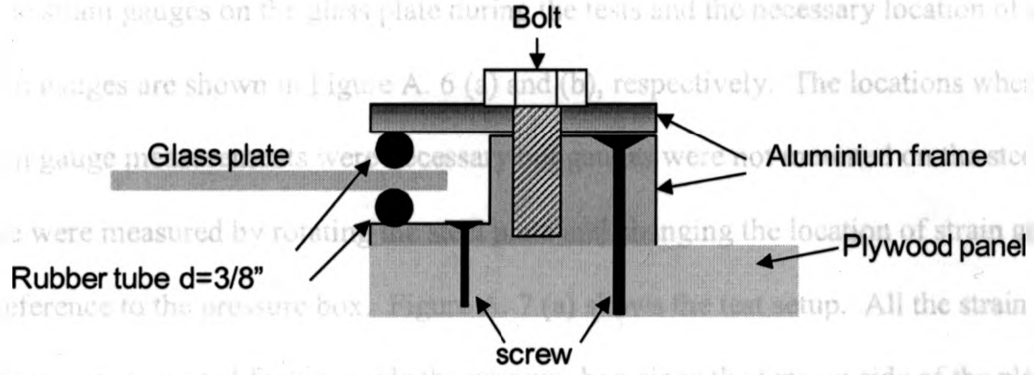

Figure A. 4 Glass support system

A.2.1 Device of deflection and strain measurement

In order to assess whether or not the current frame achieved the simply-support condition, the strain and deflection were measured at certain locations on the steel plate (which can be used for test repeatedly), and the resulting stress was compared with the one from finite element analysis (FEA, Appendix D). The location of the steel plate deflection measurement is shown in Figure A. 5. The *x*-, *y*-, *xy*- (45 degree inclined from *x*- direction) direction normal strains (ε_x, ε_y, ε_{xy}) were measured by three-axial strain gauges, and only one direction of the strain was measured by one-axial strain gauge. Note that in order to calculate the principle stress which would be used to compare the results from FEA, ε_x, ε_y, γ_{xy} (shear strain) were necessary, and γ_{xy} was calculated using the data obtained from measurement and substituted into the following equation:

$$\gamma_{xy} = 2\varepsilon_{xy} - (\varepsilon_x - \varepsilon_y) \qquad \text{(A. 1)}$$

The location where a given axial strain gauge was mounted was where it was known that the maximum principle strain would be equal to either ε_x or ε_y. The actual configuration

of the strain gauges on the glass plate during the tests and the necessary location of the strain gauges are shown in Figure A. 6 (a) and (b), respectively. The locations where the strain gauge measurements were necessary but gauges were not mounted on the steel plate were measured by rotating the steel plate and changing the location of strain gauge in reference to the pressure box. Figure A. 7 (a) shows the test setup. All the strain gauges were mounted facing inside the pressure box since the tension side of the plate under suction loading was the principal concern of this testing (Figure A. 7 (b)). All tests were conducted under the same pressure trace as Figure A. 3.

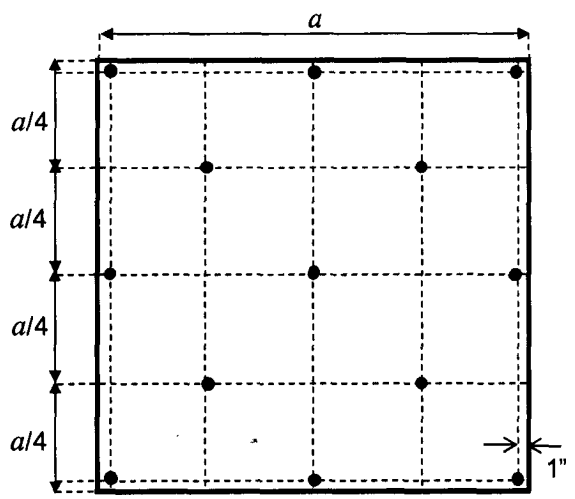

Figure A. 5 Location of steel plate deflection measurement

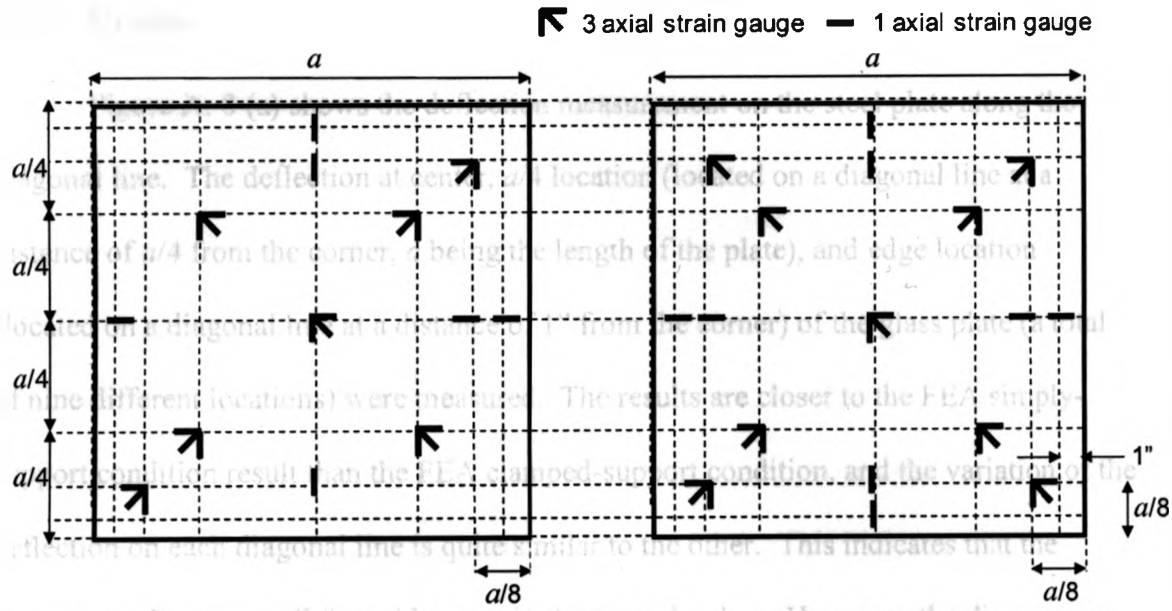

Figure A. 6 Configuration of strain gauge measurement

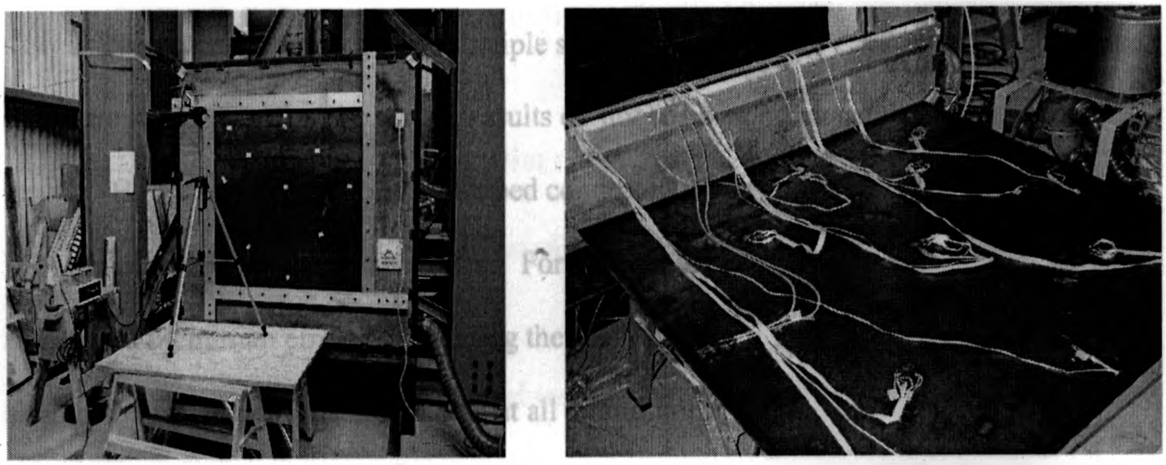

(a) Pressure box (b) Strain gauges on steel plate

Figure A. 7 Test setup

A.2.2 Results

Figure A. 8 (a) shows the deflection measurement on the steel plate along the diagonal line. The deflection at center, *a*/4 location (located on a diagonal line at a distance of *a*/4 from the corner, *a* being the length of the plate), and edge location (located on a diagonal line at a distance of 1" from the corner) of the glass plate (a total of nine different locations) were measured. The results are closer to the FEA simply-support condition result than the FEA clamped-support condition, and the variation of the deflection on each diagonal line is quite similar to the other. This indicates that the support conditions on all four sides are similar to each other. However, the discrepancy between FEA results and measurements becomes larger as the location moves from the corner of the plate to its center.

The calculated maximum principle stress in testing and FEA results are compared in Figure A. 8 (b) - (d). The testing results do not correspond closely to either set of FEA results. However, relative to the clamped condition, the testing results are closer to the FEA simply-support condition results. Fortunately we know that any discrepancy was not caused by human error in tightening the four aluminum frames; in other words, similar support conditions are created at all aluminum frames.

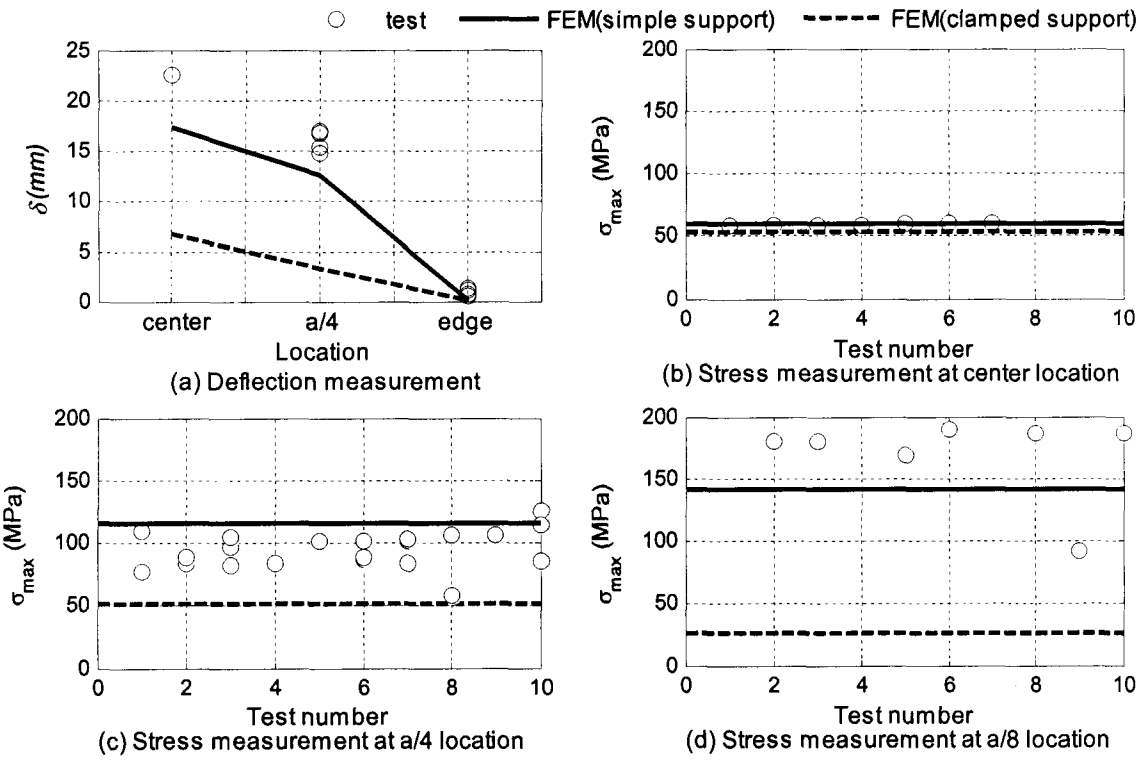

Figure A. 8 Comparison of deflection and principle stress on a glass plate

A.3 Possible explanations for discrepancy

At this point, there are several possible reasons for this incongruous result, such as:

1. The aluminum frame is fixed tighter than it is supposed to be;
2. Several material properties (e.g. Young's modulus, Poisson ratio) are not exactly correct in FEA;
3. The simply-support condition is not successfully reproduced in FEA;
4. SAP 2000 is not the proper FEA software for this type of test;
5. The strain gauges are not working properly; and/or

6. Pressure is not correctly applied by the PLA

In the second place, it is difficult to obtain exact material properties from material suppliers. Therefore, standard values of these properties have been used in FEA.

In the third and fourth place, the FEA results (deflection and stress) were validated by comparing them to those from the theoretical equation (Appendix D), and therefore, these reasons are unlikely to cause the discrepancy.

In the fifth place, different strain gauges at the same location on the steel plate recorded similar values. For this reason, it is unrealistic to consider that all the strain gauge measurements were wrong. However, it is also true that different components of strain gauges at the same location (ε_x, ε_y) sometimes record the different values which are expected to be the same. Based on these results we may conclude that these strain measurements by gauges may be less trustworthy than deflection measurements made by LDTs.

In the sixth place, all pressure traces (input and output) were recorded for each test, and the time history of input and output pressure data matched very well in each testing. The amount of leakage from the pressure box, which could cause significant difference in pressures, was also within the allowable range. Finally, a calibration of the pressure transducer was carried out, and all the testing results were corrected based on the calibration results. Therefore, a difference in pressure is unlikely to have caused the discrepancy.

A.4 Verification of simply-support condition with glass plate and new frames

A.4.1 Description of test 1

Considering the above, the most probable causes for the discrepancy recorded between test and FEA results would be possibilities 1 and 5. In an attempt to resolve the first possible cause, several materials, sizes and tightness of the support head were tested out in the glass plate support system. In terms of materials, silicone tubes and rubber tubes of different diameters [1/2" (12.7mm), 3/8" (9.525mm)] were used, and the tightness of the support was adjusted by adding washers of 1/16" in thickness between the aluminum frames (Figure A. 9).

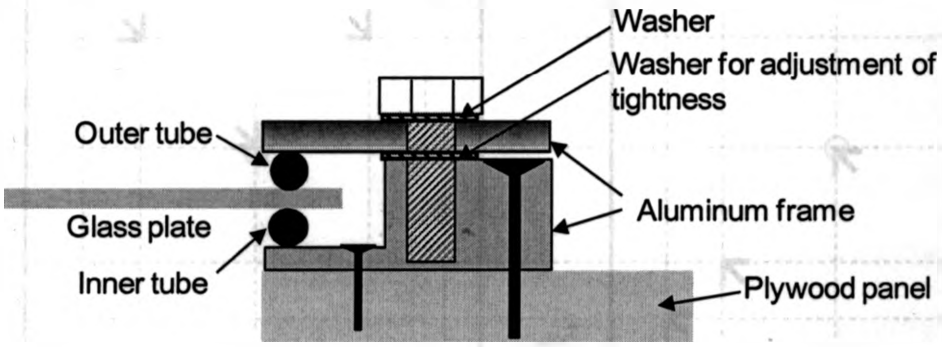

Figure A. 9 New glass plate support system

A sheet of steel of 1 x 1 x 0.003 m had been used in order to conduct the test repeatedly. However, it was discovered that the steel plate was becoming concave toward its center after being exposed to suction pressure several times and this seemed to

have begun causing an error in deflection and strain measurements. Thus, it was decided to use a glass plate of 1 x 1 x 0.006 m for this preliminary test thereafter.

The suitability of the support head was checked by comparing the deflection at the center of the plate and the strains at several locations of the plate from measurement and FEA. Deflection and strain were measured by LDT and strain gauge, respectively. Note that strain gauges were mounted only on ½ of the area of the plate (five three-axial strain gauges) in order to minimise the effect of heat from the soldering iron used to attach the strain gauge to glass plate, and the measurement of the whole plate was achieved by rotating the plate 180° (see Figure A. 10).

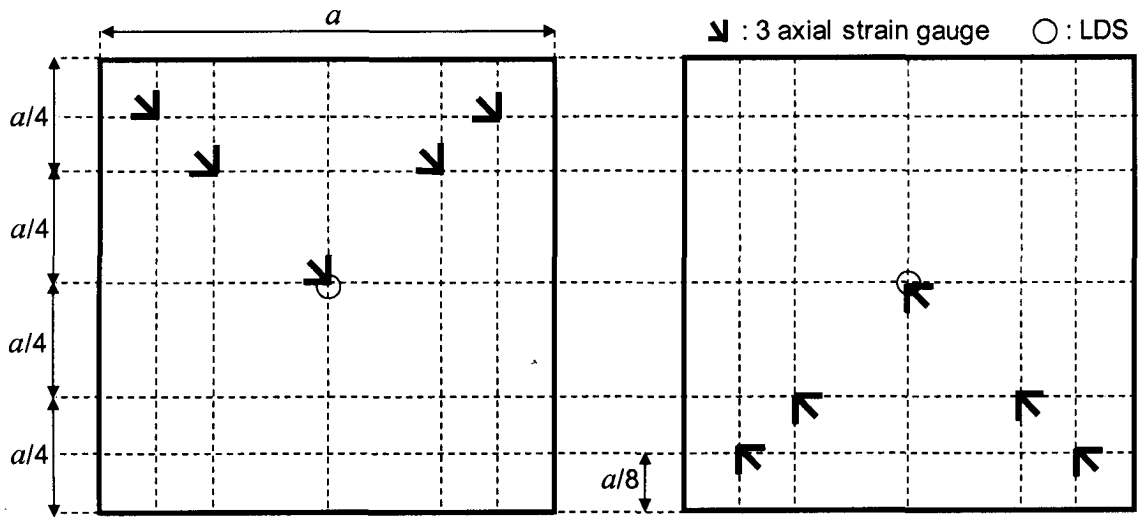

Figure A. 10 Location of LDT and strain gauge measurement on a glass plate

A.4.2 FEA inputs

The commercial software SAP 2000, was utilized, the same which was used for analysis of the steel plate, and the standard material properties of glass were assumed for this analysis as follows:

Young's modulus: E =70.3 (GPa)

Poisson ratio: $\nu' = 0.23$

Density: ρ =2190 (kg/m^3)

Glass should not exhibit large differences in its physical properties from supplier to supplier, and the standard values of material parameters should be quite appropriate for use with an in-service glass plate. The only element which might vary and affect testing results is glass thickness (Werthwein 2007). Therefore, the thickness of glass plate was precisely measured by calliper. The glass plates used in this preliminary test and the following breakage test came from the same supplier, and the average of the measured thickness was 5.79 mm. This falls squarely within the range of dimensional tolerance for transparent flat glass for designation as 6 mm glass plate, as specified in ASTM C1036-01 (ASTM 2001), which is 5.66 – 6.20 mm. For further discussion on the validation of FEA, refer to Appendix D.

A.4.3 Description of test 2

After several trials, three configurations of the support system seemed to be most appropriate. In order to choose the best among the three, and to verify the repeatability of

the measurement, the deflection at center, $a/4$ location and $a/8$ location (located on a diagonal line at a distance of $a/8$ from the corner) of the glass plate were measured. Then, the glass plate was rotated by 90° to measure the strains at different location. This process was repeated four times so that the strain gauge measurements could be captured for the surface of the entire plate. Obtaining several measurements at each location further served to improve the repeatability of the tests (see Table A. 2). The same glass plate with the same strain gauges attached was used in all three configurations. The input pressure trace is shown in Figure A.11.

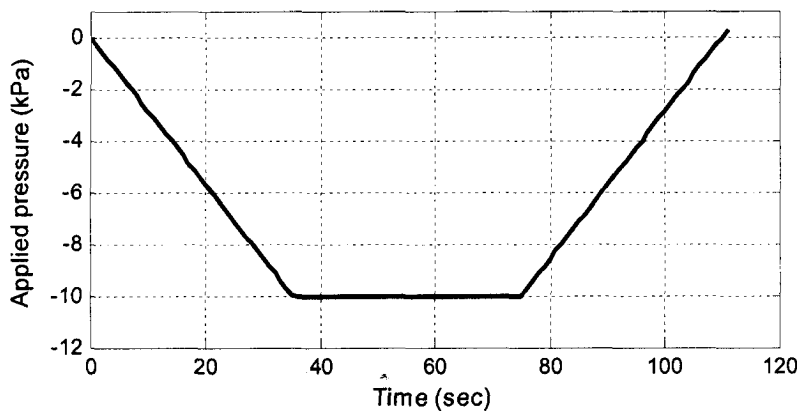

Figure A. 11 PLA pressure trace

Table A. 2 Test arrangement

Displacement	Strain gauge location			
	Upper half	Left half	Bottom half	Right half
Center	Test 1	Test 10	Test 19	Test 28
a/4 upper right	Test 2	Test 11	Test 20	Test 29
a/8 upper right	Test 3	Test 12	Test 21	Test 30
a/4 lower right	Test 4	Test 13	Test 22	Test 31
a/8 lower right	Test 5	Test 14	Test 23	Test 32
a/4 upper left	Test 6	Test 15	Test 24	Test 33
a/8 upper left	Test 7	Test 16	Test 25	Test 34
a/4 lower left	Test 8	Test 17	Test 26	Test 35
a/8 lower left	Test 9	Test 18	Test 27	Test 36

These three configurations of glass plate support system are following:

Configuration 1:

Outer tube: 1/2" (12.7mm) silicone tube, inner tube: 3/8" (9.525mm) rubber tube, tightness: adding 2 washers

Configuration 2:

Outer tube: 3/8" (9.525mm) rubber tube, inner tube: 3/8" (9.525mm) rubber tube, tightness: adding 2 washers

Configuration 3:

Outer tube: 3/8" (9.525mm) rubber tube, inner tube: 3/8" (9.525mm) rubber tube, tightness: adding 1 washer

A.4.4 Results

Comparisons of displacement and strain from testing and FEA are shown in Figure A. 12. Note that all three tests were conducted on different dates, but the testing conditions (temperature, etc.) were monitored and maintained as consistent as possible.

The stresses calculated from strain measurements with assumed E and ν' are significantly lower than those predicted by FEA. Although stress results from the apparent dead strain gauges are not included in the figure, this discrepancy is quite large and thus the strain measurement data must be considered suspect. These measurements may be improved by obtaining the actual material properties (E, ν', etc) from the flexural test.

As for deflection, the measurement results from all configurations are relatively close to those from FEA. However, Configuration 3 in particular enjoys the following advantages over the others:

- The leakage which affects the performance of the PLA under dynamic loading is smaller
- The test setup is relatively easier
- The standard deviation is smaller

For the above reasons, Configuration 3 is selected to be the appropriate support system to create the simply-support condition in the present study.

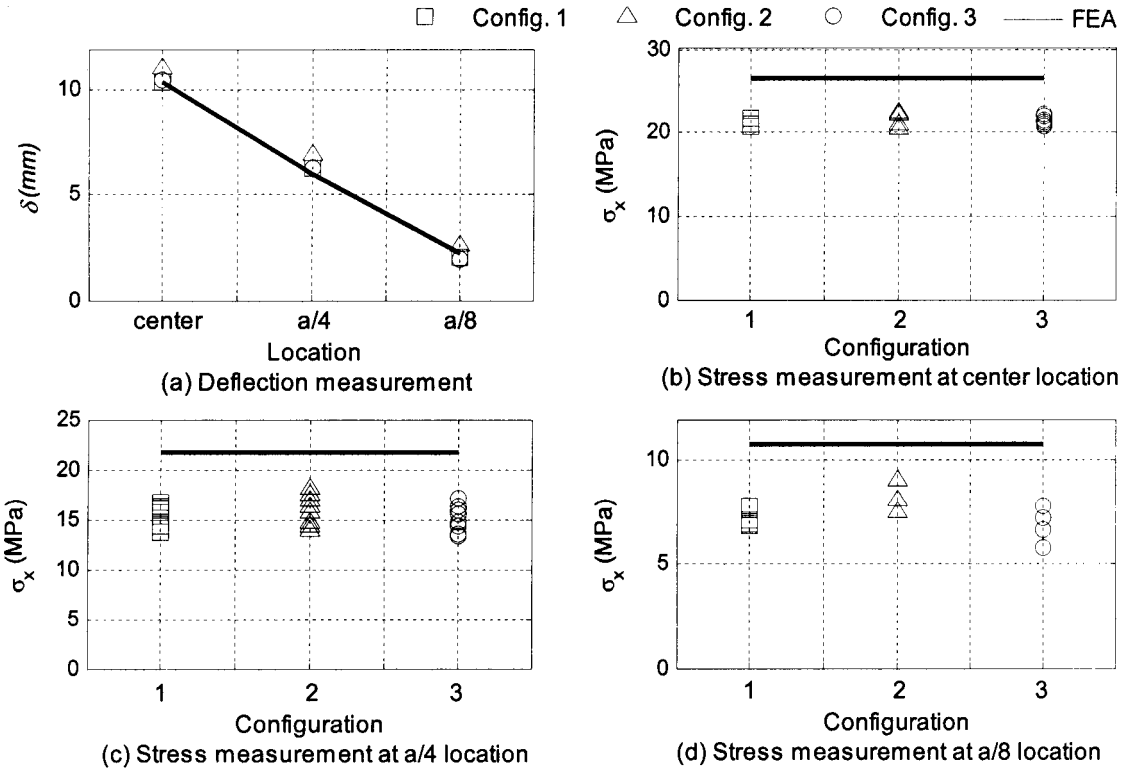

Figure A. 12 Test results

In order to further ensure that the simply-support setup was created on the pressure box using the configuration 3 for glass plate support system during the actual testing, deflection at the center of the plate was measured by a Laser Displacement Transducer at certain applied pressure levels during the preliminary test (R0, Appendix B), and compared with those from FEA in Figure A. 13. Deflections from FEA and testing matched at all pressure levels within 10 kPa, which may be taken as a sufficient proof to establish that the simply-support setup functioned successfully on the pressure box during the actual testing. Note that the uncertainty analysis on the correspondence between measured and calculated deflection at the center of glass plate was performed

and its total uncertainty was calculated as 3.35%, which is acceptable (For details, the reader is referred to Appendix H).

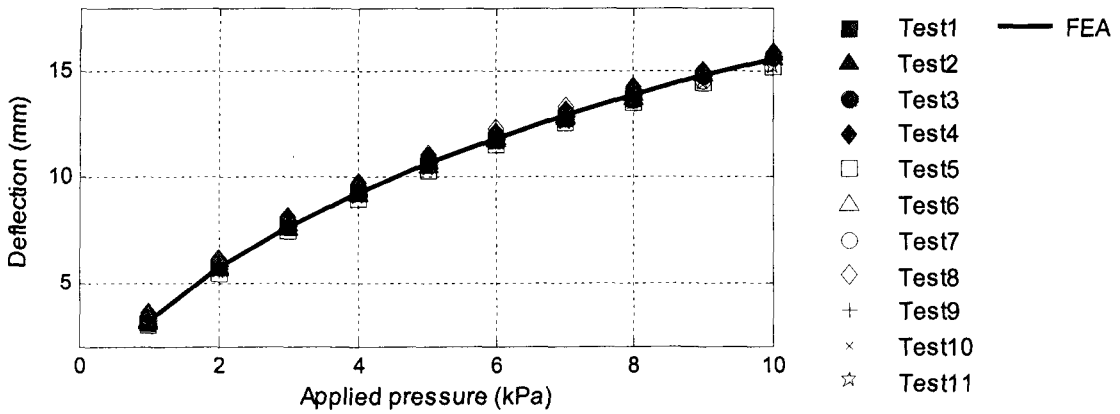

Figure A. 13 Comparison in deflection at center of a glass plate

APPENDIX B Preliminary test results

As mentioned in Chapter 3, the preliminary tests under ramp and saw-tooth loadings were conducted. Since we did not notice the importance of initial glass strength, the very first test series were conducted as follows: The necessary number of glass plates was ordered for one configuration at one time, and if more glass plates were necessary, additional ones were ordered. After one series of test, the results were analyzed, and based on them the configuration of the next test series was chosen. This procedure was repeated until the end of last series. This means that all the glass plates used for any given series necessarily came from the same batch of glass, having undergone the same conditions during the production process and having been exposed to particular wear during the delivery process. After having conducted these tests, it was found out that the test results seemed to be affected by the order of testing, and by the initial glass strength, which varied on account of the production of the plates in different batch. Based on the experience from these preliminary tests, the actual tests whose results are presented in Chapter 3 were conducted in a way explained in the Chapter 3. Even though these test results were suspicious in terms of the randomness of initial glass strength, they helped to understand the phenomena well and let us notice the importance of initial glass strength. Though the entire tests presented here, the thickness of a glass plate was measured from time to time and its averaged was determined as 5.79 mm.

B.1 Ramp loading test

The ramp rate of 16.4 Pa/sec was chosen as the very first loading to compare the test results of Kawabata (1996) who used the same glass plate dimension, type and same loading type for the verification of test methodology. Figure B. 1 (a) is the pressure trace applied to a glass plate by the PLA with this ramp rate until its failure. This loading case is called 'Ramp loading 0 (R0)' for convenience hereafter.

Table B. 1 shows the general test results. The temperature (T) was measured inside the Safety Guard (three layers tarp which covers the whole pressure box to prevent broke glass pieces to shatter in the lab). Only in this test series, the deflection at the center of a glass plate was measured by the laser displacement transducer in order to confirm the simply-support condition by comparing the FEA results (These results are in Appendix A). The "Failure deflection δf" is the measured deflection at the moment of failure.

In this test, the variation of temperature was quite small, therefore, the testing condition was assumed to be consistent in all trials. Also, the coefficient of variation (COV) of the failure pressure was quite small, which points out that the variation of each test run was small and the repeatability of test was satisfactory as mentioned in Appendix A. Moreover, the results of fifteen trials seemed accurate enough to statistically represent this test series, hence, the additional trials have not been conducted after fifteen pieces of glass plate.

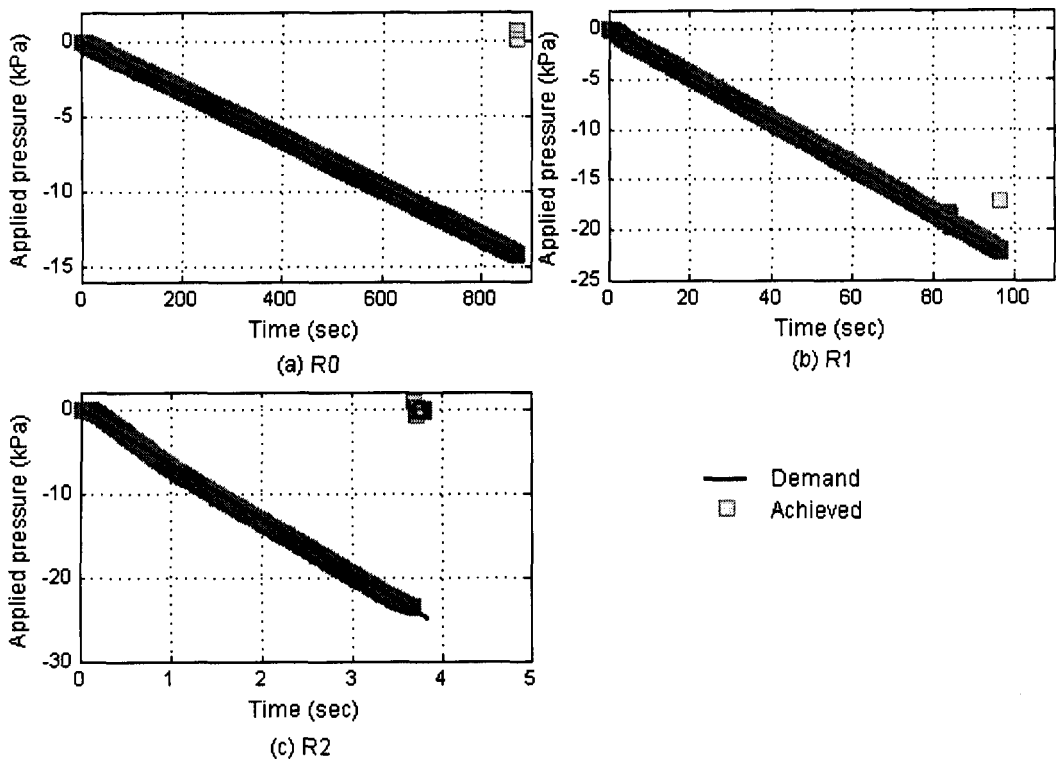

Figure B. 1 PLA pressure trace for ramp loading

Table B. 1 Test results for R0

Trial	T (° C)	p_f (kPa)	t_f (sec)	δ_f (mm)	Trial	T (° C)	p_f (kPa)	t_f (sec)	δ_f (mm)
1	18	8.30	506.52	16.52	9	22	12.91	788.46	21.08
2	21	10.01	610.01	18.45	10	20	12.03	733.32	20.46
3	22	10.73	651.81	19.15	11	22	10.49	642.14	18.66
4	22	10.77	658.72	19.42	12	22	10.24	624.68	19.13
5	21	12.26	748.01	21.04	13	21	14.28	873.58	22.51
6	22	8.35	507.53	16.53	14	20	12.24	748.04	20.92
7	21	9.73	593.80	17.95	15	20	13.86	846.51	22.41
8	21	8.35	508.94	17.18					
						Ave	10.97	669.47	19.43
						S.D	1.92	117.89	1.94
						COV	0.18	0.18	0.10

Following to the R0, the test of loading rate of 230 Pa/sec (Ramp loading 1, R1) with fifteen glass pieces, the test of loading rate of 6500 Pa/sec (Ramp loading 2, R2) with fifteen glass pieces were carried out in this order. Their applied pressure traces are shown in Figure B. 1 (b) and (c). The purpose and all the details of these tests were explained in Chapter 3. The general test results are shown in Table B. 2 and B.3.

For the R1, the results of first fifteen pieces of glass plate had a relatively large variance compared to those of the R0 and R2. Therefore, five pieces of glass plate were additionally tested in order to reduce this variability afterward.

Table B. 2 Test results for R1

Trial	T (° C)	p_f (kPa)	t_f (sec)	Trial	T (° C)	p_f (kPa)	t_f (sec)
1	20	17.69	76.60	11	21	18.64	81.13
2	22	14.49	62.87	12	21	13.36	57.97
3	19	14.40	62.50	13	20	14.55	63.16
4	20	18.71	81.11	14	22	12.33	53.53
5	20	10.33	44.92	15	21	14.27	62.01
6	20	11.33	48.76	16	20	16.68	72.38
7	22	22.22	96.58	17	20	14.47	62.81
8	21	17.38	75.57	18	21	17.01	73.76
9	20	13.78	59.78	19	20	12.75	56.08
10	23	19.92	86.41	20	20	14.04	60.58
					Ave	15.42	66.92
					S.D	3.03	13.14
					COV	0.20	0.20

Table B. 3 Test results of R2

Trial	T (° C)	p_f (kPa)	t_f (sec)	Trial	T (° C)	p_f (kPa)	t_f (sec)
1	22	17.51	2.63	9	20	20.86	3.17
2	20	18.42	2.76	10	22	22.54	3.44
3	20	16.96	2.57	11	20	17.72	2.68
4	20	23.40	3.64	12	21	14.96	2.26
5	20	23.56	3.68	13	21	19.33	2.93
6	20	16.89	2.56	14	20.5	23.21	3.57
7	20	16.45	2.47	15	20	18.01	2.73
8	20	18.05	2.74				
					Ave	19.19	2.92
					S.D	2.81	0.46
					COV	0.15	0.16

B.2 Saw-tooth loading tests

Following ramp loading, a trace that is closer to realistic wind fluctuating load than ramp loading was pursued, since it seemed too large a step to jump directly to fluctuating load with the current understanding of the glass failure under pressure loadings. A cyclic loading was another possibility to apply since there were a few researchers who used cyclic loading in their full-scale tests as a next step of ramp loading (Calderone 1999). However based on the reasons mentioned in Chapter 3, the saw-tooth loading was selected instead of cyclic loading.

The first saw-tooth loading test had a loading rate of 6500 Pa/sec and a pressure amplitude of 14.9 kPa. The same loading rate as R2 was selected because results of R0 and R2 seemed more statistically appropriate than R1, and higher loading rate is a closer situation to the realistic wind. The amplitude of 14.9 kPa was chosen to cause one failure

in a first cycle out of 20 trials based on the results of R2. This saw-tooth loading pattern is called Saw-tooth loading 1 (S1).

After conducting S1, two things to be investigated came up given that they seem to affect the glass strength. They were an amplitude and a loading rate of saw-tooth loading. Since our understanding of glass failure was too little to predict the results and our main interest was the effect of amplitude at that time, this was investigated first by applying the saw-tooth loading which has the same loading rate as S1 but has a lower amplitude than S1. The lower amplitude was selected in order not to have more failures in the first cycle and also 14.9 kPa was close to the pressure which the PLA could achieve with current setup with loading rate of 6500 Pa/sec. After several trial tests, 12.35 kPa was chosen based on the supposition that 2.5 kPa might be enough pressure difference to see the effect but not to bring significantly long time duration until its failure. This saw-tooth loading is called Saw-tooth loading 2′ (S2′). The relative humidity (RH) at Wet Lab began to be measured from this test series since we found that the humidity might affect glass strength from literature (Wiederhorn et al. 1980).

In order to check the other effect on glass strength, the effect of loading rate, the loading rate of 230 kPa/sec which is the same as R1 with the peak pressure of 12.78 kPa was chosen. 12.78 kPa was selected based on the same reason for S2'. This saw-tooth loading is called Saw-tooth loading 3′ (S3′). Note that the pressure amplitude of S2′ and S3′ were set not to be the same in this preliminary test since we did not notice the hypothesis – the failure time should be the same as long as the pressure amplitude is the

same regardless the loading rate– mentioned in Chapter 3 until all the preliminary tests were conducted and their data were analyzed.

Figure B. 2 depicts a time history of the pressure applied to a glass plate by the PLA under S1, S2′, and S3′.

Table B. 4- B. 6 shows the general test results of saw-tooth loading.

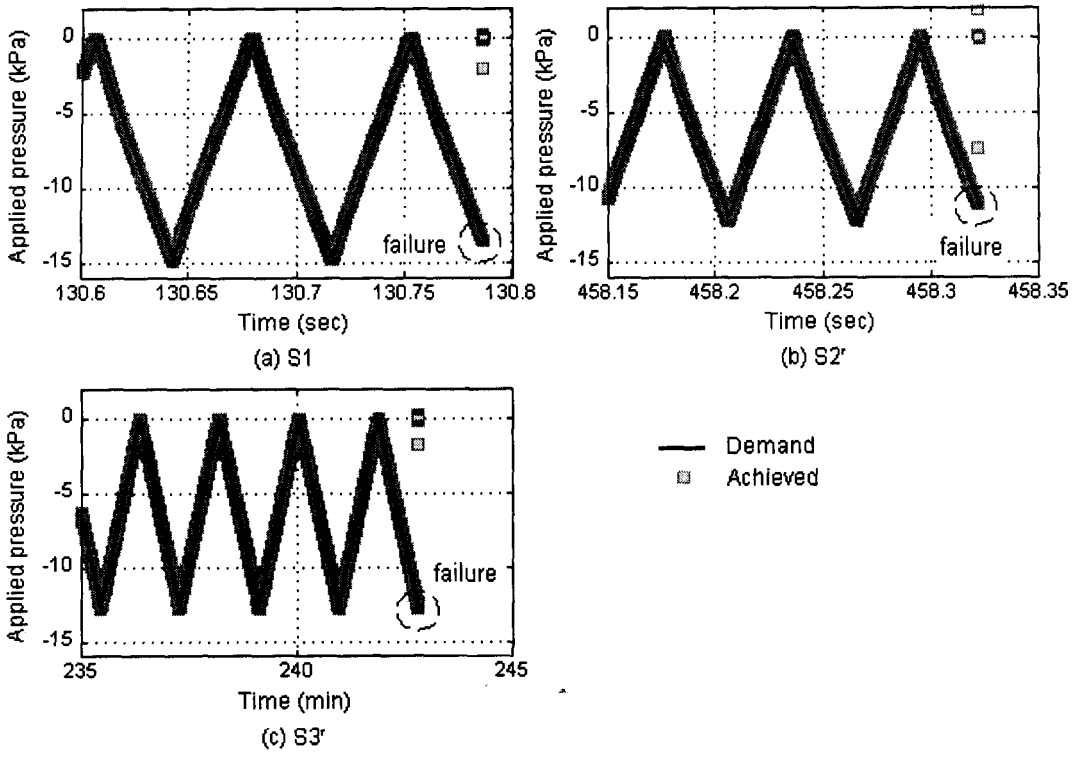

Figure B. 2 PLA pressure trace for saw-tooth loading

Table B. 4 Test results for S1

Trial	T (° C)	p_f (kPa)	t_f (sec)	Trial	T (° C)	p_f (kPa)	t_f (sec)
1	20	14.89	85.78	11	19	13.50	7847.20
2	21	10.43	2806.70	12	22	14.22	28.48
3	20	11.69	234.89	13	21.5	14.42	934.94
4	21.5	13.84	384.82	14	19	14.80	574.21
5	19	14.68	4534.10	15	18.5	14.69	1132.90
6	20	11.31	547.23	16	19.5	14.06	2.07
7	21	12.76	969.85	17	20	12.48	1986.20
8	20.5	13.59	235.18	18	21	14.86	11.23
9	21	12.50	50.21	19	21	14.42	327.73
10	21	13.89	6905.60	20	20	13.67	318.80
					Ave	13.53	1495.91
					S.D	1.28	2306.71
					COV	0.09	1.54

Table B. 5 Test results for S2′

Trial	T (° C)	RH (%)	p_f (kPa)	t_f (sec)	Trial	T (° C)	RH (%)	p_f (kPa)	t_f (sec)
1	21	75	8.79	47.38	11	(-)	(-)	10.61	44.11
2	21	76	11.64	15.85	12	20	80	10.92	2894.70
3	21	77	12.58	1.81	13	22	77	10.05	413.23
4	24	68	12.23	4560.00	14	23	78	10.46	222.13
5	22	77	11.51	612.23*	15	21	76	9.97	594.27
6	22	81	11.92	11518.00	16	22	74	11.19	4602.40
7	20	7	11.19	27542.00	17	23	67	12.25	158.00
8	21	77	12.31	1027.70	18	22	67	10.66	8.68
9	22	76	12.04	10698.00	19	22	75	12.20	4655.80
10	20	77	10.30	29.89	20	22.5	77	10.93	470.17
						Ave		11.19	3505.82
						S.D		0.99	6625.89
						COV		0.09	1.89

Table B. 6 Test results for S3′

Trial	T (° C)	RH (%)	p_f (kPa)	t_f (sec)	Trial	T (° C)	RH (%)	p_f (kPa)	t_f (sec)
1	22	77	12.58	6654.40	11	23	76	12.01	162.23
2	20	78	11.87	58.57	12	23	88	12.20	3682.60
3	21	78	11.49	280.28	13	22	73	11.86	608.57
4	21	79	11.63	10839.00	14	24	81	10.20	4575.90
5	22.5	78	12.67	55.05	15	20	71	10.32	3915.20
6	22	75	12.00	51.62	16	(-)	(-)	12.68	1484.80
7	22	74	11.72	13251.00	17	23	74	12.50	274.08
8	22	76	12.55	14569.00	18	22	77	10.53	45.46
9	23	75	12.31	55.67	19	22	78	10.86	46.79
10	23	77	11.44	500.53	20	22	73	12.64	275.41
						Ave		11.80	3069.31
						S.D		0.79	4668.62
						COV		0.07	1.52

B.3 Equivalent 3 seconds load

Following the procedure explained in Chapter 3, the equivalent 3-sec loads for all the preliminary test results were calculated and are given in Figure B. 3. Compared to the same figures shown in Chapter 3, the results from different loading cases are not corresponding to each other and the possible reason for this is the difference in initial glass strength between glass batches or delivery process as mentioned earlier. From this result, it became clear that the initial strength of glass varies significantly among different batches/production lines.

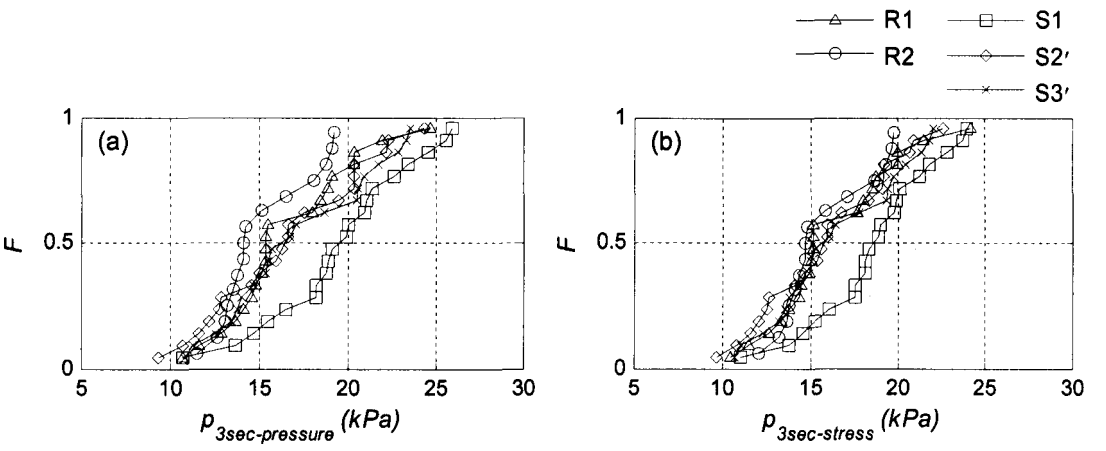

Figure B. 3 CDF of (a) $p_{3\_pressure}$ and (b) p_{3_stress}

APPENDIX C General results of full-scale glass breakage test

Table C. 1 Test results for R1

Trial	T (° C)	RH (%)	p_f (kPa)	t_f (sec)	Trial	T (° C)	RH (%)	p_f (kPa)	t_f (sec)
1	21	70	19.24	83.72	11	21	59	18.50	80.30
2	22	72	8.62	37.45	12	22	67	15.66	68.09
3	22	75	18.29	79.43	13	20	64	18.21	79.18
4	21	74	10.81	46.62	14	20	55	12.57	54.58
5	21	74	12.02	51.94	15	23	51	14.04	60.94
6	20	63	13.08	56.77	16	20	50	10.87	46.83
7	20	67	15.12	65.66	17	22	49	11.48	49.34
8	20	54	14.04	60.87	18	19	49	10.72	46.36
9	22	59	14.25	61.94	19	20	45	9.54	41.02
10	20	54	14.76	64.05	20	20.5	49	9.94	42.79
						Ave		11.80	3069.31
						S.D		0.79	4668.62
						COV		0.07	1.52

Table C. 2 Test results for R2

Trial	T (° C)	RH (%)	p_f (kPa)	t_f (sec)	Trial	T (° C)	RH (%)	p_f (kPa)	t_f (sec)
1	22	72	15.48	2.34	11	20	67	16.31	2.47
2	20	70	9.69	1.43	12	20	52	19.26	2.92
3	22	73	18.94	2.87	13	20	66	19.61	2.98
4	20	72	18.42	2.78	14	23	49	18.22	2.76
5	22	72	16.26	2.46	15	20	53	24.57	4.11
6	21	63	15.43	2.33	16	20	51	15.87	2.40
7	20.5	58	21.49	3.28	17	21	49	13.98	2.11
8	18.	55.5	19.02	2.89	18	23	52.5	11.55	1.72
9	19	62	17.56	2.66	19	20	50	14.33	2.18
10	20	54	21.75	3.31	20	20	54	15.52	2.34
						Ave		17.16	2.62
						S.D		3.49	0.59
						COV		0.20	0.22

Table C. 3 Test results for S1

Trial	T (° C)	RH (%)	p_f (kPa)	t_f (sec)	# *of cycle*	Trial	T (° C)	RH (%)	p_f (kPa)	t_f (sec)	# *of cycle*
1	20	71	14.85	32.97	7	11	21	56	13.77	107.60	24
2	21	74	14.70	2.33	1	12	20	65.5	15.04	19.78	4
3	20	74	13.53	2013.16	457	13	20	54	14.50	81.32	18
4	20	67	14.24	1990.90	452	14	22	67	13.91	2.01	0
5	22	74	14.67	41.74	9	15	23	50	12.33	6.18	1
6	22	74.5	12.72	361.68	144	16	19.5	51	11.74	1.65	0
7	20	68	12.23	1.74	0	17	21	49	13.37	1.90	0
8	20.5	60	13.70	1704.80	387	18	19.5	51	12.08	1.73	0
9	20	59	13.75	7530.40	1711	19	21	49	11.59	1.64	0
10	19	58	14.23	2.05	0	20	20	49	11.93	1.69	0
								Ave	13.44	695.36	
								S.D	1.13	1748.86	
								COV	0.08	2.52	

Table C. 4 Test results for S2

Trial	T (° C)	RH (%)	p_f (kPa)	t_f (sec)	# *of cycle*	Trial	T (° C)	RH (%)	p_f (kPa)	t_f (sec)	# *of cycle*
1	20	74	12.36	30.71	8	11	18	62	13.06	12.72	3
2	22	74	11.02	1.67	0	12	20	56	12.16	1477.70	410
3	21	75	12.46	135.32	37	13	22	62.5	12.29	1344.20	372
4	21	74	10.88	759.38	210	14	20	69	12.71	2.03	1
5	20	68	10.98	1.73	0	15	19	50	12.33	55.91	15
6	23	74	10.46	6977.10	1936	16	20	51	11.02	1.55	0
7	21	74	12.75	5.51	1	17	20	51	12.35	1.74	0
8	18	68	12.89	1.88	0	18	20	52	12.34	19.82	5
9	20	58	12.30	6717.60	1868	19	21	49	12.83	1.95	1
10	24	55	10.61	1607.40	445	20	21.5	46	12.81	1.83	0
								Ave	12.03	957.89	
								S.D	0.85	2085.40	
								COV	0.07	2.18	

Table C. 5 Test results for S3

Trial	T (° C)	RH (%)	p_f (kPa)	t_f (sec)	# *of cycle*	Trial	T (° C)	RH (%)	p_f (kPa)	t_f (sec)	# *of cycle*
1	20	70	12.36	161.59	1	11	20	56	11.44	2626.50	24
2	20	73	11.16	48.12	0	12	20	68	12.04	162.81	1
3	20	75	11.33	797.84	7	13	24	54	10.16	171.41	2
4	20	74	10.28	44.25	0	14	22	58	12.03	266.01	2
5	22	72	11.74	157.51	1	15	24	49	12.50	2729.10	25
6	20	70	12.15	8401.70	78	16	19.5	52	11.88	51.29	0
7	19.5	64	12.32	23072.00	215	17	20	50	11.68	370.66	3
8	24	52	12.27	6903.00	64	18	20	49	12.28	54.74	1
9	19	63	12.49	267.98	2	19	20.5	45	9.36	40.21	0
10	Failure did not occur after 20 hours of load application					20	18.5	51	9.58	41.38	0
								Ave	11.53	2440.43	
								S.D	0.99	5541.67	
								COV	0.09	2.27	

Table C. 6 Test results for F1

Trial	T (° C)	RH (%)	p_f (kPa)	t_f (sec)	# *of cycle*	Trial	T (° C)	RH (%)	p_f (kPa)	t_f (sec)	# *of cycle*
1	21	69	10.34	165.18	0	11	(-)	(-)	13.18	219.06	0
2	19.5	72	13.84	711.40	2	12	20	54	16.82	286.11	0
3	20	70	12.82	153.62	0	13	19	68	10.22	30.59	0
4	20	72.5	15.73	153.77	0	14	23	57	15.50	322.73	0
5	20.5	72	12.45	8.06	0	15	20	48	15.79	1834.70	5
6	19.5	68	11.96	527.29	1	16	21	52	12.45	7.74	0
7	20	53	10.65	37480.00	111	17	Failure did not occur after 20 hours of load application				
8	20	57	1121	307.38	0	18	19	52	12.25	7.714	0
9	20	59	10.12	23.54	0	19	20	44	10.04	23.528	0
10	19.5	69	14.51	47.22	0	20	24	50	12.13	8.025	0
								Ave	12.74	2227.24	
								S.D	2.13	8547.44	
								COV	0.17	3.84	

APPENDIX D Validation of finite element analysis results

For deflection and stress analysis on glass plate, the commercial finite element analysis (FEA) software SAP 2000 was employed. Linear plate theory can be used while the out-of-plane deflections of glass plates are less than its thickness under lateral loads. However, once they become relatively larger than the thickness of the plate under lateral loads, bending of a plate is accompanied by strain in the middle plate, and these supplementary stresses, called membrane stresses, must be taken into account. At that point, non-linear plate theory must be employed, and fortunately SAP 2000 can also handle this non-linear analysis.

D.1 Simply-support condition

The necessary components from SAP 2000 in this research were deflections of and stresses on a uniformly loaded thin glass plate with boundary conditions defined as simply-support, but allowing for in-plane movement. The results of this analysis were used to confirm the appositeness of the testing rig (pressure box) by comparing them to the deflection measurements from testing, and also to provide glass plate stress data to be used as input for the glass failure prediction simulation (Chapter 4). In order to reduce the calculation time, only 1/4 of the entire area of a square plate was modeled in SAP 2000. The support conditions were arranged as shown in Figure D. 1.

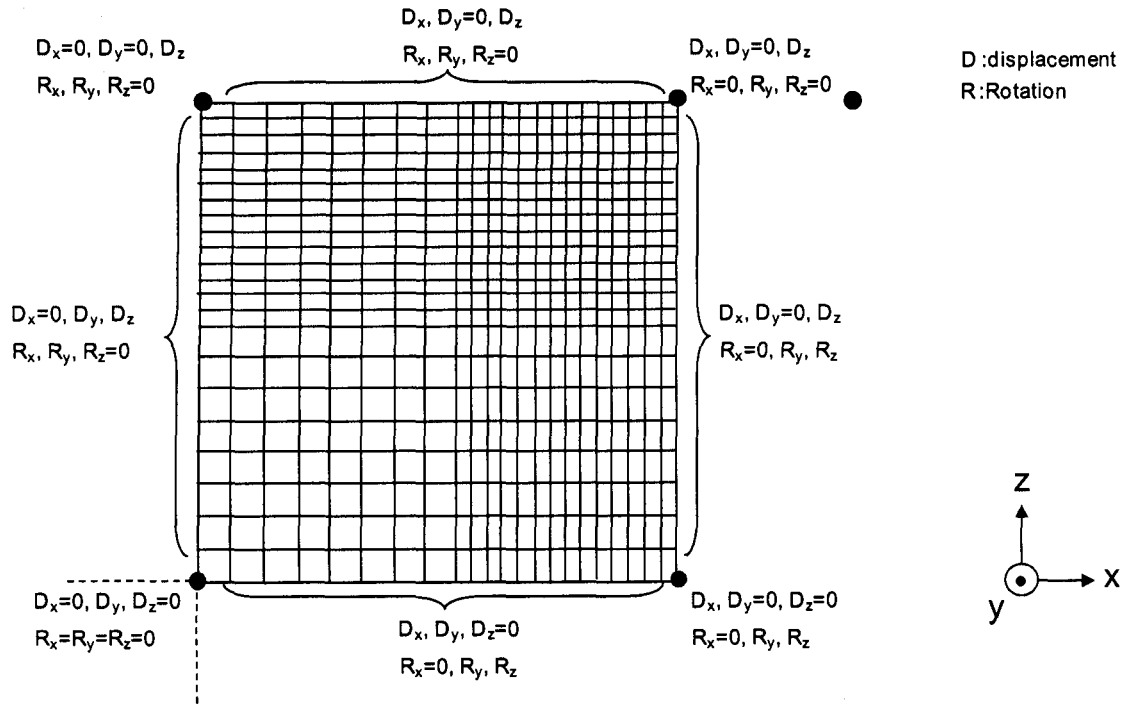

Figure D. 1 Support condition setup in FEA

The accuracy of FEA results were validated by comparing them with results from the theoretical equation and those from other researchers.

Seaman's theoretical equation (1967) which is a modification of Timoshenko's formulation (Timoshenko & Woinowsky-Krieger 1959) with a correction for movable edges in the plane of the plate when $\nu' = 0.23$, is stated as:

$$\frac{p}{E}\left(\frac{a}{h}\right)^4 = 21.7\left(\frac{\delta}{h}\right) + 2.8\left(\frac{\delta}{h}\right)^3 \qquad \text{(D. 1)}$$

where p is applied uniform pressure, a is the length of a square plate, h is the thickness of the plate, and δ is the central deflection. δ may be obtained for a given value of p, which

in turn may be used to calculate the components of applied pressure contributing to bending and membrane action, respectively p_1 and p_2, expressed in the following way:

$$p_1 = 21.7\frac{\delta E h^3}{a^4} \tag{D. 2}$$

$$p_2 = 2.80\frac{\delta^3 E h^3}{a^4} \tag{D. 3}$$

Using the calculated values of p_1 and p_2, the maximum bending and membrane stress on plate, respectively σ_1 and σ_2, are obtained through the following relationship:

$$\sigma_1 = 0.2874\frac{p_1 a^2}{h^2} \tag{D. 4}$$

$$\sigma_2 = 0.243\left[\frac{p_2 a^2 E}{h^2}\right]^{1/3} \tag{D. 5}$$

The sum of σ_1 and σ_2 is the maximum stress induced on the plate.

Fisher-Cripps and Collins (1995) conducted stress analysis on a 1 x 1 x 0.004 m glass plate under the uniform pressure of 2.2 kPa using a commercially-available finite element software package, and their deflection and stress results are reported in their paper.

Table D. 1 compares the deflection and stress results from Fisher-Cripps and Collins (1995), Seaman's theoretical equation (1967), and SAP 2000 for a 1 x 1 x 0.004 m glass plate under the uniform pressure of 2.2 kPa. For the purposes of this analysis, the

glass plate was modeled as a shell element, and the following material properties[i] were used:

Young's modulus: E=70.3 (GPa)

Poisson ratio: $\nu' = 0.23$

Density: ρ=2190 (kg/m^3)

Table D. 1 Comparison of induced stress and deflection at the center of glass plate

		Stress		Deflection
		σ_{center} (MPa)	σ_{max} (MPa)	δ_{center} (mm)
Seaman's equation	Non-linear	(-)	23.9	11.2
Fisher-Cripps & Collins	Linear	37.5	37.5	22.0
	Non-linear	17.3	20.8	10.5
Present	Linear	37.4	37.4	22.6
	Non-linear	17.7	22.6	10.6

With respect to results from non-linear analysis, as may be quickly gleaned from the above table, stresses from Fisher-Cripps and Collins are lower than the others, and deflection from Seaman's equation is larger than the others. Considering the assumed material properties in Fisher-Cripps and Collins results, present results correspond quite well with others. Therefore, this comparison concluded that SAP 2000 can successfully conduct non-linear analysis on thin glass plates, and also that the inputs in SAP 2000 were appropriate.

[i] Note that since the material properties of glass were not mentioned in Fisher-Cripps and Collins' paper, they were assumed to be the same as those used in current FEA.

D.2 Grid independence

As for the grid independence, the current results were obtained by dividing one quarter of the glass area in 22 x 22 grids. Figure D. 2 shows the principal stress distribution on the current grid and on the grid which is doubled (44 x 44 grids). Although the double grid results show smoother transition of stress from one grid to another, the stress values do not change significantly at the locations needed for the numerical simulation. Moreover, the computational time is much longer when using 44 x 44 grids than with the current grid. Therefore, it was concluded that the properties of the current grid proved adequate to confirm grid independence.

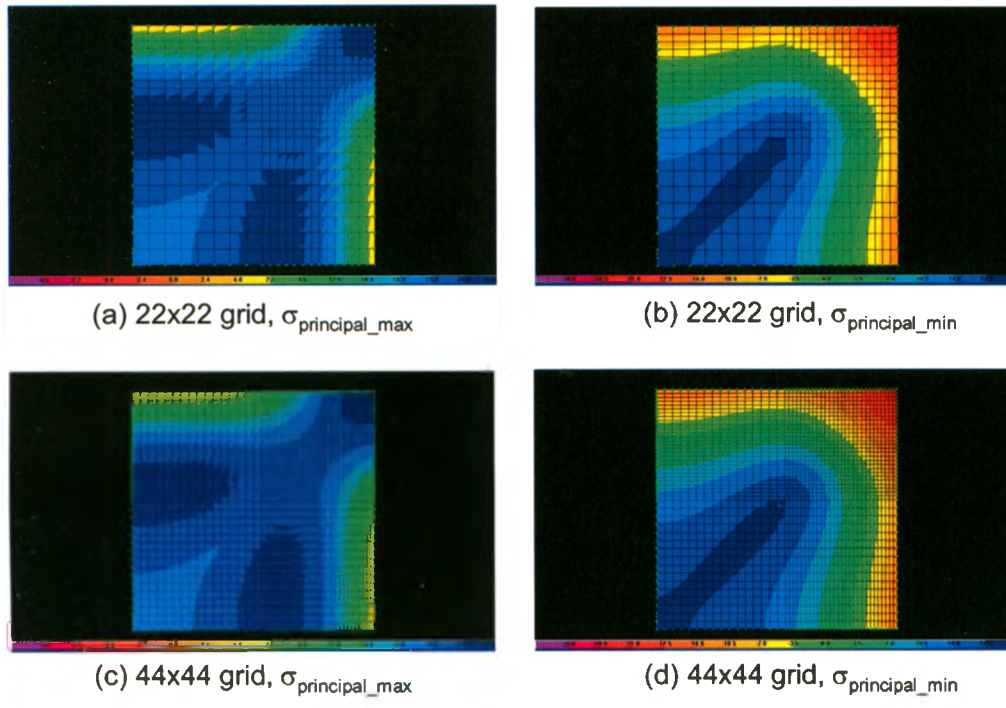

(a) 22x22 grid, $\sigma_{principal\_max}$ (b) 22x22 grid, $\sigma_{principal\_min}$

(c) 44x44 grid, $\sigma_{principal\_max}$ (d) 44x44 grid, $\sigma_{principal\_min}$

Figure D. 2 Principal stress distribution

APPENDIX E Statistics of failure location

Since Brown's integral is valid only at the critical crack location on a glass plate, this location is essential information to calculate the equivalent 3-sec load p_{3_stress} for each glass plate broken in the full-scale tests. However, as mentioned in Chapter 3, it was difficult to capture the location where glass plate began to break, —the critical crack location—, in the current test. Therefore, the statistics of critical crack location/direction on a plate was calculated using the numerical simulation results (Chapter 4) in order to obtain p_{3_stress} as a statistically most reliable value.

For each loading case (R1, R2, S1, S2, S3, F1), the modified numerical simulation was conducted using the input coefficients producing the closest results to the test results (Chapter 4) (repetition of 10000), and the 10000 results of failure location, M_j (j =1~225) and direction, α_k (k =1~10) were obtained. The number of failure at each M_j and α_k was counted, and a probability of failure at each M_j and α_k was calculated by dividing it by the total repetition number (=10000). For example, if the number of failure at M_j =1 and α_k =8 was 3, its probability of failure was $P(M_1, \alpha_8)$ = 3/10000. This calculation was repeated at all M_j and α_k, and the results were kept as a table for each loading case. Using the method explained in Chapter 3, p_3 (M_j, α_k) was calculated at each M_j and α_k, and the statistically most reliable value of p_3 (M_j, α_k), p_{3_stress} for the loading case was calculated as:

$$p_{3\_stress} = \sum_{j=1}^{225} \sum_{k=1}^{10} p_3(M_j, \alpha_k) \cdot P(M_j, \alpha_k) \qquad \text{(E. 1)}$$

APPENDIX F Cumulative distribution function

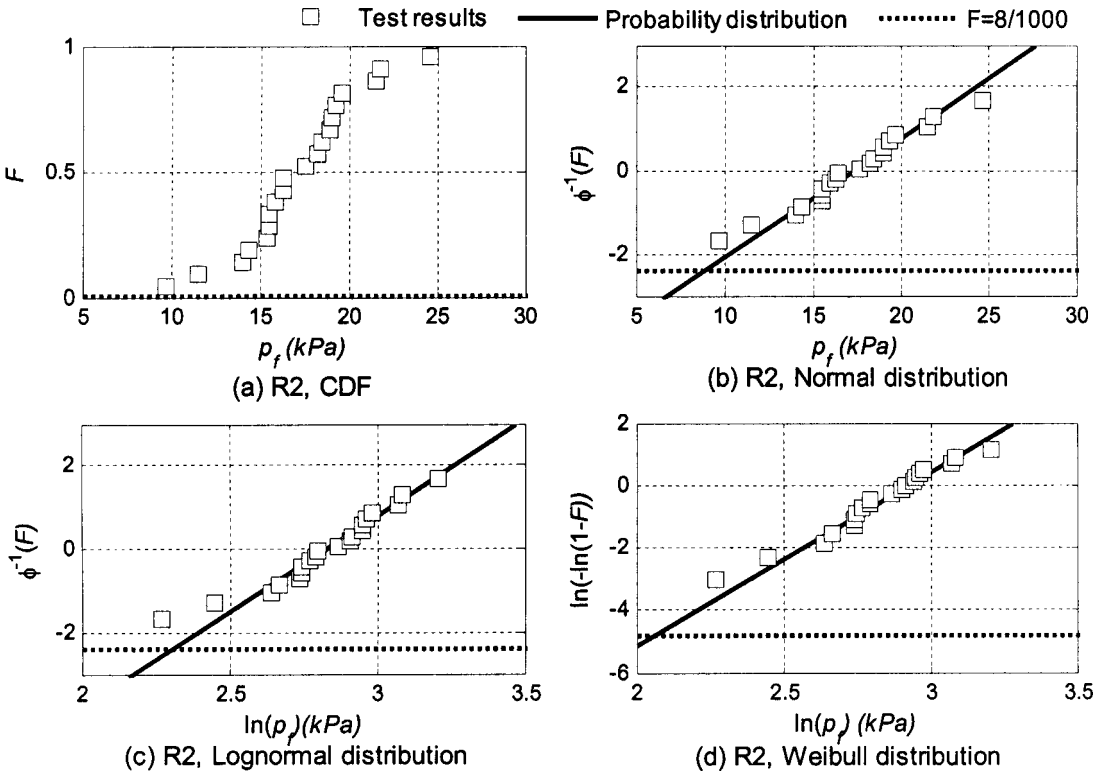

Figure F. 1 CDF of failure pressure (R2)

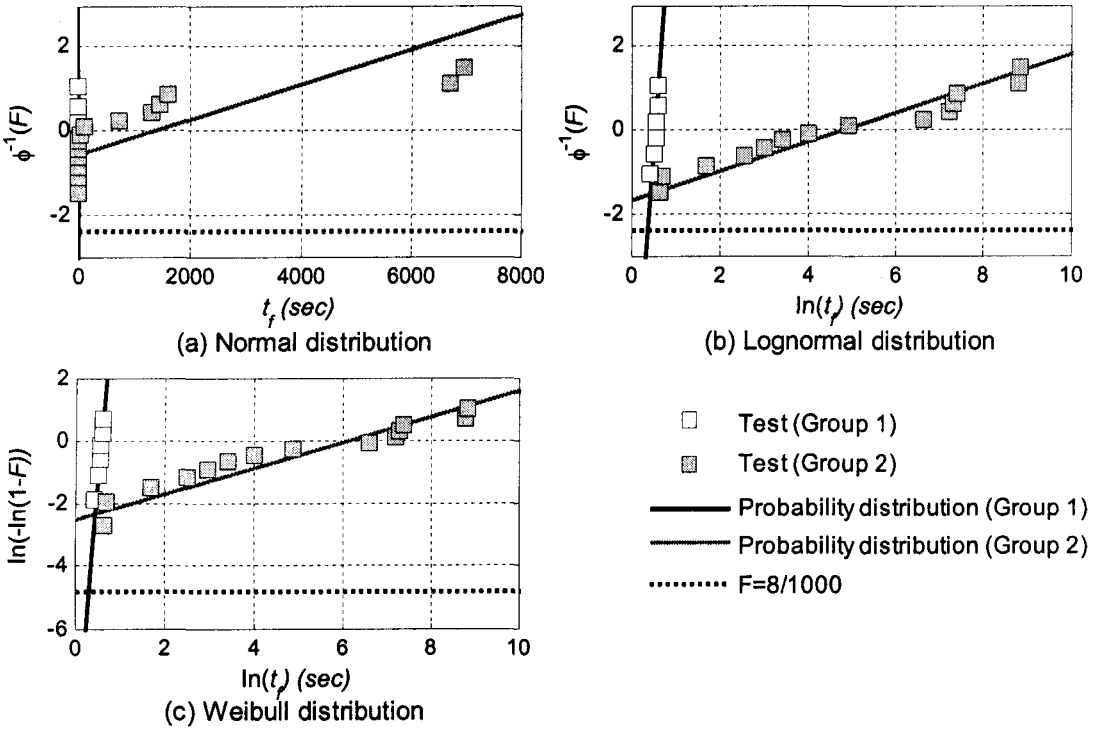

Figure F. 2 CDF of failure time (S2)

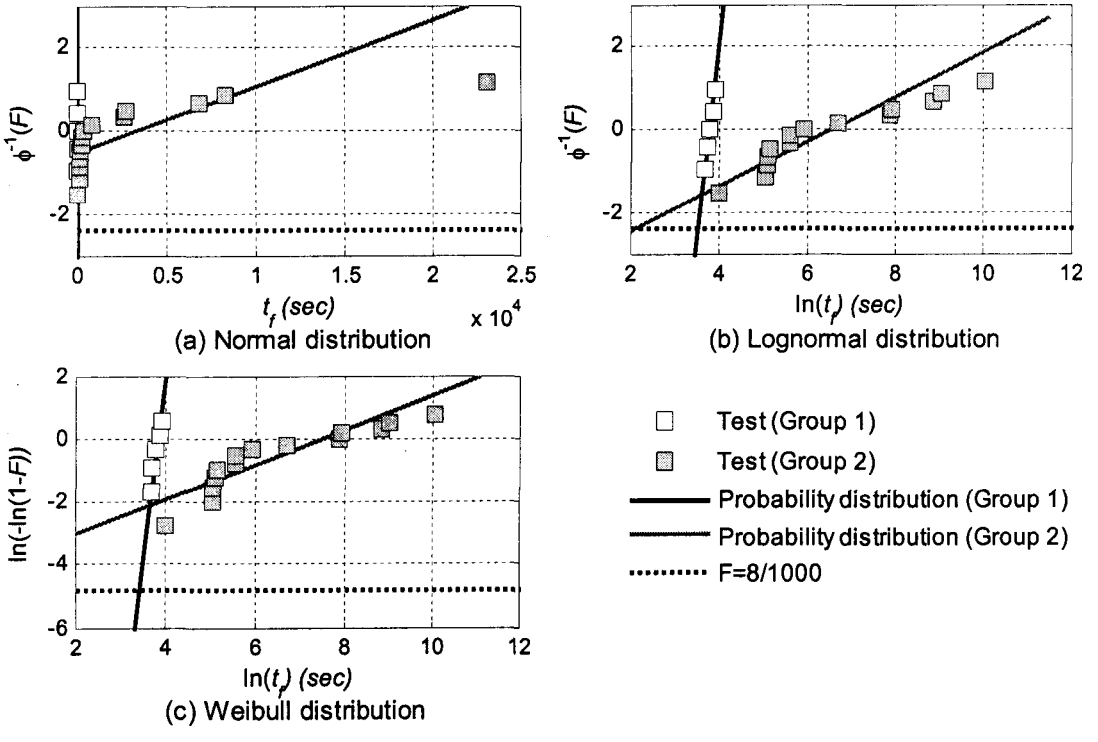

Figure F. 3 CDF of failure time (S3)

APPENDIX G Estimation of surface crack coefficients

In order to estimate the surface crack coefficient, the same method as Haldimann (2006) was used in the present research. Haldimann selected the results of ramp loading test (loading rate of 15 kPa/sec) on 3.721m^2 float glass, assuming that 15 kPa/sec is the minimum ramp loading necessary to create the inert condition in their test setup, namely, a glass size of 3.721 m^2 and a simply-support condition without lateral displacement. However, the challenge here is that the loading rate which produces the inert condition for our test conditions—namely, a glass size of 1 m^2 and simply-support condition with lateral displacement—was unknown. Moreover the test results which correspond to this loading rate may not be the same as the one used in the current experiment (230 Pa/sec, 6500 Pa/sec). These issues needed to be resolved before proceeding further.

G.1 Desired loading rate

The surface coefficients of S_0 (A_0=1m^2) = 63 (MPa), m = 8.1, which were estimated by Haldimann for 6 mm annealed glass, can be converted to S_0 (A_0=3.721m^2) = 53.6 (MPa), m = 8.1 using the following relationship:

$$\left(\frac{S_{0,A_1}}{S_{0,A_2}}\right)=\left(\frac{A_2}{A_1}\right)^{1/m} \tag{G.1}$$

where A_1 and A_2 correspond to different glass areas. For the test results which Haldimann chose as the inert condition, the average failure time of this test results was 0.44 sec. Hence, it can be interpreted that the inert condition was created for glass size of 3.721 m^2

since the loading rate of 15 kPa/sec made the applied stress reach 53.6 MPa in 0.44 sec and cause failure at that point. Since the time duration required for failure in the inert condition for the current test setup was unknown, it was assumed to be 0.44 sec for glass size of 1 m^2, the same as the average failure time of Haldimann's selected test results whose glass size was 3.721 m^2. From the above discussion, the desired loading rate for the present test setup (1 m^2) was interpreted as the loading rate which would make the applied stress reach 63 MPa in 0.44 sec. From the FEA, this loading rate was calculated as 82 kPa/sec. This loading rate seemed appropriate, having compared it to other researchers' results (15kPa/sec for a surface area of 3.721 m^2 in a simply-support condition without lateral displacement (Haldimann 2006), 1235kPa/sec for a surface area of 0.00342 m^2 (Kawabata 1996)).

G.2 Estimation of *m*

The coefficient *m* may be obtained from:

$$\frac{m}{m_f} = \frac{n'-2}{n'+1} = \frac{16-2}{16+1} = 0.824 \qquad \text{(G.2)}$$

where *m* is a surface crack parameter for initial strength and m_f is the one for the failure strength. In order to calculate m_f, the induced stress at failure under R1 and R2 were calculated using the FEA[ii], and were fitted to the Weibull distribution properly with the

[ii] The failure stress was calculated at several different locations on a glass plate and a final stress was obtained as their area average.

parameter of m_f = 6.2 and 7.2, respectively, by the method of maximum likelihood. Accordingly, m was obtained as 5 and 6 for R1 and R2, respectively from equation (G.2).

G.3 Estimation of S_0

In terms of actual test results at a loading rate of 82 kPa/sec, the failure pressure of different loading rates can be predicted using the relationship between failure pressure and loading rate, based on a modification of Brown's integral (equation (1.2)). Using the R1 and R2 test results, the failure pressures under a loading rate of 82 kPa/sec were predicted using equation (1.2), and are shown as CDF in Figure G. 1, with those from the lifetime prediction model, based on the different values of S_0 (A_0=1m^2) and m = 5 and 6 for R1 and R2, respectively. Values of S_0 (A_0=1m^2) = 67 and 69 (MPa) were obtained, which showed the best fit using the least square method. Differences in these values are not significant, and m = 6 seemed more appropriate when compared to the values obtained by other researchers. Hence, m = 6 and S_0 (A_0=1m^2) = 69 will be used as the surface crack coefficients in the discussion below.

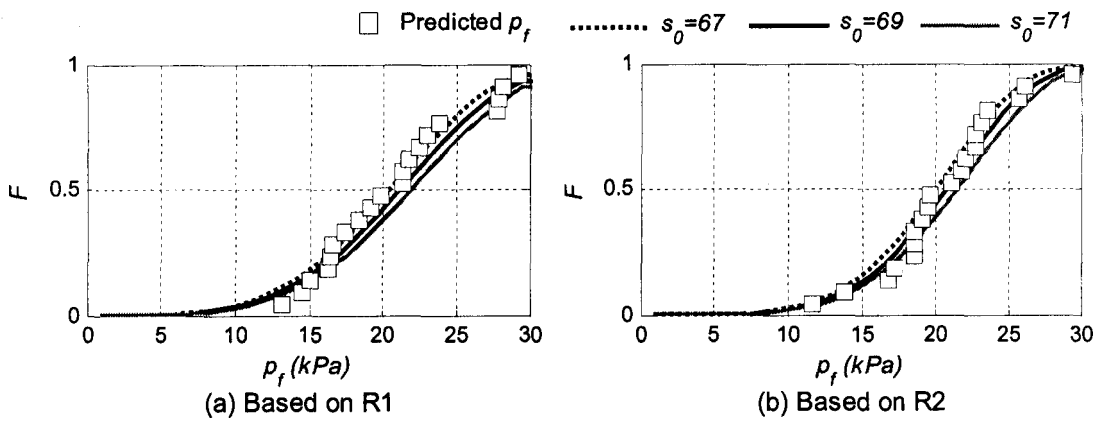

Figure G. 1 Predicted failure pressure under loading rate of 82 kPa/sec with results of life time prediction model

APPENDIX H Uncertainty analysis on correspondence between measured and calculated deflections

H.1 General procedure of analysis

In order to ensure the reliability of obtained and calculated deflection measurements at the center of the glass plate, an uncertainty analysis was conducted.

On the one hand, uncertainty exists in the measured deflection as a result of bias and precision errors. In turn, these errors come from two sources: the Laser Displacement Transducer (LDT) and Data Acquisition System (DAQ). These errors can be calculated using the following equations (Wheeler & Ganji 1996):

$$B_x = \sqrt{\sum_{i=1}^{k} B_i^{\,2}} \tag{H. 1}$$

$$S_x = \sqrt{\sum_{i=1}^{m} S_i^{\,2}} \tag{H. 2}$$

$$T_x = \sqrt{B_x^{\,2} + (t' S_x)^2} \tag{H. 3}$$

where B_x is the bias limit, S_x is the precision index, T_x is the total uncertainty for the quantity x, k, m are the number of sources of uncertainty, and t' is the value of Student-t statistics for the degrees of freedom ν'' and for a selected level of confidence. In this study, $t' = 2$ was used for a 95% confidence level.

On the other hand, uncertainties from the measured quantities that are a function of deflection must be known in order to evaluate the uncertainty of calculated deflection. The deflection at the center of a square glass plate was calculated from the following

equation developed by Timoshenko and Woinowsky-Krieger (1959) and modified by Seaman (1967), which was introduced in Appendix D:

$$\frac{p}{E}\left(\frac{a}{h}\right)^4 = 21.7\left(\frac{\delta}{h}\right) + 2.8\left(\frac{\delta}{h}\right)^3 \qquad \text{(H. 4)}$$

where p is the applied uniform pressure, a is the length of the glass panel, E is Young's modulus of glass panel, δ is the displacement at the center of the glass panel, and h is the thickness of the panel. This cubic equation can be solved using the method developed by Gerolamo Cardano (1954). The answer for this equation was obtained as;

$$\delta = \left(-\frac{B_1}{2} + \sqrt{\left(\frac{B_1}{2}\right)^2 + \left(\frac{A_1}{3}\right)^2}\right)^{1/3} + \left(-\frac{B_1}{2} - \sqrt{\left(\frac{B_1}{2}\right)^2 + \left(\frac{A_1}{3}\right)^2}\right)^{1/3} \qquad \text{(H. 5)}$$

where $A_1 = 7.75h^2$ and $B_1 = -\frac{1}{2.8}\frac{p}{E}\frac{a^4}{h}$. When a quantity Q is a function of l number of measured variables $x_1, x_2, ,,,,, x_l$ as is the current case, the maximum uncertainty in Q can be expressed as:

$$T_Q = \sqrt{\sum_{i=1}^{l}\left(T_{x_i}\frac{\partial Q}{\partial x_i}\right)^2} \qquad \text{(H. 6)}$$

The measured deflection should be the same as the value obtained from the calculation if no error exists in the deflection measurement and in the measured functions of deflection. Therefore, all errors affecting the total uncertainty of the correspondence between measured and calculated deflection at the center of the glass can be evaluated as $Q=\delta_{measurement}/\delta_{calculation}$. The value of this relationship was calculated as:

$$\frac{T_Q}{Q} = \sqrt{\left(\frac{T_{\delta_{measurement}}}{\delta_{measurement}}\right)^2 + \left(\frac{T_{\delta_{calculation}}}{\delta_{calculation}}\right)^2} \quad \text{(H. 7)}$$

The following sections conduct the calculation according to the approach mentioned above.

H.2 Uncertainties in measured deflection

H.2.1 Errors from laser displacement transducer

The followings were the possible bias and precision errors from the LDT:

Bias error: accuracy, linearity

Precision error: repeatability, temperature fluctuation due to sensor head, temperature fluctuation due to controller

In order to obtain the accuracy and repeatability of LDT, a simple test using steel bar was conducted. The test setup is shown in Figure H. 1. The laser was pointing at the steel bar vertically downwards. Each measurement was performed by inserting and removing the steel bar from the target spot of LDT. The measurement was repeated 10 times and the results are shown in Table H. 1.

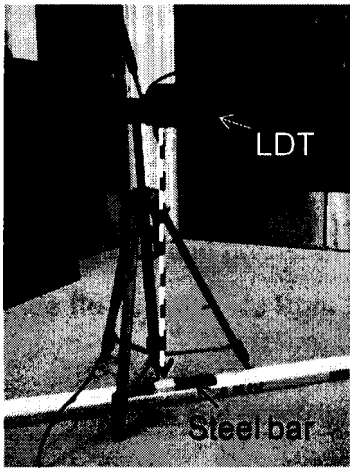

Figure H. 1 Test setup

Table H. 1 Measurement results

	Measurement (mm) δ	Deviation (mm) $\Delta\delta$
1	13.40	0.42
2	13.42	0.44
3	13.41	0.43
4	13.42	0.44
5	13.37	0.39
6	13.36	0.38
7	13.34	0.36
8	13.41	0.43
9	13.38	0.40
10	13.35	0.37
Max	13.4	0.44
Min	13.3	0.36

In Table H. 1, the deviation which is the difference between the measured value and the actual thickness of the steel bar (12.979 mm) measured by callipers is included. The measuring range of this laser displacement sensor is $\pm 100\,\text{mm}$. Using these data, the accuracy and repeatability of measurement were calculated as follows:

Accuracy: $\dfrac{\Delta\delta_{\max}}{\delta_{\max}} = \dfrac{0.44}{13.42} = 0.00328 = +3.28\%$

$$\frac{\Delta\delta_{\min}}{\delta_{\max}} = \frac{0.36}{13.42} = 0.00266 = +2.66\%$$

Repeatability: $\frac{\Delta\delta_{\max} - \Delta\delta_{\min}}{\delta_{\max}} = \frac{0.44 - 0.36}{13.42} = 0.0062 = 0.62\% \text{ or } \pm 0.31\%$

Table H. 2 summarizes all the bias and precision errors from LDT. The values of errors of linearity and temperature fluctuations are from the specification of LDT.

Table H. 2 Summary of bias and precision errors from LDT

Bias Limit	
Accuracy	$\pm\frac{3.28}{100}\times 100 = \pm 3.28(mm)$
Linearity	$\pm\frac{0.1}{100}\times 100 = \pm 0.1(mm)$
Precision index	
Repeatability	$\pm\frac{0.31}{100}\times 100 = \pm 0.31(mm)$
Temperature fluctuation due to sensor head	$\pm\frac{0.02}{100}\times 100 = \pm 0.02(mm)$
Temperature fluctuation due to controller	$\pm\frac{0.01}{100}\times 100 = \pm 0.01(mm)$
Total uncertainty	$\sqrt{3.28^2 + 0.1^2 + (2*0.31)^2 + (2*0.02)^2 + (2*0.01)^2}$ $= \pm 3.336(mm)$

H.2.2 Error from data acquisition system (DAQ)

Following the same method used in H.2.1, the uncertainty from DAQ was calculated assuming that both accuracy and repeatability are 0.1% for a measurement range of 100mm. The relevant summary is given in Table H. 3.

Table H. 3 Summary of bias and precision errors from DAQ

Bias Limit	
Accuracy	$\pm\frac{0.1}{100}\times 100=\pm 0.1(mm)$
Precision index	
Repeatability	$\pm\frac{0.1}{100}\times 100=\pm 0.1(mm)$
Total uncertainty	$\sqrt{0.1^2+(2*0.1)^2}=\pm 0.224(mm)$

H.2.3 Total uncertainty of measured deflection

Based on the results obtained until this point, the total uncertainty in deflection measurement that may be attributed to equipment was calculated and the results are shown in Table H. 4. The total uncertainty in the measured deflection at the center of the glass plate is 3.344/100=3.344% of the full-scale reading, or ± 3.344 mm.

Table H. 4 Summary of uncertainty in measured deflection

Combined Bias limit	$\sqrt{3.28^2+0.1^2+0.1^2}=\pm 3.280(mm)$
Combined Precision index	$\sqrt{0.31^2+0.02^2+0.01^2+0.1^2}=\pm 0.325(mm)$
Total uncertainty	$\sqrt{3.280^2+(2\times 0.325)^2}=\pm 3.344(mm)$

H.3 Uncertainties of calculated deflection

According to equation (H.5), deflection at the center of the glass plate is a function of applied uniform pressure p, Young's modulus E, glass panel length a, and glass plate thickness h. Hence, the uncertainty of the deflection at the center of the glass

plate due to these measured quantities also needs to be evaluated by the following equation:

$$T_\delta = \sqrt{\left(T_q \frac{\partial \delta}{\partial q}\right)^2 + \left(T_a \frac{\partial \delta}{\partial a}\right)^2 + \left(T_E \frac{\partial \delta}{\partial E}\right)^2 + \left(T_t \frac{\partial \delta}{\partial t}\right)^{2^2}} \qquad \text{(H. 8)}$$

All of the variables in equation (H.5) are listed in Table H.5. The current calculation assumed a uniform load of 5 kPa applied to a 1m x 1m x 6 mm glass plate. Based on equation (H.5), the total deflection at the center of the plate should be 10.74(mm) in this case. Using equation (H.8) and the values in Table H.5, the total uncertainty of calculated deflection due to the measured functions was calculated as

$$T_\delta = \sqrt{\left(100 \cdot 1\times10^{-6}\right)^2 + \left(7.03\times10^{8} \cdot 2.1\times10^{-28}\right)^2 + \left(0.01 \cdot 0.02\right)^2 + \left(1.2\times10^{-4} \cdot 0.62\right)^2}$$

$$=0.237 \text{ (mm)}$$

Or, 0.237/10.74=2.2% of correctly calculated deflection.

Table H. 5 Summary of bias from functions of deflection

Bias Limit	
Uniform pressure q	Bias error = 2% $T_q = \pm\frac{2}{100}\times 5000(N/m^2) = 100(N/m^2)$ $d\delta/dq = 1\times 10^{-6}$
Young's modulus E	Bias error = 1% $T_E = \pm\frac{1}{100}\times 7.03\times 10^{10}(N/m^2) = 7.03\times 10^{8}(N/m^2)$ $d\delta/dE = -2.1\times 10^{-28}$
Glass plate length a	Bias error = 1% $T_a = \pm\frac{1}{100}\times 1(m) = 0.01(m)$ $d\delta/da = 0.02$
Glass thickness h	Bias error = 2% $T_h = \pm\frac{2}{100}\times 0.006(m) = 1.2\times 10^{-4}(m)$ $d\delta/dh = -0.62$

H.4 Total uncertainty

Using equation (H.7) and the results obtained so far, the total uncertainty between measured and calculated deflections at the center of the glass plate was determined as:

$$\frac{T_Q}{Q} = \sqrt{\left(\frac{3.344}{100}\right)^2 + \left(\frac{2.2}{100}\right)^2} = 3.35\%$$